Syntrophic interactions between anode-respiring bacteria and non-anode-respiring bacteria in microbial electrochemical cells

by

Yaohuan Gao

A thesis

presented to the University of Waterloo

in fulfilment of the

thesis requirement for the degree of

Doctor of Philosophy

in

Civil Engineering

Waterloo, Ontario, Canada, 2015

Author's Declaration

This thesis consists of material all of which I authored or co-authored: see Statement of Contributions included in the thesis. This is a true copy of the thesis, including any required final revisions, as accepted by my examiners.

I understand that my thesis may be made electronically available to the public.

Statement of Contributions

A version of Chapter 3 was published as the paper: Yaohuan Gao, Hodon Ryu, Jorge W. Santo Domingo, and Hyung-Sool Lee. "*Syntrophic interactions between H_2-scavenging and anode-respiring bacteria can improve current density in microbial electrochemical cells*" Bioresource Technology 153, 245–253, 2014

I carried out all experimental work in Chapter 3, except for the sequencing of biofilm and planktonic cells. Here is a summary of my major tasks associated with Chapter 3.

- Design of the sandwich-type microbial electrochemical cells (MECs)
- Operation of an anaerobic digester and the MECs mentioned in this study
- Set-up of a multi-channel potentiostat for MEC experiments
- Establishment of analytical methods for biogas composition and dissolved methane using a GC-TCD and volatile fatty acids (VFAs) using a GC-FID
- Analyses of all gaseous and liquid samples (gas compositions and VFAs)
- Collection and preparation of biofilm and planktonic cells for molecular biology analyses
- Data interpretation (current density, VFAs, gas composition, sequencing data, etc.) under the supervision of Prof. Hyung-Sool Lee

Below are the contributions of co-authors (Dr. Hodon Ryu and Dr. Jorge W. Santo Domingo) to Chapter 3.

- DNA extraction, Sanger sequencing, and pyrosequencing
- Provision of raw data from sequencing studies

A version of Chapter 4 was published as the paper: Yaohuan Gao, Junyeong An, Hodon Ryu, and Hyung-Sool Lee. "*Microbial Fuel Cells as Discontinuous Portable Power Sources: Syntrophic Interactions with Anode-Respiring Bacteria*" ChemSusChem, 7 (4), 1026–1029, 2014

I carried out all experimental work related to MECs in Chapter 4, except for the sequencing of biofilm and planktonic cells. Here is a summary of my major tasks associated with Chapter 4.

- Design of the sandwich-type MECs
- Operation of the MECs mentioned in this study
- Establishment of the methods for acetate analysis using a GC-FID and the method for dissolved and gaseous methane analysis using a GC-TCD

- Design of the acetate medium injection tests
- Establishment of the Nile-red staining method
- Image analysis of stained biofilms with an epifluorescence microscope
- Collection and preparation of biofilm and planktonic cell samples for molecular biology analyses
- Data interpretation (current density, acetate concentration, microscopic images, sequencing data, etc.) under the supervision of Prof. Hyung-Sool Lee

Below are the contributions of co-authors (Dr. Junyeong An and Dr. Hodon Ryu) to Chapter 4.

- Confirmation tests with microbial fuel cells (Dr. Junyeong An)
- Sequencing study and provision of the raw data from sequencing (Dr. Hodon Ryu)

For Chapter 5, I carried out all the experimental work and conducted data organization and data interpretation under the supervision of Prof. Hyung-Sool Lee. DNA-Stable isotope probing (SIP) and associated sequencing work was carried out in Prof. Josh Neufeld's lab in the Department of Biology.

Abstract

Microbial electrochemical cells (MECs), a promising technology for recovering value-added products from waste biomass and wastewater, require syntrophic interactions between anode-respiring bacteria (ARB) and non-ARB for high performance and versatile functionality. However, understanding of the syntrophic interactions is limited. Controlling the growth of unfavorable non-ARB, such as methanogens, is challenging, and the proliferation of these microorganisms seriously decreases energy recovery from MECs. Small-sized microbial fuel cells (MFCs), one kind of the MECs, have recently gained attention as renewable and portable power suppliers to small electronics. In spite of this potential, the serious deterioration of ARB's catabolism in the absence of exogenous substrate limits the real-world application of small-sized MFCs. Additionally, MECs can be useful biosensors for various targets (e.g., volatile fatty acids, protons, and heavy metals), but the potential of sensing dissolved methane by anode biofilm has never been reported although methanogenesis and dissolved methane have been frequently observed in MECs.

Therefore, the objective of this study was to explore the potentials of three new syntrophic interactions that can catalyze the applications of MECs to be (1) a sustainable anaerobic wastewater treatment technique, (2) portable power sources, and (3) biosensors for methane or methanogenesis detection.

High current density of 10.0–14.6 A/m^2 and high chemical oxygen demand (COD) removal up to 96% were obtained in an MEC fed with digestate at hydraulic retention time (HRT) of 4 day and 8 day. Volatile fatty acids (VFAs) became undetectable in the MEC effluent (HRT 8 day), except for low levels of acetate (4.16 ± 1.86 mg COD/l). Accumulated methane only accounted for 3.42% of removed COD.

Pyrosequencing analyses showed abundant fermenters (*Kosmotoga* species) and homoacetogens (*Treponema* species) in anolytes. In the anode biofilm, propionate fermenters (*Kosmotoga* species and *Syntrophobacter* species), homoacetogens (*Treponema* species), and ARB (*Geobacter* species and *Dysgonomonas* species) were dominant. These results implied that syntrophic interactions among fermenters, homoacetogens, and ARB would enable MECs to maintain high current density and coulombic efficiency despite the presence of methanogens.

Steady current density around 1.5 A/m^2 in a dual-chamber MEC was sustained for over four days without exogenous electron donors. High efficiency, close to 100%, of electron recovery can be achieved once acetate was provided. The air-cathode MFC inoculated by this MEC showed stable anode-respiring activity over a seven-day starvation period. Nile red staining revealed that lipid-accumulating bacteria were abundant in the anode biofilm. Taken together, these results suggested that lipid-accumulating bacteria in syntrophy with ARB generated current without exogenous electron donors. This study implied that small-sized MFCs can be used as portable power sources in a discontinuous feeding manner.

A long term of enrichment and growth of anode biofilm in MECs with dissolved methane, ~800 days, resulted in a syntrophy between *Methanobacterium* species and *Geobacter* species, which is the first anode-respiration-dependent anaerobic oxidation of methane (AOM) discovered so far. In this proposed syntrophy, *Methanobacterium* species anaerobically oxidize methane molecules and transfer electrons or certain reducing powers derived from methane to *Geobacter* species for anode respiration. No common electron mediators found in MECs were detected; instead, ethanol- or dimethyl ether-like compounds were detected. Electric current (2-12 mA/m^2) was consistently produced from an MEC using methane as the sole carbon and electron source for over 440 days, whereas nitrogen gas sparging of the anolyte

decreased the current to near zero. Deoxyribonucleic acid (DNA)-stable isotope probing (SIP) experiments employing $^{13}CH_4$ combined with denaturing gradient gel electrophoresis (DGGE) demonstrated that the labeled carbon was found in DNA of dominant bacteria (*Geobacter*) and archaea (*Methanobacterium*). Fluorescence *in situ* hybridization (*FISH*) targeting the two genera clearly showed that *Methanobacterium* and *Geobacter* formed biofilm together on the surface of anode fibers. These results and the available information from literature support the explanation that AOM archaea and ARB built syntrophy for generating current from dissolved methane under anaerobic conditions.

Acknowledgements

Without a doubt there are many people to recognize who have helped me along the way, and I greatly appreciate their effort. First and foremost, I would like to express my sincere gratitude to my adviser, Prof. Hyung-Sool Lee, for his expert guidance and continuing support in my research. Meanwhile, I would like to greatly appreciate the guidance and input from Prof. Wayne J. Parker, my former co-adviser, during my PhD study. I would also like to thank the other members of my committee, Prof. Monica B. Emelko, Prof. William B. Anderson, and Prof. Zhongwei Chen for the assistance they provided at all levels during my study. I would like to thank Prof. John M. Regan from the Department of Civil and Environmental Engineering at the Pennsylvania State University for sparing his precious time to serve as my external examiner.

I am deeply grateful to our technicians, Mark Sobon, Mark Merlau, Terry Ridgway, and Anne Allen for their assistance in instrument troubleshooting and for their commitment to maintaining the equipment from our department in good conditions without which my laboratory life would be much more difficult. My sincere thanks goes out to Dr. Hodon Ryu, from the US EPA, for his instructions and training on qPCR and his effort spent during the sequencing of some of my biomass samples.

In addition, I would like to thank all the members in Waterloo Environmental Biotechnology Lab, past and present, for making my experience in Waterloo so interesting and exciting. Specially, I would like to thank Dr. Weiwei Du, Yu Hou, and Mohammed A. Galib who initiated the anaerobic digester and maintained the reactor before my test. I should also give my thanks to Chao Jin, Dr. Maria M.F. Mesquita, and Dr. Christina Smeaton for teaching me, at different stages of my PhD study, how to operate different models of epifluorescence microscopes.

I would like to thank Prof. Josh D. Neufeld and his student, Sara Victoria Coyotzi, for providing technical support for the DNA-SIP and subsequent DGGE analyses, and I thank Prof. Neufeld for allowing me to involve in the lab work.

Finally, and most importantly, I would like to thank my family for the exceptional support they provided me through my entire life.

Table of Contents

List of Figures

List of Tables

Nomenclature

AD	Anaerobic Digester
AEM	Anion Exchange Membrane
Ag/AgCl	Silver/Silver Chloride reference electrode
ANME	ANaerobic MEthanotrophic archaea
AOM	Anaerobic Oxidation of Methane
ARB	Anode-Respiring Bacteria
BES	BromoEthaneSulfonate
BOD	Biological Oxygen Demand
CE	Coulombic Efficiencies
COD	Chemical Oxygen Demand
DGGE	Denaturing Gradient Gel Electrophoresis
DNA	DeoxyriboNucleic Acid
EET	Extra-cellular Electron Transfer
FISH	Fluorescence *in situ* Hybridization
GC-FID	Gas Chromatography with a Flame Ionization Detector
GC-TCD	Gas Chromatography with a Thermal Conductivity Detector
H-MECs	H-type Microbial Electrochemical Cells
HRT	Hydraulic Retention Time
ILIs	Intracellular Lipophilic Inclusions or Intracellular Lipid Inclusions
MCA	Membrane-Cathode Assembly
MECs	Microbial Electrochemical Cells
MFCs	Microbial Fuel Cells
NMR	Nuclear Magnetic Resonance
PCR	Polymerase Chain Reaction
PDB	Pee Dee Belemnite
PEM	Proton Exchange Membrane
PHAs	PolyHydroxyAlkanoates
PHBs	PolyHydroxyButyrates
qPCR	quantitative Polymerase Chain Reaction
16s rRNA	16s ribosomal RiboNucleic Acid
SCOD	Soluble Chemical Oxygen Demand
SIP	Stable-Isotope Probing
SMP	Soluble Microbial Products
SRT	Solid Retention Time
TCOD	Total Chemical Oxygen Demand
TSS	Total Suspended Solid
UHP	Ultra High Purity
VFAs	Volatile Fatty Acids
VPDB	Vienna Pee Dee Belemnite
VSS	Volatile Suspended Solid

Chapter 1 Introduction

1.1. Background of microbial electrochemical cells

Conventional aerobic biological wastewater treatment converts organic content and nutrients into carbon dioxide, water, and their oxidized forms (e.g., ammonium to nitrate) using oxygen molecules as the terminal electron acceptor; hence intensive aeration is essential for aerobic biological wastewater treatment. This aeration can account for around half of the total energy consumption by wastewater treatment plants (McCarty et al., 2011). Generally speaking, around 0.26-0.84 kWh/m^3 of electrical energy is necessary for a plant using aerobic processes (Singh et al., 2012). Thus, for a plant employing an aerobic processes with a daily flow of 1 MGD (3785 m^3/day), the energy input will be around 984-3179 kWh/day. Reflecting this energy investment, the annual cost for municipal wastewater treatment is estimated at $ 1.5-2 billion in Canada (Environment_Canada, 2010).

As issues like energy security, climate change, and sustainability become significant, the demand on energy- and cost-efficient biotechnologies for wastewater treatment is increasing. In fact, most wastewater contains reduced forms of organic compounds, typically expressed as biochemical oxygen demand (BOD), which means that the wastewater can be renewable energy resource. Heidrich *et al*. (2011) reported that the energy content in domestic wastewater ranges from 5 to 16 kJ/l, which means approximately 5261-16835 kWh/day of energy flows through a normal wastewater treatment plant (assume a flow rate of 3785 m^3/day). This energy is over five times higher than the energy input for aerobic treatment. Municipal wastewater could be treated in energy-neutral manners assuming that the energy recovered from the

wastewater is equal to or higher than the energy consumption for treatment. There are several wastewater treatment biotechnologies capable of recovering energy, such as anaerobic digestion, dark fermentation, and microbial electrochemical cells (MECs); among them, MECs is a standout because of their versatile functionality and applicability (Figure 1-1), including recovery of electricity and generation of hydrogen gas, hydrogen peroxide, and acetate (Logan and Rabaey, 2012). In addition, MECs can be used as biosensors to detect toxic chemicals (Gil et al., 2003, Xu et al., 2014).

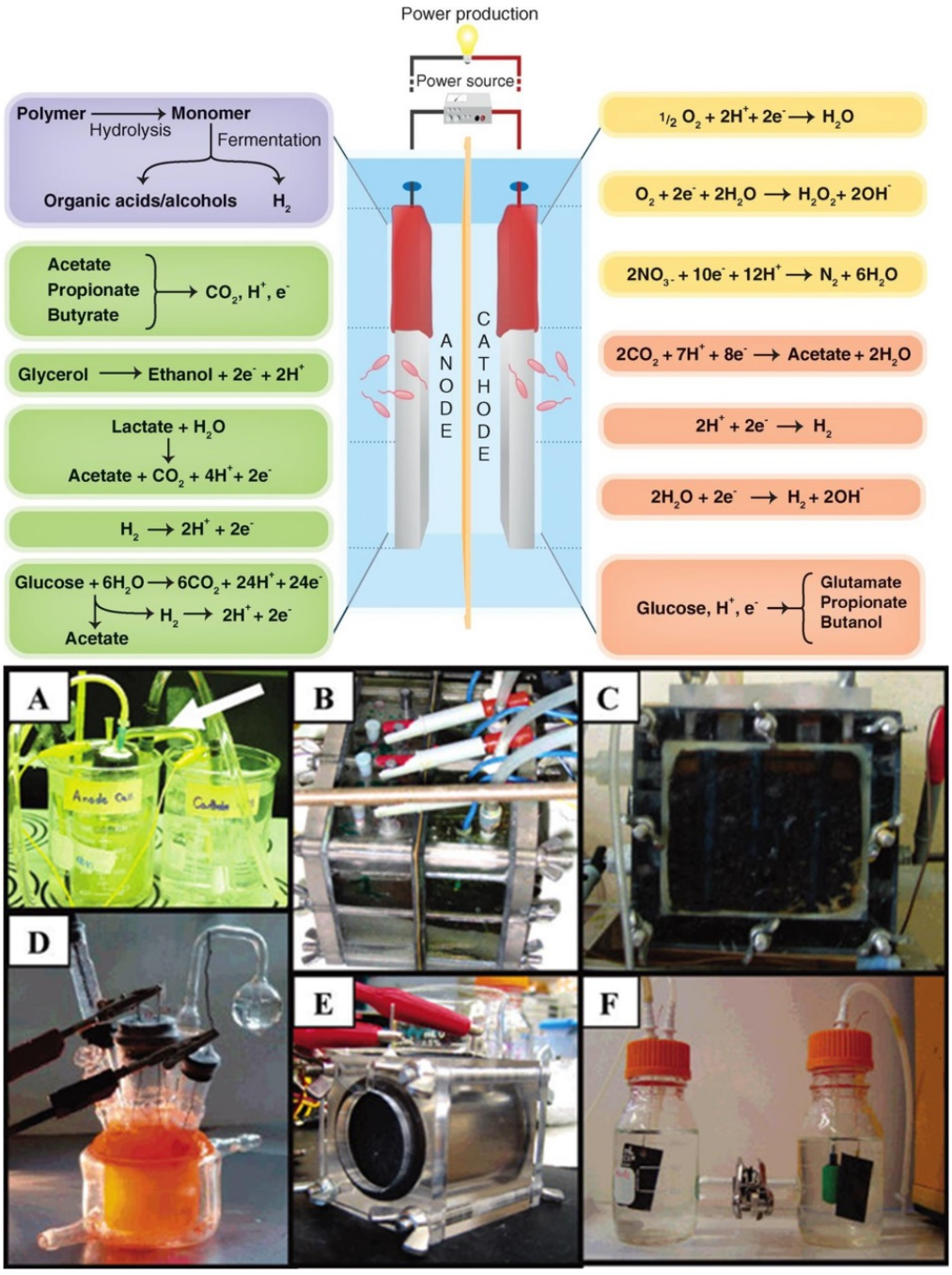

Figure 1–1. Overview of the functions of microbial electrochemical cells (MECs) (Top figure) and types of MECs used in various studies (Bottom figure). (A) a salt-bridge MEC (B) four batch sandwich-type MECs where the chambers are separated by the membrane; (C) sandwich-type MEC with a continuous flow-through granular graphite anode; (D) photoheterotrophic MEC; (E) air-cathode MEC; (F) H-type MEC (Logan et al., 2006, Logan and Rabaey, 2012).

An MEC merges an electrochemical cell with an anaerobic bioreactor (Logan, 2004, Liu et al., 2005, Lee et al., 2008b), which allows the conversion of chemical energy stored in organics in wastewater into electrical energy (Rabaey and Verstraete, 2005, Rabaey and Rozendal, 2010). An MEC normally consists of an anode chamber, a cathode chamber, and an ion-selective membrane (a reference electrode is optional) (Figure 1-1). Generally, the anode chambers of MECs function like conventional anaerobic bioreactors except that conductive materials (i.e., electrodes) are provided to support biofilm growth and to facilitate electron transfer (Logan, 2004, Rabaey and Verstraete, 2005). These electrochemically active bacterial species among the microorganisms that form biofilms on electrodes are commonly known as exoelectrogenic bacteria (Logan, 2009) or anode-respiring bacteria (ARB) (Torres et al., 2008b) because they can respire on electrode surfaces—a distinct feature from typical anaerobes. In contrast to conventional electrochemical cells, these microorganisms themselves serve as electrode catalysts, facilitating electron transfer from donor substrate to electrodes. Meanwhile, in MECs, the basic thermodynamic rules of a conventional fuel cell still hold true: after the anode receives electrons from microbial catabolism, the anode circuits the electrons through a wire to the cathode in the cathodic chamber where electrons react with oxidants (Figure 1-1); this cathodic reaction can spontaneously occur when the coupled anodic and cathodic reaction is thermodynamically favorable (i.e., a microbial fuel cell), and if the coupled anodic and cathodic reaction is not thermodynamically favorable, an external power source needs to be added to force the flow of electrons by manipulating the electrode potentials (i.e., a microbial electrolysis cell). Since all of the MECs used for experimental studies in this thesis are microbial electrolysis cells, unless stated otherwise, a microbial electrochemical cell is interchangeable with a microbial electrolysis cell in the following sections.

1.2 Microbial syntrophic interactions

Microbial syntrophy (Figure 1-2) can be defined as a "thermodynamically interdependent lifestyle where the degradation of a compound, such as a fatty acid, occurs only when degradation end products, usually hydrogen, formate, and acetate, are maintained at very low concentrations" (McInerney et al., 2009). This lifestyle requires a consortium of microorganisms to complete a series of interconnected redox reactions. Syntrophy plays an important role in both natural and engineered processes. For instance, petroleum in a natural reservoir or a contaminated site is biodegraded through the collaboration of multiple microorganisms: syntrophic fermenters for the initial fermentative degradation and methanogens, sulfate-reducing bacteria, and denitrifiers for scavenging the fermentation end products. Regarding engineered processes, anaerobic digestion is an excellent example. One of the most important reactions during anaerobic digestion is methanogenesis, which has been treated as a classic case of syntrophy: fermentative bacteria supply hydrogen gas, simple acids, or formate to methanogens that maintain the intermediate compounds at low concentration and facilitate the degradation of organic compounds.

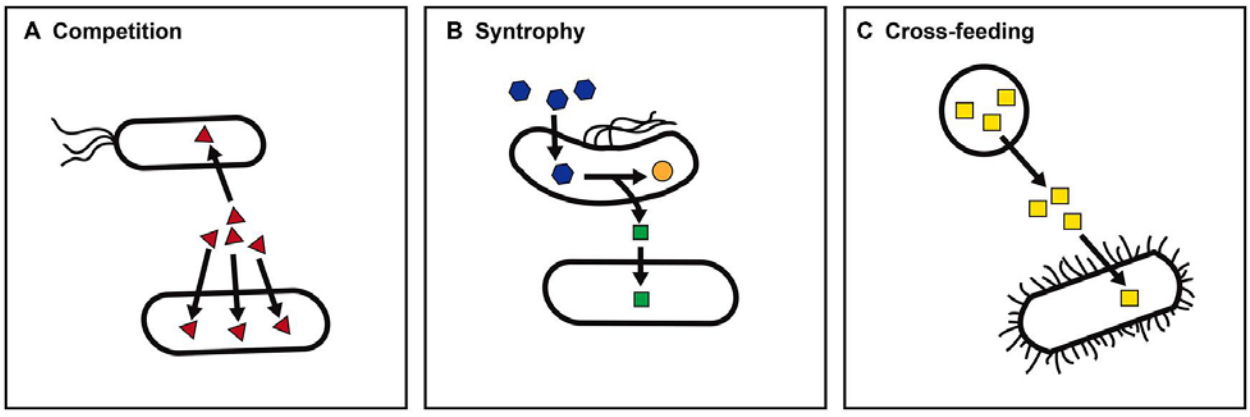

Figure 1–2. Nutritional interactions between microorganisms. (A) Nutrient competition. Different species compete for a limited nutrient (red triangles) for survival. (B) Syntrophic metabolism. The consumption of an intermediate or end

product, such as hydrogen (green squares), by a partner organism allows an otherwise energetically unfavorable reaction, for example, fermentation of propionate (blue hexagons) to acetate (orange circles) to support growth. (C) Nutrient cross-feeding. The presence of a microbe that produces an essential nutrient, such as folate (yellow squares), enables auxotrophs to survive (Seth and Taga, 2014).

Various types of syntrophy have been discovered in the past, and these syntrophic interactions can often be conveniently categorized according to the reducing power shared among partners. Hydrogen gas, formate, and acetate are the commonly encountered reducing powers in both methanogenic and non-methanogenic conditions. For instance, with the assistance of hydrogen-utilizing bacteria, *Desulfovibrio* strain G11, *Syntrophomonas wolfei* can ferment butyrate into acetate (McInerney et al., 1981). Some other species, such as *Syntrophobacter fumaroxidans*, are able to ferment propionate in the presence of formate-utilizing methanogens, whereas co-culture with hydrogen-utilizing methanogens cannot support the growth of *Syntrophobacter fumaroxidans* (Harmsen et al., 1998). Other than the conventional reducing powers and the relevant syntrophic interactions, recent studies demonstrated that microorganisms are able to directly share electrons among them, which suggests in some circumstances electrons themselves become the direct interspecies reducing power. For example, methanogens and *Geobacter* species have been reported to exchange electrons via conductive iron oxide and biochar, which were thought to serve as "wires" for electron transfer (Kato et al., 2012, Chen et al., 2014). Moreover, two *Geobacter* species, *Geobacter metallireducens* and *Geobacter sulfurreducens,* are found to share electrons directly via the pili or "nanowire" on cell membrane surfaces (Shrestha et al., 2013).

Generally, these syntrophy in normal anaerobic environment can also be significant in MEC environment, especially during the treatment of complex organic compounds (industrial wastewater, sludge, and animal manure). Since ARB cannot

directly utilize complex forms of organic compounds present in typical waste and wastewater and they cannot efficiently break complex compounds into smaller ones, the microorganisms that are able to hydrolyze and ferment complex organics into simple acids and alcohols are essential for the MECs using complex organics as feed (Fornero et al., 2010, Inoue et al., 2013). Although such kind of microbial syntrophy can be significant for MECs, there is limited information on syntrophic interactions between ARB and fermenters in MECs. One significant advantage of MECs over other anaerobic biotechnologies is their versatile applications in areas from waste treatment to biosensors. Therefore, in order to promote the development of MEC technology, it is highly valuable and probably critical to explore new syntrophic interactions between ARB and non-ARB in order to engineer MECs for given purposes (e.g., small power suppliers, biosensors, etc.).

1.3 Research needs

MECs were initially applied in wastewater treatment to achieve energy-neutrality, but most studies have commonly reported low energy recovery. For instance, MECs usually demonstrate an energy recovery of 1.6-14.3% of the degraded COD, whereas existing anaerobic technologies, such as anaerobic membrane bioreactors (AnMBR) and upflow anaerobic sludge blanket (UASB) reactors, can achieve 24-35% of energy recovery (Shoener et al., 2014). Moreover, electrical energy usually accounts for a small part, around 10%, of the total energy recovered from MECs (e.g., electricity, methane, and hydrogen gas) (Min et al., 2005, Ge et al., 2013). Several limitations of MEC systems have been identified, including low substrate utilization rates, poor ability in handling particulate organic matter, and multiple energy losses at the electrode surfaces and membrane surfaces (Arends and Verstraete, 2012). All these

drawbacks need to be overcome to give MECs competitive advantages over existing anaerobic technologies. Among them, improving the functions of the anodic biofilm is crucial because anodic reactions catalyzed by ARB and their syntrophic partners are one of the major limiting factors in MEC performance (Clauwaert et al., 2008, Shoener et al., 2014).

In recent years, small-sized MECs have been studied to develop portable bio-battery or biosensors after realizing the challenges of recovering massive energy from wastewater using MECs (Qian and Morse, 2011, Ren et al., 2012). Although small-sized MECs as portable power suppliers show great potentials, one significant challenge is that ARB are very sensitive to changes in environmental conditions, such as starvation. However, portable MECs mean that fuels will be fed to the MECs in a discontinuous manner (e.g., fed-batch). Although portable MECs show promises as renewable power sources for small electronic devices, the development of portable MECs seems unrealistic without addressing the sensitivity of ARB to starvation conditions.

MEC application to biosensors has been expanded recently, due to its energy independence and sustainability. Volatile fatty acids, BOD, pH, and heavy metals sensors based on MECs have been developed (Chang et al., 2004, Tront et al., 2008, Di Lorenzo et al., 2009, Liu et al., 2011, Kaur et al., 2013, Liu et al., 2014) but these MEC-based biosensors seems unfeasible because of the limited advantages over existing abiotic sensors. The significance of MEC-based biosensors will increase if the sensors can detect compounds or reactions that current devices are unable to detect, such as methanogenesis or dissolved methane.

The following sections briefly summarize the research advances on MECs and identify the research needs and opportunities for improving the energy recovery of

MECs using wastewater and exploring the potentials of using MECs as portable power sources and dissolved methane detectors.

1.3.1 Fermentable substrates degradation in microbial electrochemical cells

Despite the fact that MECs can generate electricity directly from organic feed, recent studies show that MECs cannot replace anaerobic digestion due to limited energy recovery (Arends and Verstraete, 2012, Ge et al., 2013). Therefore, it has been concluded that MECs could only be implemented as a supplementary treatment process to anaerobic digesters or dark fermentation for treating low strength wastewater. In a sequential anaerobic digestion-MEC treatment process, anaerobic digesters act as a pretreatment unit for hydrolysis of particulate organic matters and fermentation of complex organics (i.e., proteins, carbohydrates, and fatty acids), which complements MECs for better energy recovery since ARB are poor at hydrolyzing and fermenting complex and particulate organic feeds (Pant et al., 2010, Ge et al., 2013, Li et al., 2014). Furthermore, MECs in this sequential arrangement would improve the quality of effluent from anaerobic digestion or dark fermentation (Barker et al., 1999, Chernicharo, 2006).

Nevertheless, attempts to use MECs to further treat anaerobic effluent for obtaining a higher quality effluent is challenging. First, in an MEC originally inoculated with an environmental sample (e.g., activated sludge), methanogens can easily divert the reducing powers from organic substrates to methane production when fermentable substrates are present (He et al., 2005, Clauwaert and Verstraete, 2009, Lee et al., 2009b, Cusick et al., 2011). Second, although ARB can readily utilize acetate for anode respiration, slow degradation of propionate, butyrate, or valerate has been reported (Freguia et al., 2010, Choi et al., 2011), probably because of either

lack of fermentative bacteria or the accumulation of fermentative products, such as hydrogen gas, in anode biofilm. Due to either loss of electrons to methane or lack of essential syntrophic partners in anode biofilm, limited amount of reducing power can be recovered by MECs (Rozendal et al., 2008, Chae et al., 2010).

In order to overcome these limitations, substantial effort has been invested in optimizing the design and operating conditions of MECs to inhibit the activity of methanogens (Chae et al., 2010, Logan, 2012). Recent studies with fermentable substrates show that ARB can establish syntrophic interactions with H_2-scavengers, such as homoacetogens, for an improved energy recovery when methanogens are inhibited (Parameswaran et al., 2009, Freguia et al., 2010, Parameswaran et al., 2011, Parameswaran et al., 2012). However, the addition of chemical inhibitors undermines the practical application of these studies. The low recovery of energy and low electric current in these studies imply that there is still room for improvement. Hence, the syntrophic interactions among ARB and non-ARB in an inhibitor-free condition should be more closely examined for a better treatment of fermentable substrates.

1.3.2 Intracellular lipophilic inclusions generation in anode biofilm

The application of lipid-accumulating organisms in MECs has been mostly focused on photosynthetic electrochemical reactors in which the photosynthetic microorganisms (i.e., cyanobacteria and microalgae) synthesize triacylglycerols (TAGs) or triglyceride (TG) as storage products or source of energy. Some of these studies rely on the cell lysis of algae and use algae as substrates for anode-respiration, while others applied these photosynthetic microorganisms as a metabolic entity in an integrated photo-electrochemical bioreactor; the latter case includes recovery of electrons from

oxidation of intracellular carbon storage during dark phases from cyanobacterial species, anode respiration of photosynthetic hydrogen gas, and coupled photosynthesis and heterotrophic anode-respiration (Mu et al., 2006, Rosenbaum et al., 2010).

In addition to TAGs, polyhydroxyalkanoates (PHAs) are another kind of common intracellular inclusion that can be generated inside bacterial cells (Stahl, 2010). PHAs usually accumulate as discrete granules that can, in certain instances, account for as much as 90% of cell dry weight (López-Cortés et al., 2008). Some bacteria naturally accumulate PHAs under normal conditions while many others synthesize PHAs only under environmental stress, such as nitrogen or phosphate limiting conditions and alternating feast and famine condition (Bengtsson et al., 2008). Polyhydroxybutyrate (PHB) is a kind of PHAs with 3-hydroxybutyrate as the monomer, and it is the mostly studied PHA so far. Although PHB accumulation is commonly observed in sequencing batch reactors (SBR) and biological phosphorus removal processes (Mino et al., 1998), anode biofilms acclimated from activated sludge are rarely shown to accumulate PHB or PHAs. Until today, only one study has reported that an anode biofilm synthesized lipids as storage compounds (Freguia et al., 2007). The authors found lipophilic inclusions in anode biofilm when glucose was intermittently supplied to the anode biofilm in an electron balance study. The turnover of the lipids was shown to be fast during a "feast and famine" cycle on the anode.

Microbial fuel cells (MFCs) are usually being portrayed as power sources; however, minimal levels of substrate have to be always available for a normal metabolic function of the ARB and a stable power output. In reality, discontinuous

feeding condition would be common if MFCs are to be used as portable power sources. Since lipid-accumulating microorganisms are more resistant to the feast and famine cycle, the collaboration between lipid-accumulating bacteria and ARB holds potential for a self-sustainable MFC in which intracellular storage becomes the energy source for anode respiration in the absence of external substrate. The new syntrophy between lipid-accumulating bacteria and ARB would allow MFCs to be used as a normal battery with a continuous power output even when substrate is fed intermittently. To engineer MFCs for portable energy sources, the potential for establishing a syntrophy between lipid-accumulating bacteria and ARB should be explored.

1.3.3 Dissolved methane oxidation in microbial electrochemical cells

Methane gas is a well-known greenhouse gas with strong infrared absorption, and its global warming potential is 25 times higher than that of carbon dioxide (EPA, 2010). Methane is emitted into the atmosphere from both natural and anthropogenic sources. Although the details of the source of methane from geological emissions is not clear, most of the other significant sources (red boxes in Figure 1-3) are considered to be strongly related to the decomposition of organic matter through methanogenesis.

The microbial production of methane is a net result of two counteracting processes. One is methanogenesis and the other is methanotrophy during which methane is oxidized by microorganisms. Methanogenesis is carried out by a special group of archaea named methanogens, and it has been engineered for biogas production in wastewater treatment facilities all over the world. As regards methanotrophy, two kinds of methanotrophs have been discovered so far. The first is

the aerobic methanotrophs, which inhabit in soils and other environmental niches where oxygen is available (equation 1-1). Their ability to aerobically oxidize methane has been extensively studied (Mancinelli, 1995).

$$CH_4\ (g) + 2O_2 \rightarrow CO_2\ (g) + 2H_2O \qquad (1\text{-}1)$$

Although many details of the aerobic oxidation of methane are known, the second kind of methanotrophy, anaerobic methanotrophy is not well understood (Knittel and Boetius, 2009a). The oxygen-independent methanotrophy, commonly known as anaerobic oxidation of methane (AOM), has been observed in a number of anoxic environments, such as marine sediments, methane seeps, vents, and peatlands (Alperin, 1985, Boetius, 2000, Smemo, 2007, Beal, 2009).

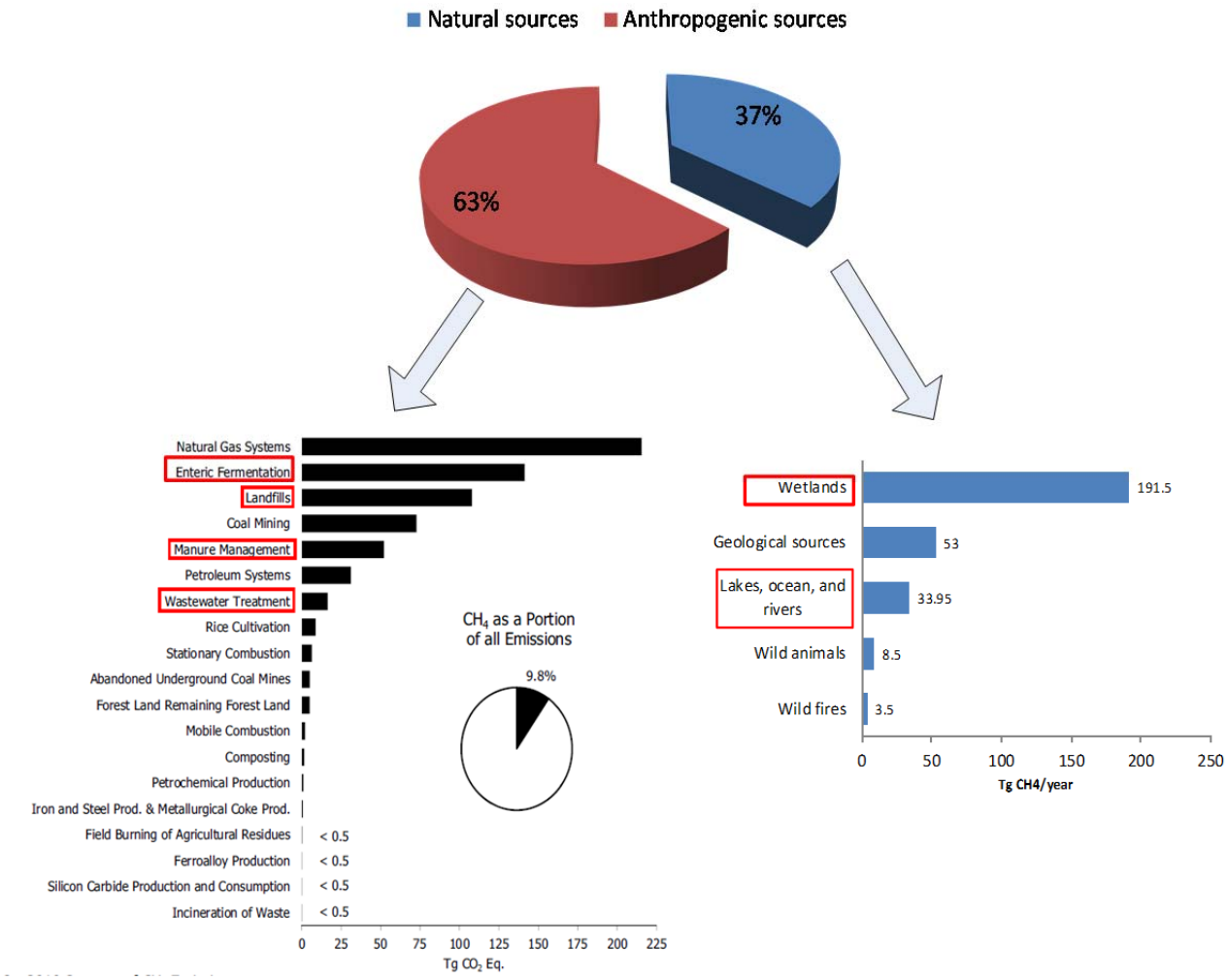

Figure 1–3. The methane gas emitted into the atmosphere as reported by US EPA (EPA, 2010, US-EPA, 2012). The numbers illustrate the relative importance of each source in total methane emission; note that the bar chart on the left-hand side shows methane emission from USA in 2010 and the chart on the right-hand side shows estimated global methane emission.

Numerous studies have reported AOM in natural habitats with sulfate, iron, manganese, nitrite, and nitrate as terminal electron acceptors (Grossman et al., 2002, Nauhaus et al., 2002, Orphan et al., 2002, Knittel, 2009, Ettwig et al., 2010, Thauer, 2011, Shi et al., 2013), but published results in engineered systems that incorporate the concept of AOM are rare, mainly due to the complexity of the microbial consortia undertaking AOM and their slow growth rate. The limited knowledge on the

metabolism of AOM-microorganisms is a main hindrance to the engineering of the AOM concept. Until now there are no publications and reports on AOM coupled to EET (extracellular electron transfer) in MECs, but exploration of AOM in MECs has significant implications. First, syntrophic interactions between AOM-microorganisms and ARB allow better understanding of AOM in syntrophy with metal-oxide reducers in natural environment, usually subsurface environment: since it is difficult to quantify AOM in natural environment, studies on AOM in MECs can improve the understanding of how significant the contribution of AOM coupled metal-oxides reduction to global methane sink could be. Second, syntrophic interactions between AOM and ARB enable the sensing of methanogenesis reactions that occur in anaerobic nature because electric current generation in MECs from AOM can be an indicator of methanogenesis. Besides, the application of AOM-MEC for sensing dissolved methane could be significant in locations where human access is seriously limited, such as permafrost zones. Hence, a proof of concept study of AOM in MECs will not only contribute to the understanding of AOM microorganisms that use solids as the terminal electron sink, but also lay the foundations for one possible engineering application in monitoring methanogenesis (possibly methane emissions) in both natural and engineered systems (Walter Anthony et al., 2012).

1.4 Objectives

This study examined the syntrophic relationships on anode electrode surfaces in microbial electrochemical cells. The specific objectives were to

- cultivate an anode microbial consortium that degrades volatile fatty acids in the presence of methanogens
- demonstrate that a lipid-accumulating anodic microbial community allows an microbial fuel cell to work as a potential self-sustainable power source

- Show anaerobic oxidation of methane can be achieved on an anode of a microbial electrochemical cell

1.5 Structure of the thesis

This thesis is comprised of six chapters, references, and appendices. Chapter one introduces the problems under investigation, identifies the research needs, and defines the objectives of the current research. Chapter two includes the literature review on syntrophic relationships in microbial electrochemical cells and anaerobic oxidation of methane. Chapters three, four, and five are organized in manuscript format with a distinct syntrophic relationship in each chapter. Chapter six concludes the whole study and offers the recommendations for future research.

Chapter 2 Literature review

2.1 Syntrophy in anode biofilm of microbial electrochemical cells

In both natural and engineered systems, various groups of microorganisms often have to work together to propel some reactions to their thermodynamically unfavourable directions; this kind of cooperation is called syntrophy or syntrophic interactions. One good example in engineered systems is the syntrophic interaction between fermenters and methanogens in anaerobic digesters. An anode biofilm is usually comprised of numerous kinds of microorganisms, not only the anode-respiring bacteria (ARB) but also fermenters, methanogens, and others, collectively called non-ARB. The role of ARB is obvious; however, the functions of non-ARB can be complex. It is likely that syntrophic interactions would be important for MECs treating complex organics (e.g., during anaerobic wastewater treatment) because ARB are not good at utilizing complex organics. Unlike ARB, fermenters hydrolyze and break down complex organic compounds into simple and small molecules, such as acids and alcohols, efficiently, and hence fermenters are indispensable for anode respiration in MECs treating waste and wastewater. Fermentation generally accumulates simple acids and solvents at neutral pH (Patakova et al., 2011), along with hydrogen gas, implying that hydrogen gas consumption is significant for building the syntrophy between fermenters and ARB since ARB cannot efficiently consume hydrogen gas as electron donors. Depending on the objectives of MECs, syntrophic interactions can be more diverse. This section reviews the syntrophic interactions in anode biofilm of MECs, including syntrophy for cellulose utilization in MECs, syntrophy under chemolithotrophic conditions in MECs, syntrophy for ethanol utilization in MECs,

and uncertain syntrophy for the utilization of glucose and/or glucose fermentation products in MECs.

2.1.1 Syntrophy during cellulose utilization in microbial electrochemical cells

Rismani *et al* (2007) conducted a study using cellulose as a substrate and rumen microorganisms as an inoculum for power production in an MFC. The analysis of the 16s rRNA genes of the anode biofilm showed that most of the species on anode electrodes were from the phyla *Firmicutes* and *Deferribacteres*. Although they proposed a collaboration of hydrolytic and respiratory microorganisms during the utilization of cellulose for current production, detailed studies are unavailable. In a research study on the degradation of cellulose by a defined binary culture (Ren et al., 2007), *Clostridium cellulolyticum*, which is capable of hydrolyzing cellulose and fermenting glucose, supplied fermentation products, such as acetate and hydrogen gas, to *Geobacter sulfurreducens* for anode respiration. Neither of the two strains alone can respire on the anode surface with cellulose as a substrate, and thus, this study demonstrates that hydrolytic microorganisms are necessary for breaking down the big molecules before the energy in cellulose is available to ARB. In a more complex situation where methanogens are present, the syntrophic interaction between fermentative bacteria and methanogens could be dominant in MECs, compared to the syntrophic interaction between fermenters and ARB (Gregoire and Becker, 2012).

2.1.2 Syntrophy under chemolithotrophic conditions in microbial electrochemical cells

Some research demonstrated that enriched photosynthetic microorganisms can form a close relationship with anode-respiring microorganisms so that a benthic MFC can be

self-powered without any organic substrate. He *et al* (2009) found that, when a benthic MFC is exposed to alternate light and dark conditions for months, the microorganisms developed a clear organic synthesis and consumption cycle in the light and dark phase, respectively. In another similar study, *Cyanobacteria* and *Betaproteobacteria* were shown to dominate in the anode biofilm of a photosynthetic MFC with maximum power density of 9 mW/m^2, where the only carbon source is bicarbonate (Nishio et al., 2010); in comparison, MFCs fed with organics commonly show a power density of approximately 100-5000 mW/m^2 (Logan and Rabaey, 2012). Nevertheless, more recently, some green algae and *cyanobacteria* strains were shown to independently respire on the anode in photosynthetic MFCs (McCormick et al., 2011). One cyanobacterium, *Synechocystis* strain PCC 6803, was shown to even have conductive pili, which are proposed to be involved in anode respiration (Gorby et al., 2006). Therefore, the newly proposed syntrophy between photosynthetic microorganisms and heterotrophic ARB should be carefully scrutinized.

2.1.3 Syntrophy during ethanol utilization in microbial electrochemical cells

As for ethanol utilization in an MEC, early studies showed that ARB cannot effectively utilize ethanol until it is fermented to acetate and hydrogen gas (Kim et al., 2007, Richter et al., 2007). Thus, fermentative bacteria are crucial for supplying preferred substrates to ARB when ethanol is the sole substrate. In addition to fermentative bacteria, hydrogen gas scavengers, such as methanogens and homoacetogens, are also shown to be necessary during the anode respiration of ethanol. For example, Parameswaran *et al* (2009) reported that anode respiration increases with methanogenesis, thereby supporting the fact that hydrogen gas

consumption relieves the thermodynamic constraint for ethanol fermentation ($CH_3CH_2OH + H_2O \rightarrow 2H_2 + CH_3COO^- + H^+$, $\Delta G^{o\prime}$=9.7 kJ/mol ethanol). Unlike methanogens, the role of homoacetogens has been documented to be significant under low hydraulic retention time (e.g., 1 hour) or in the presence of bromoethanesulfonate (BES), which inhibits the activity of methanogens (Parameswaran et al., 2010, Parameswaran et al., 2011). In this syntrophy involving homoacetogens, the hydrogen gas and carbon dioxide are synthesized to acetate, which then enters anode respiration. The above syntrophy among ARB, fermentative bacteria, and homoacetogens demonstrates that microorganisms have the ability to switch their partners for a complete anode respiration. Unless hydrogenotrophic methanogens are inhibited, the methanogens usually out-compete homoacetogens for the hydrogen gas generated from fermentation in a naturally acclimated anode biofilm system (Chae et al., 2010).

2.1.4 Syntrophy during glucose and/or glucose fermentation products utilization in microbial electrochemical cells

During the utilization of glucose and the fermentation products derived from glucose (e.g., common VFAs and solvents), fermentative bacteria and hydrogenotrophic methanogens are revealed to be syntrophic partners of ARB as a H_2-scavenger. Methanogenesis by hydrogenotrophic methanogens drives glucose fermentation to acetate, which is then consumed by ARB during anode respiration. Studies on the utilization of glucose in an MEC demonstrated that hydrogenotrophic methanogens are crucial for anode respiration as they scavenge hydrogen gas accumulated in fermentation (Min and Logan, 2004, Freguia et al., 2008, Lee et al., 2008b). In a study using a dual-chamber MEC with waste activated sludge as the feed, taxonomic

classification of pyrosequencing data showed that fermentative acidogenic bacteria, such as *Paludibacter*, *Petrimonas*, *Oscillibacter*, etc., accounted for over 10% of the total reads and ARB accounted for over 13% of the total reads, whereas in the domain of archaea, hydrogenotrophic methanogens were enriched for one order of magnitude compared with that in the inoculum (Lu et al., 2012). In contrast, acetoclastic methanogens, although they consume acetate during methanogenesis, are rarely observed to be dominant in anode biofilm since they are kinetically inferior to ARB in acetate consumption (Lee et al., 2009c). Examination from the kinetic perspectives of acetate consumption by ARB and acetoclastic methanogens shows that ARB usually demonstrate an acetate half saturation constant (Ks) around 119-176 mg COD/l (Torres et al., 2007, Lee et al., 2009c), which are lower than these reported for acetoclastic methanogens, 180-430 mg COD/l (Lee et al., 2010). A lower Ks together with a higher maximum specific growth rate of ARB, compared to acetoclastic methanogens, determine that ARB can outcompete methanogens for acetate (Lee et al., 2009c).

Although methanogenesis is instrumental in scavenging the hydrogen gas for a healthy fermentation process, it inevitably diverts some electrons from electricity production to methane production; more methane production means less energy recovery by MECs. In order to maximize the energy recovery, various measures were examined to suppress methanogenesis. Reducing the external resistance of an MFC (Chae et al., 2010, Jung and Regan, 2011), aeration during operation (Call and Logan, 2008, Freguia et al., 2008, Lee et al., 2009b, Chae et al., 2010), and manipulation of pH and temperature (Hu et al., 2008, Chae et al., 2010) were all tested but none of them can be applied as a general method in controlling methanogenesis. The limitation of these approaches is that the inhibition of hydrogenotrophic methanogens can adversely affect the metabolism of ARB, due to hydrogen gas accumulation and

repression of glucose fermentation. Ideally, the consumption of hydrogen gas should not be greatly compromised when methanogens are inhibited; however, it is difficult to simultaneously achieve these two conflicting goals.

Alternatively, homoacetogens, which synthesize acetate by oxidizing hydrogen gas as an electron donor, are ideal H_2-consumers for ARB because acetate production also stimulates the growth of ARB and current generation in MECs. Some studies (Parameswaran et al., 2009, Parameswaran et al., 2012) reported the syntrophy between homoacetogens and ARB, but only under the circumstances in which methanogens are inhibited. Homoacetogens generally are found to be inferior to methanogens for hydrogen gas consumption, but there are environmental niches where high local hydrogen concentration or temperature below 20 ^{o}C allow homoacetogens to co-exist or to compete for hydrogen gas with methanogens (Conrad et al., 1989, Schmitt-Wagner and Brune, 1999). Thus, manipulation of operating conditions or reactor configurations for preferential growth of homoacetogens over methanogens may help establish syntrophic interactions between homoacetogens and ARB despite the presence of hydrogenotrophic methanogens. Once such syntrophic interactions are established, MECs can recover more energy when fed with fermentable substrates, such as glucose, while the whole biodegradation process is also free of the thermodynamic constraint, i.e. no accumulation of hydrogen gas from fermentation.

In summary, the syntrophy observed in cellulose degradation and under chemolithotrophic conditions indicate that new syntrophy can be established when special functional microorganisms are introduced to degrade their favorite substrates together with ARB during anode respiration. Meanwhile, the syntrophy from ethanol-MECs and glucose-utilizing MECs imply that homoacetogens would be a strong syntrophic partner of ARB if operational conditions favor homoacetogens over

methanogens.

2.2 Syntrophy in anaerobic oxidation of methane

This section covers the research progress in sulfate, nitrate/nitrite, and ferric/manganese oxide-driven anaerobic oxidation of methane (AOM). Due to the intrinsic slow reaction rates and the complexity of the metabolic pathways, some reactions mentioned in this section are still under investigation.

AOM has been extensively studied in the past decades since the discovery of simultaneous consumption of sulfate and methane in marine sediment (Martens and Berner, 1974). The general trajectory of AOM research has been reviewed elsewhere (Knittel and Boetius, 2009a, Thauer, 2011). Anaerobic methanotrophs (ANME) or anaerobic methanotrophic archaea (Figure 2-1) were demonstrated to be responsible for initiating the oxidation of the dissolved methane in various environmental niches (Hinrichs et al., 1999, Knittel et al., 2005, Beal, 2009). Because the isolation of ANME is technically difficult, researchers temporarily grouped ANME into three lineages, i.e. ANME-1, ANME-2, and ANME-3, according to the phylogenetic analysis of their 16S rRNA genes. The analysis shows that ANME-2 and ANME-3 are close to *Methanosarcinales*, whereas ANME-1 forms a distinct group. Historically, detection of ANME-1 and ANME-2 has been more frequently reported since they are involved in the most common AOM in marine sediment systems where sulfate serves as the electron acceptor; this AOM might be the most important methane sink at the sea water-sediment interface (Knittel and Boetius, 2009b, Milucka et al., 2012). A recent model to elucidate sulfate-reduction-coupled AOM, though not fully understood,

proposes that ANME conducts both methane oxidation and the reduction of sulfate with their bacterial partner (*Desulfosarcina*/*Desulfococcus* cluster) recycling disulfide to sulfate (equations 2-1a, 2-1b and 2-1c) (Milucka et al., 2012). The two species thus formed a syntrophic relationship for a complete re-cycling of sulfate.

Step 1: $7CH_4\ (aq) + 8SO_4^{2-} + 5H^+ \rightarrow 7HCO_3^-(g) + 11H_2O + 4HS_2^-$ (2-1a)

Step 2: $4HS_2^- + 4H_2O \rightarrow 7HS^- + 5H^+ + SO_4^{2-}$ (2-1b)

Overall reaction: $CH_4\ (aq) + SO_4^{2-} \rightarrow HCO_3^- + HS^- + H_2O$ (2-1c)

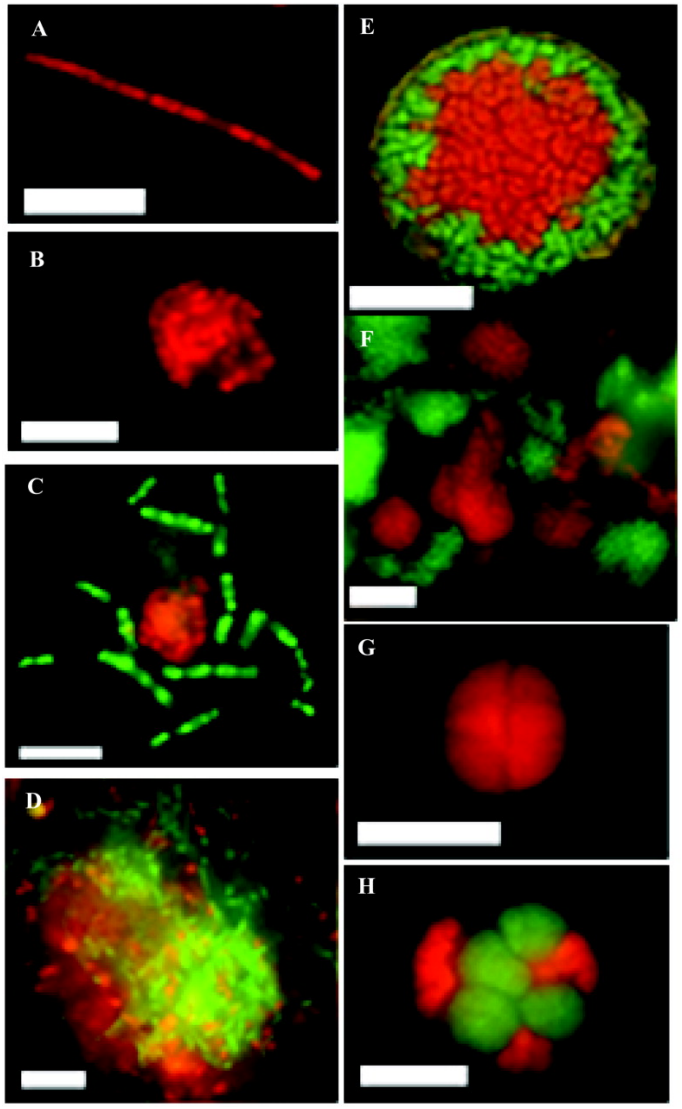

Figure 2–1. Individual cells and cell aggregates of ANME-1 and ANME-2 archaea, visualized with fluorescent-labeled oligonucleotide probes. Unless otherwise indicated, scale bar represents 5 μm. (A) An ANME-1 archaeal filament (B) Tightly associated cluster of ANME-1 rods (C) archaeal ANME-1 rods (green), and *Desulfosarcina* species (red). (D) Large archaeal ANME-1/sulfate-reducing *Desulfosarcina* aggregate. Scale bar = 10 μm. (E) An aggregate showing a core of ANME-2 Archaea surrounded by sulfate-reducing *Desulfosarcina*. (F) Large aggregation of loosely associated, individual micro-colonies of ANME-2, and *Desulfosarcina*. (G) Monospecies aggregate of archaeal ANME-2 not affiliated with a bacterial partner. (H) An association of the ANME-2 archaea (green) with a bacterial partner (red) not affiliated with the sulfate-reducing *Desulfosarcina*. Extracted from a reference (Orphan et al., 2002).

Unlike the sulfate-driven AOM, the nitrite-driven AOM (Ettwig et al., 2008, Ettwig et al., 2010) were shown to be conducted by intracellular oxygenic oxidation of methane or reverse methanogenesis pathway. Oxygenic AOM is unique in that oxygen molecules are generated from reduction of nitrite to N_2 ($2NO_2^- \rightarrow 2NO \rightarrow N_2 + O_2$), and the oxygen is used for oxidizing methane to carbon dioxide, similar to typical aerobic methane oxidation pathway (Ettwig et al., 2010). A bacterium, *Candidatus Methylomirabilis oxyfera*, is known to employ this oxygenic AOM pathway. Interestingly, when ammonium or nitrate is abundant, ANME-2-like archaea can establish a syntrophic relationship with anammox bacteria or *Candidatus Methylomirabilis oxyfera* in AOM (Haroon et al., 2013, Shi et al., 2013). Reverse methanogenesis-dependent AOM coupled to reduction of nitrite or nitrate is not fully understood, but metagenomic analysis has commonly shown all genes essential for reverse methanogenesis; ANME-2 groups are usually found in this AOM coupled to denitrification (Haroon et al., 2013). In contrast to these studies on sulfate and nitrate/nitrite driven AOM, ferric oxide (equation 2-2) and manganese oxide reduction coupled AOM are rarely reported (Beal, 2009), though the potential energy gain from iron or manganese respiration could be larger. For instance, the Gibbs free energy gain (pH=7) of ferric oxide-driven AOM is -270.4 kJ/mol CH_4, whereas sulfate-driven AOM only provides -28.8 kJ/mol CH_4 (Appendix Table A5). The solidity nature of these metal oxides, which causes the much slower AOM rate, compared with the rate of sulfate-driven AOM, could be one of the reasons why such kind of studies is sparse and the role of iron in AOM is still ambiguous (Schubert et al., 2011). Additionally, the inherent difficulty in analyzing the reduced form of either iron or manganese could be another reason for "low AOM rate". Noticeably, lack of long term observation or enrichment could be another important reason why the reported AOM rate is low

(Nauhaus et al., 2005). In spite of all these reports, a more recent study on the AOM activity in sediment from the Middle Valley hydrothermal vent shows that ferric iron dependent AOM might be dominant in high temperature environment where sulfate reduction ceases (Wankel et al., 2012). According to this study, ferric iron dependent AOM is much more active at 90 ^{o}C and ANME-1a archaea and *Verrucomicrobia*, putative iron reducers involved in the AOM process. Like sulfate-driven AOM, a syntrophy may exist between the ANME-1a archaea and bacteria from the phylum *Verrucomicrobia*, although some bacteria from *Verrucomicrobia* are methanotrophs (Jensen et al., 2008). In another study where manganese oxide was provided as an electron acceptor, a group of potential metal reducing proteobacteria were enriched together with ANME-3 although the analysis of the 16S rRNA genes showed that ANME-1 and ANME-3 accounted for around 5% of the total in the incubation (Beal, 2009). This evidence, together with the aforementioned, indicate that AOM in metal reducing environment might also involve a syntrophy between archaeal and bacterial species and the reduction of metals during AOM might be underestimated and requires more in-depth study.

$$CH_4 + 8Fe(OH)_3 + 15H^+ \rightarrow HCO_3^- + 8\,Fe^{2+} + 21H_2O \qquad (2\text{-}2)$$

In summary, the previous notion of AOM has been substantially changed through all these milestone studies. The ability of activating and oxidizing methane anaerobically might be owned by a more diverse group of microorganisms, not only ANME. Moreover, when different electron acceptors are available, various syntrophic interactions could be induced for a complete AOM. Therefore, the study of AOM in an MEC is a valuable exploration of potential new syntrophic relationships.

Chapter 3 Syntrophy between anode-respiring bacteria and H_2-consuming bacteria in microbial electrochemical cells

3.1 Introduction

Microbial electrochemical cells (MECs) including microbial fuel cells, microbial electrolysis cells, and microbial desalination cells are able to capture substrate electrons and to produce value-added products from organic wastes and wastewaters (e.g., H_2O_2, acetate, ethanol, etc.) (Logan and Rabaey, 2012). A key feature of MECs is their ability to use bacteria, i.e. anode-respiring bacteria (ARB), as anode catalysts for oxidizing reduced forms of compounds and transferring donor electrons to an anode. The electrons then move to a cathode at which they react with oxidants. MECs can achieve high substrate conversion rates (i.e., high current or current density), but only using simple acids (e.g., acetate) as substrate (Pant et al., 2010). ARB have shown low coulombic efficiency (CE) and substrate degradation rates when particulates and complex substrates are used as feed (Oh and Logan, 2005, Ren et al., 2007, Pant et al., 2010, Ge et al., 2013). In contrast, anaerobic digestion is very efficient for stabilizing complex organic waste (Lettinga, 1995). For instance, COD removal rates typically range from 16 to 26 kg COD/m^3-d in anaerobic digestion, corresponding to 2,233-3,629 A/m^3. In comparison, the volumetric current density is around 6 A/m^3 for MECs using complex organics as feed, although the volumetric current density can be as high as 5050 A/m^3 in MECs using acetate (Qian and Morse, 2011). To improve current density of MECs for treating complex substrate, syntrophic interactions among hydrolytic bacteria, fermenters, and ARB seem essential since hydrolysing and fermentative

bacteria can more efficiently break down complex organics to simple forms (Lee and Rittmann, 2010, Pant et al., 2010). Hydrogen gas accumulation is unavoidable in fermentation, and hence hydrogen gas consumption reactions (e.g., methanogenesis) are necessary for maintaining the progress of fermentation reactions. Some ARB utilize hydrogen gas as an electron donor (Bond and Lovley, 2003), meaning that ARB are potentially H_2-scavengers. CE and current density can increase simultaneously if ARB efficiently consume the hydrogen gas generated from fermentation. Several studies, however, reported low CE, 15–39%, and methane accumulation in MECs fed with fermentable substrate (Teng et al., 2010, Catal et al., 2011), whereas CE values are normally 65–98% from MECs fed with acetate (Logan and Rabaey, 2012). Some studies (Lee et al., 2009b, Lee and Rittmann, 2010) demonstrated that hydrogenotrophic methanogens proliferated in MECs, suggesting these methanogens could kinetically outcompete ARB for hydrogen gas. Consequently, methane accumulation seems inevitable in MECs employing fermentable or complex organics as feed (Freguia et al., 2007, Pant et al., 2010).

Despite their negative effect on CE, H_2-utilizing methanogens are an efficient H_2-scavenger in MECs. For instance, current generation was depressed in ethanol-fed MECs when hydrogenotrophic methanogens were selectively inhibited by 2-bromoethanesulphonate (Parameswaran et al., 2010). Methanogenesis by hydrogenotrophic methanogens makes acetogenesis reactions thermodynamically favourable ($1/2CH_3CH_2CH_2COO^- + H_2O \rightarrow CH_3COO^- + H_2(g) + 1/2H^+$, $\Delta G^{0\prime}$=28.4 kJ/mol H_2; $H_2(g) + 1/4HCO_3^- + 1/4H^+ \rightarrow 1/4CH_4(g) + 3/4H_2O$, $\Delta G^{0\prime}$=-33.9 kJ/mol H_2), providing acetate for ARB to generate current density (Parameswaran et al., 2010). Hence, hydrogenotrophic methanogens, fermenters, and ARB build syntrophic interactions in order to utilize complex organics in these MECs. Interestingly, Parameswaran *et al*. (2011) demonstrated that homoacetogens in syntrophy with fermenters and ARB

simultaneously improved CE (84%) and current density (10 A/m^2) in MECs in which methanogens were inhibited by BES (50 mmol/L). It seems challenging to build a syntrophy among fermenters, homoacetogens, and ARB in the presence of hydrogenotrophic methanogens because these methanogens gain more benefits over homoacetogens from both thermodynamic and kinetic perspectives (Stams et al., 2003). Specifically, the standard Gibbs free energy gain at pH 7 ($\Delta G^{0\prime}$) for hydrogenotrophic methanogens is -32.68 kJ/mol H_2, whereas $\Delta G^{0\prime}$ for homoacetogens is relatively small, -23.73 kJ/mol H_2 (Peters et al., 1998). In addition, the Michaelis–Menten constant (K_m) for hydrogenotrophic methanogens ranges from 50 to 190 Pa H_2 (390–1,482 nmol H_2/L at 25°C), whereas the K_m for homoacetogens is relatively high at 190–520 Pa H_2 (1,482–4,056 nmol H_2/L at 25°C) (Kotsyurbenko et al., 2001, Stams et al., 2003). As a result of these advantages of hydrogenotrophic methanogens, the hydrogen gas threshold pressure for hydrogenotrophic methanogens is several orders of magnitude lower than that for homoacetogens (Kotsyurbenko et al., 2001), and this ability to utilize low levels of hydrogen gas dictates the predominance of hydrogenotrophic methanogens in an anaerobic digester where hydrogen gas partial pressure can be as low as 1.33–1,330 Pa (10–10^4 nmol H_2 /l at 35°C) (McCarty and Smith, 1986).

Nevertheless, several studies suggest that homoacetogens are able to compete with hydrogenotrophic methanogens under unique conditions (e.g., psychrophilic and/or mixotrophic conditions) (Peters et al., 1998, Kotsyurbenko et al., 2001). Under mixotrophic conditions, homoacetogens can have energy benefits for cell synthesis (Peters et al., 1998), allowing them to compete with hydrogenotrophic methanogens. Based on a thermodynamic model developed by Rittmann and McCarty (2001), the energy required for synthesizing new cells under heterotrophic conditions is significantly less, compared to that in autotrophic conditions. For example, the energy

required for converting lactate to acetyl-CoA is (30.9) -(32.29) = -1.39 kJ/e equivalent (no energy required), whereas the energy requirement under autotrophic growth is (30.9)-(-78.72) = 109.62 kJ/e equivalent (Stahl, 2010). Peters *et al* (1998) reported that the maximum specific growth rate (μ_{max}) for *Acetobacterium woodii* can be increased from 0.576/d under autotrophic conditions (i.e., H_2 + CO_2) to 1.03/d under mixotrophic conditions (i.e., H_2 + lactate), which is close to μ_{max} values of 0.77–1.3/d for *Methanobacterium bryantii* M.o.H. and *Methanospirillum hungatei* JF-1 (Kristjansson et al., 1982, Karadagli and Rittmann, 2005).

Theoretically, the Gibbs' free energy at pH 7 and 25°C ($\Delta G^{0\prime}$) for homoacetogenesis can be enhanced from -7.78 kJ/mol H_2 to -12.1 kJ/mol H_2 when acetate concentration is decreased from 10 mmol/L to 0.01 mmol/l at P_{H2} = 0.000987 atm (100 Pa), P_{CO2} =0.5 atm and HCO_3^-=20 mmol/l. This $\Delta G^{0\prime}$ is close to -15.5 kJ/mol H_2 for hydrogenotrophic methanogenesis under the condition of P_{H2}=0.000987 atm (100 Pa), P_{CO2} =0.5 atm, and P_{CH4}=0.5 atm. The energetically favorable mixotrophic condition for homoacetogens opens the possibility that ARB may degrade fermentable substrates in the presence of hydrogenotrophic methanogens, which exist in many types of organic waste and wastewater (Garcia et al., 2000).

The objectives of this chapter were to prove the hypothesis that considerable acetate oxidation by ARB or ARB favor acetate could facilitate the growth of homoacetogens and could result in the establishment of a syntrophic interaction between homoacetogens and ARB in the presence of hydrogenotrophic methanogens; the second objective was to assess whether this syntrophy could allow MECs to successfully treat complex forms of organic wastewater, along with high CE and current density.

3.2 Methods and materials

3.2.1 Operating conditions of the anaerobic digester

A 20 l PVC anaerobic digester (AD) (Ø 25.8 cm and height 38.1 cm) was operated in this study. The digester was run in batch mode, and the sludge inside of the reactor was mechanically mixed by an agitator (290 ± 20 rpm). Glucose medium (5 g glucose/l) (Wiegant and Lettinga, 1985) was used as feed. The AD was inoculated with anaerobic digester sludge (5 l) from the Waterloo Wastewater Treatment Plant. Hydraulic retention time (HRT) and solid retention time (SRT) were fixed at 20 day by regularly withdrawing sludge from the AD. The pH of the glucose medium was maintained at 7.3 ± 0.2 using bicarbonate buffer (2.94 g/l of $NaHCO_3$). The temperature of the AD was controlled at 37 ± 1 ^oC with a compact industrial RTD probe (Oakton Instruments, USA) and a heater. At steady state of the AD (total suspended solids (TSS), 1170 ± 181 mg/L, volatile suspended solids (VSS), 760 ± 287 mg/L, and methane production rate 0.065 ± 0.005 CH_4 L/g COD-d), AD effluent (hereafter referred to as the digestate) was fed to an MEC at two different HRTs, 4 and 8 days.

3.2.2 Configuration and initiation of the microbial electrochemical cell

One sandwich-type MEC was used in this study (Figure 3-1). The reactor was made of Plexiglas® and was manufactured by the Engineering Machine Shop at the University of Waterloo. Working volumes of the anode and the cathode chambers were 300 ml and 122 ml, respectively. Carbon fiber (24 K carbon tow, Fiber Glast, USA) was used as the anode. In this study, carbon fiber was chosen to be the anode material for (1) its high specific surface area for biofilm attachment and (2) easiness during biofilm

recovery. The carbon fiber was sequentially cleaned in 1 mol/l of nitric acid, acetone, and ethanol, a day in each solution. A bundle of carbon fiber was held by stainless steel frame, which had a row of totally nine holes (diameter 6 mm) on both the top and the bottom. Stainless steel mesh (Type 304, McMaster Carr, USA) was used as the cathode, and the two chambers were separated by an anion exchange membrane (AEM, AMI-7001S, Membranes International, USA). The geometric area of the membrane is 28.3 cm^2; the current density was computed based on this area.

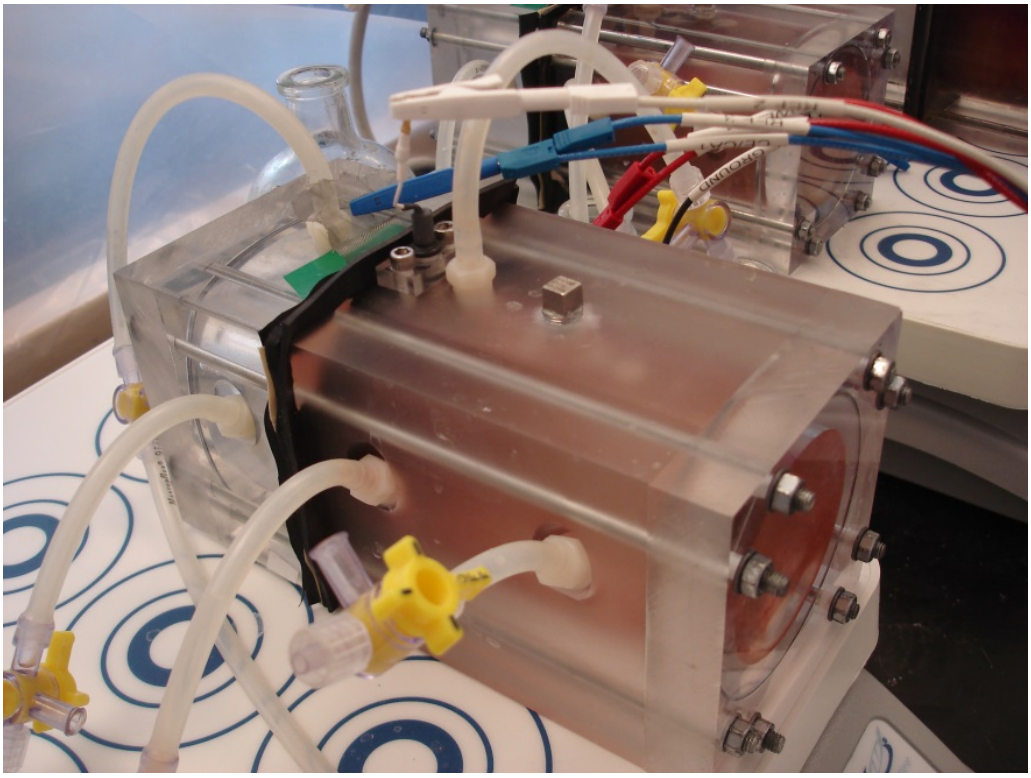

Figure 3–1. Two microbial electrochemical cells used in this study. The compartment on the right hand side is the anode chamber, and the one on the left hand side is the cathode chamber. The cell is located on top of a magnetic stirrer for a continuous mixing of the electrolytes. Three alligator leads, red, white, and blue color lines, from a potentiostat are connected with the anode, reference electrode, and cathode, respectively.

The MEC was inoculated with 10 ml of the anolyte from another MEC reactor, which was operated with methane and minimal level of acetate for around half a year.

Preliminary tests were conducted on the mother MEC, and the results (Figure A1) show that the ARB prefer acetate to other fermentable substrates. After inoculation, anolyte containing 25 mmol/l of acetate (Torres et al., 2008b) was purged with N_2/CO_2 (80:20 %, v/v) for 30 minutes. The phosphate buffer was set to 50 mmol/l in this study. The MEC was connected with a potentiostat (VSP, BioLogic, Canada) and operated in fed-batch mode. The anode potential was fixed at -0.4 V vs. Ag/AgCl reference electrode (RE-5B, BASi, USA). The same medium except for organic substrate was used as catholyte in this study. The catholyte was maintained in anaerobic condition by regularly purging with nitrogen or helium gas (99.999%, Praxair Canada). The catholyte was refreshed when the pH exceeded 10.

The MEC had been run for over one month in fed-batch mode with acetate until the current density reached a steady state value (Figure 3-2A). During the fed-batch operation, spent anolyte was exchanged by fresh acetate medium when the current was lower than 0.5 mA (~0.16 A/m^2). To avoid oxygen contamination during medium exchange, the anolyte was expelled from the anode chamber through the inlet (side opening in Figure 3-1) while nitrogen gas or helium (99.999%, Praxair Canada) was purged in from the top. When the anode chamber was empty, new medium was anaerobically fed from the side inlet. It is worth pointing out that, unlike conventional fuel cells, an MEC always demonstrates a certain degree of fluctuation with regard to the peak current density. Generally accepted standard for a steady state is that the peak current density should be within ±10% of difference in three consecutive runs.

CE was calculated using Equation (3-1) (Lee et al., 2009b):

$$Coulombic\ efficiency = \frac{e^-_{transferred}}{e^-_{donor}} \qquad (3\text{-}1)$$

where $e^-_{transferred}$ is the accumulated electron obtained from the record of electric current, and e^-_{donor} is the electron equivalents of the consumed organic electron-donor.

Current density (A/m^2) was calculated using Equation (3-2):

$$Current\ density = I/Area \quad (3\text{-}2)$$

where I is electric current (A), and $Area$ is the geometric surface area of the ion-exchange membrane (m^2).

3.2.3 Feed of digestate into the microbial electrochemical cell

Upon the steady condition with acetate medium, the digestate was fed into the MEC. After collecting the digestate with a graduated cylinder (2 l), the digestate was immediately fed into the MEC using a syringe (30 ml, BD Luer-Lok™ tip, USA) equipped with a 3-way valve and a short tube, while the headspace in the cylinder was gently purged with nitrogen gas (99.999%, Praxair, Canada) to avoid oxygen intrusion to the digestate. The MEC was operated with the digestate in fed-batch mode at two HRTs (4 day and 8 day). TCOD concentration in the digestate ranged from 2,877 to 3,561 mg/l during experiments, and propionate and acetate were the dominant VFAs; more detailed information on the characteristics of the digestate is described in Table 3-1 and Figure 3-2. The liquid inside the MEC was mixed with a magnetic stirrer (150 rpm), and the reactor was run at a temperature of 25 ± 1 °C. Electric current, potential, and applied voltage were recorded every 2 min by a personal computer (EC-lab software) connected with the potentiostat.

3.2.4 Chemical analyses

3.2.4.1 Volatile fatty acids analyses

During the initial acclimation of the ARB, the concentration of acetate was high (25 mmol/l) and it was the only substrate. Hence, Hach method (20-1,500 mg/l COD) was chosen for quantification of acetate. When the digestate was used as feed, the lower acetate concentration or a mixture of volatile fatty acids (VFAs) were analyzed on a gas chromatography (GC) (Hewlett Packard HP 5890 Series II) coupled with a flame ionization detector (FID). The GC-FID method was developed with a Nukol fused-silica capillary column (15 m × 0.53 mm, PN 25326, Sigma-Aldrich Canada). Injection volume was 1 μl. The temperature of the GC oven was started at 110 °C, ramped up at 8 °C/min to a final temperature of 195 °C, which was held for 9 min. The temperature of the injector and the detector was 220 °C and 280 °C, respectively. Helium (99.999%, Praxair Canada) was used as the carrier gas. Calibration curve was prepared with standard solution of volatile free acid mix (PN 46975-U, Sigma-Aldrich) with 10 mmol/l of each of the components (C2-C7) in 100 ml of deionized water. Seven different levels of concentrations were prepared by serial dilution. Each level was analyzed in quadruplicate. During the course of this study, calibration curves were established for multiple times.

Before analysis, samples were acidified to pH below two and then filtered through 0.20 μm syringe filter (Hydrophobic PTFE filters, Advantec, Cole-Parmer Canada). Samples that cannot be analyzed instantly were filtered, frozen and analyzed within two weeks. Standards were prepared in a similar way without filtration, without storage in the fridge.

3.2.4.2 Quantification of dissolved and gaseous methane

The method for quantification of gaseous methane was developed on a GC (SRI 310C, SRI Instruments, USA) with a packed column and a thermal conductivity detector (TCD). Helium (99.999%, Praxair Canada) was used as the carrier gas at flow rate of 10 ml/min. The operational temperature of the column oven and the detector were 41°C and 200 °C, respectively. The methane composition was obtained by converting the area from a chromatogram to the volume of methane according to a calibration equation, which was prepared using standard methane gas (99.8-99.9%, Praxair Canada). A 1 ml gas tight syringe (Hamilton, 1000 series, PTFE luer lock) was used for both the calibration and measurement.

The method for dissolved methane analysis requires a sample preparation step so that the measurement of dissolved methane can be treated as the measurement of gaseous methane. A headspace method based on the equilibrium distribution of methane in gas and liquid phases was used. The container used for creating the equilibrium was a 20 ml glass vial (headspace vial crimp top, HP Canada). At the time of measurement, 1 ml of 20 mmol/l of $HgCl_2$ (microbial activity inhibitor) was pipetted into a vial. The vial was then sealed with a rubber stopper and an aluminum crimp. The headspace was replaced by ultra-high-purity (UHP) helium gas by purging the sealed vial for 3 min. Liquid sample, 10 ml, was injected into the vial while the gas inside was expelled through a thin ventilation line. The vial was vigorously shaken with a VWR® Vortex Mixer for 5 min and then allowed to equilibrate for a few min before headspace sampling. All measurements were done in duplicate. Calibration curve for low range of methane gas quantification was created

by injecting various diluted methane gas (99.8-99.9%, Praxair Canada). Helium (99.999%, Praxair Canada) was used for the dilution.

The original dissolved methane was quantified by applying Henry's law, which was adapted to room temperature (i.e., 25 °C). A sum of the methane in the headspace and that remained in the liquid is the original dissolved methane.

3.2.5 Pyrosequencing and quantitative polymerase chain reaction analyses

3.2.5.1 Biomass collection from the anode

Before molecular biology analysis, biomass in the MEC was collected as cell pellets from both biofilm anode and the anolyte. Since the biofilm sampling occurred during operation, a sterilized spatula was used to scratch biofilm from different locations on the carbon fiber anode. The biofilm sample was then washed into a 1.5 ml microcentrifuge tube and then briefly centrifuged at 5,000 g for 30 sec to make a cell pellet (Eppendorf 5424, Germany). The pellet was stored in a freezer (-80 °C) before analysis.

Planktonic cells from the anolyte were collected by filtering the anolyte through a polycarbonate membrane (0.2 μm pore size, GE Water) using a vacuum filtration system. The filter paper with cells was stored at -80°C prior to further processing.

3.2.5.2 DNA extraction, pyrosequencing and quantitative polymerase chain reaction analyses

The DNA was extracted by using MoBio PowerSoil kit (MO BIO Laboratories, USA) according to the manufacturer's protocol. The DNA concentrations were measured using a UV spectrophotometer (Qubit® 2.0 Fluorometer, Life Tech., USA). The DNA extracts were stored at -20°C before further analysis.

Bacterial diversity was assessed using 16S rRNA gene pyrosequencing analysis. Each sample was differentiated by using different barcodes or pyrotags linked to the universal primer 28F (GAGTTTGATCNTGGCTCAG) and couple with 519R (GTNTTACNGCGGCKGCTG) as described by Dowd *et al* (2008). Barcoded libraries and sequencing were performed at the Molecular Research Laboratory (Shallowater, TX, USA). These primers cover the V1, V2, and V3 hypervariable regions of the 16S rRNA and generate approximately 500 bases (*E. coli* position 28-519).

Raw sequences were processed using Sequencher 4.10.1 software (Gene Codes, USA). Chimeric sequences detected using UCHIME (Edgar et al., 2011) were not included in downstream analyses. The clone libraries were compared using Naive Bayesian rRNA Classifier version 10 of Ribosomal Database Project (RDP) with 95% confidence threshold (Cole et al., 2009). For 16S rRNA gene sequences, homology searches of DNA sequences in the GenBank (NR) database were undertaken with the National Center for Biotechnology Information (NCBI) BLAST (http://www.ncbi.nlm.nih.gov/BLAST/) (Altschul et al., 1997).

Two qPCR (quantitative polymerase chain reaction) assays with hydrolysis probes (i.e., BACT2 and ARCH1) were performed against anlyotes and biofilm

samples in 25 μl reaction mixtures containing 1× TaqMan universal PCR master mix with AmpErase uracil-N-glycosylase (Applied Biosystems, Foster City, CA, USA) and 0.2 μg/μl bovine serum albumin (Suzuki et al., 2000). Ten-fold dilutions of each DNA extract were used to test PCR inhibition (Toledo-Hernandez et al., 2013). The amplification protocol involved an initial incubation at 50°C for 2 min to activate uracil-N-glycosylase, followed by 10 min of incubation at 95°C to activate AmpliTaq Gold enzyme, and then 40 cycles at 95°C for 15 sec and at the optimum annealing temperature (i.e., 56°C and 59°C for BACT2 and ARCH1, respectively) for 1 min. The qPCR assays were performed using a 7900 HT Fast Real-Time Sequence Detector (Applied Biosystems, Foster City, CA, USA). All assays were performed in triplicates in MicroAmp Optical 96-well reaction plates with MicroAmp Optical Caps (Applied Biosystems, USA). PCR data were analyzed using ABI's Sequence Detector software (version 2.2.2). Four independent standard curves for each qPCR assay were generated by plotting threshold cycle (C_T) values against the number of target copies corresponding to serially diluted plasmid standards purchased from IDT (integrated DNA technologies, Coralville, USA). The target copy numbers (T) were estimated by the following equation.

$$T = [D/(PL \times 660)] \times 6.022 \times 10^{23} \qquad (3\text{-}3)$$

where D (g/μl) is plasmid DNA concentration, and PL (bp) is plasmid length in base pairs. Each standard curve was generated from at least five 10-fold plasmid dilutions in triplicates. Two no-template controls per PCR plate were used to check for cross-contamination.

3.2.6 Monitoring of biogas production

Biogas generated from the MEC was collected in a one liter gas sampling bag (Tedlar, Cole-Parmer Canada). The composition of the biogas was monitored during the study. Since no methane can be detected in most of the fed-batch cycles and the addition of a gas flow meter (Ritter MGC meter, USA) to the reactor system increases the internal pressure of the anode chamber, a gas flow meter was not incorporated in the system except for cycle 13 and 16. In order to avoid backflow of packing liquid from the gas flow meter, an empty 40 ml vial was connected in between the top outlet of the reactor and the inlet of the gas flow meter. The gas production was read from the gas flow meter and recorded.

3.3 Results and discussion

3.3.1 Electric current generation from digestate and the effluent quality

The new MEC was fed with 25 mmol/l acetate for over a month until the biofilm anode was ready. Figure 3-2A shows the current density profile of the new MEC in fed-batch mode when 25 mmol/l of acetate was the substrate. The peak current density ranged from 13.7 to 16.6 A/m^2 during this phase. When the feed was switched to digestate, the peak current density dropped around 1-2 A/m^2, ranging from 11.3 to 14.6 A/m^2 under HRT 4 day condition (Figure 3-2B). Although there was fluctuation, these peak current densities, which ranges from 0.097 to 0.96 A/m^2, were much higher than those from other studies using digestate or VFAs as feed (Pant et al., 2010, Teng et al., 2010, Catal et al., 2011). Over 60% of particulate matter (TSS and VSS) were reduced in the MEC, and TCOD and SCOD removals were 56% and 58%, respectively, when HRT was 4 days (Table 3-1). Propionate (1,023.6 ± 297.6 mg COD/L) and acetate

(804.8 ± 192.5 mg COD/L) were the dominant VFAs in the digestate at HRT 4 day, which accounted for 53.8 ± 34.6% and 42.3 ± 30.5% of SCOD concentration, respectively; isobutyrate (<0.6%) and isovalerate (<2.5%) were trivial (Figure 3-3A). Acetate concentration in MEC effluent was as low as 12.8 ± 6.0 mg COD/L (98.4 ± 34.1% removal efficiency), and propionate was partially reduced to 555.3 ± 258.0 mg COD/L (45.7 ± 25.2% removal efficiency).

Some ARB species, such as *Geobacter sulfurreducens* and *Geobacter psychrophilus*, cannot utilize propionate but others, such as *Geobacter metallireducens* and *Shewanella oneidensis*, can oxidize propionate anaerobically (Aklujkar et al., 2009, Pinchuk et al., 2010). Hence, ARB acclimated from different inocula may perform differently with fermentable substrate as feed. Some research shows that acetate can be accumulated during anode respiration of fermentable substrates (e.g., glucose, starch, propionate, and butyrate), resulting from slower anode respiration than fermentation (Velasquez-Orta et al., 2011, Yu et al., 2012). In this study, however, little acetate was accumulated; the residual propionate observed in this study (Section A3-1) implies that the anode respiration may not be a rate limiting step. It was observed that SS (suspended solids) were accumulated in the anode chamber, although the MEC was continuously mixed at 150 rpm with a magnetic stirrer. This accumulation of particulate matters in the MEC could have caused contradictory outcome between SS and COD removals (Table 3-1).

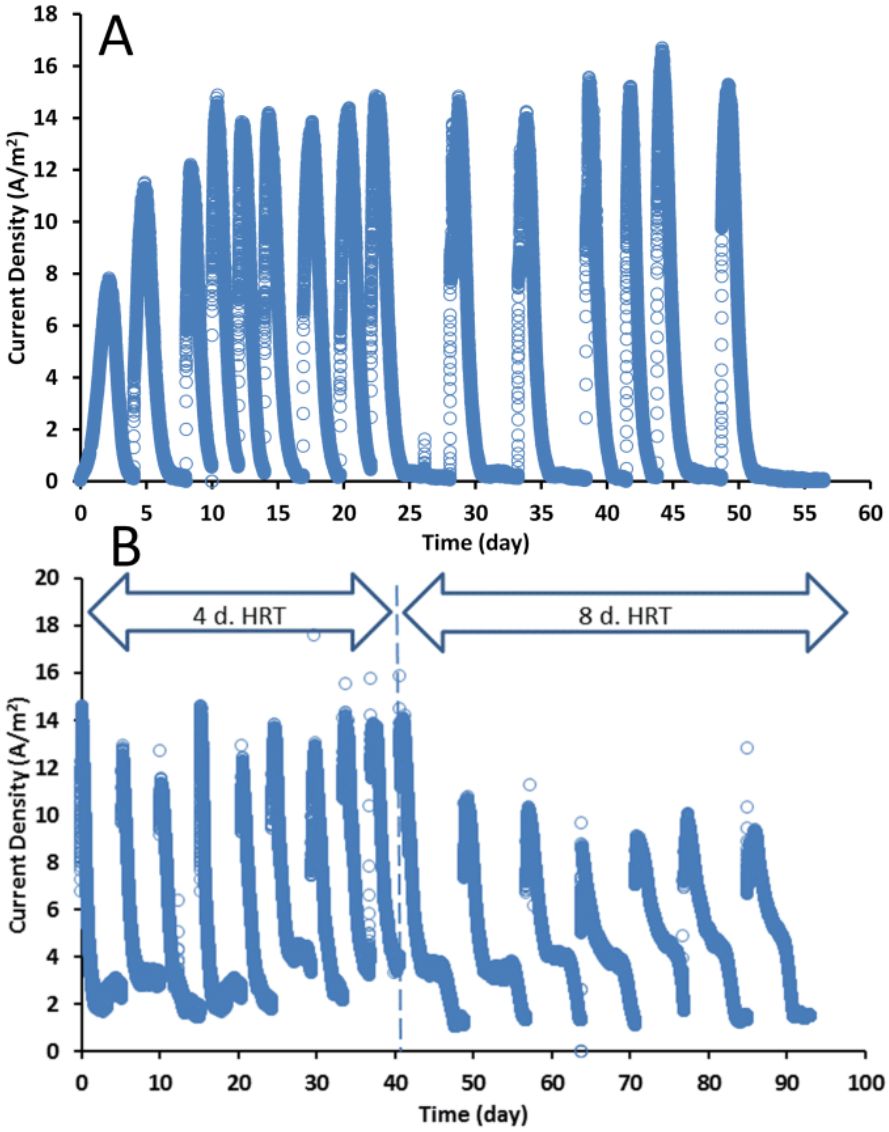

Figure 3–2. Current density profiles of the microbial electrochemical cell during acclimation with acetate (A) and operation with digestate (B). The experiment with AD effluent (B) followed the last batch cycle in (A)

At HRT 8 day, the peak current density slightly decreased to 10 ± 1 A/m^2, as compared to HRT 4 day (Figure 3-2B). The lower current density as well as CE at longer HRT (Figure 3-4) indicates that longer HRT favored the growth of non-anode-respiring microorganisms. In addition, the SS in the digestate, once attached on biofilm, may also negatively affect the transfer of substances in and out at the liquid-biofilm interface, thereby causing a decrease of anode respiration. Nevertheless, the

anode-respiring activity is still much higher than these reported in literature when digestate is used as feed in MECs. Propionate and acetate were still the dominant components in the digestate at HRT 8 day, which were 1,214.7 ± 267.3 mg COD/L (57.1 ± 7.1% of SCOD) and 778.7 ± 172.4 mg COD/L (36.8 ± 8.0% of SCOD), as shown in Figure 3-3A. COD removal was substantially improved at HRT 8 day. Table 3-1 shows that the TCOD concentration dropped to 604.7 ± 240.0 mg/L (percentage of removal 83.2 ± 7.1%), and SCOD was 121.5 ± 80.7 mg/L (percentage of removal 95.6 ± 3.4%). All VFAs, except for acetate (4.2 ± 1.8 mg COD/L), were under detection limits (Table A2 in Appendix Section B) in effluent from the MEC. These results indicate that the planktonic fermenters were able to hydrolyze and transform particulate/fermentable organics to acetate and hydrogen gas at longer HRT, and ARB subsequently oxidized these fermentation products for current generation; almost complete utilization of fermentable substrates also indicates that some hydrogen consumers, e.g. homoacetogens or hydrogenotrophic methanogens, effectively scavenged hydrogen gas, releasing the thermodynamic constraint during fermentation.

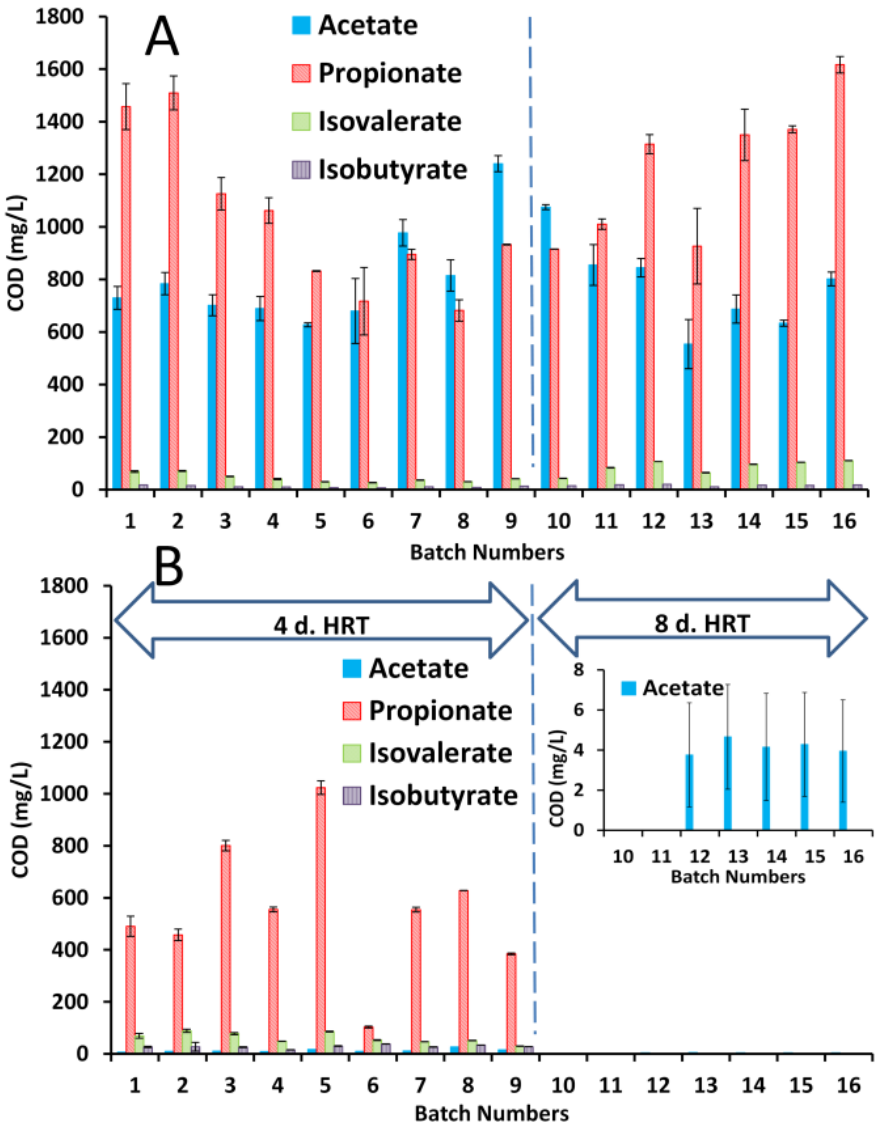

Figure 3–3. The concentrations of major volatile fatty acid components in the digestate (A) and the effluent from the microbial electrochemical cell (B) during experiments. The insertion in (B) shows the magnified residual concentrations of acetate. Error bars denote one standard deviation from quadruplicate analyses.

Table 3-1. Concentrations ± standard deviation of TSS, VSS, TCOD, and SCOD in the digestate and the effluent from the microbial electrochemical cell at HRTs of 4day and 8day.

	HRT 4 day		HRT 8 day	
	TSS	VSS	TSS	VSS
Digestate	1,164.67±162.27	911.22±281.41	1,177.67±217.50	565.71±148.76
MEC effluent	441.85±201.59	294.00±125.20	554.57±160.12	310.00±102.14
	TCOD	SCOD	TCOD	SCOD
Digestate	3,219.21±341.81	2,063.61±354.47	3,606.82±459.79	2,776.91±398.19
MEC effluent	1,343.07±373.24	914.51±260.63	604.73±239.97	121.50±80.69

3.3.2 Coulombic efficiency and methane gas production in the microbial electrochemical cell

The MEC consistently showed high CE during the experiments. Average CE (calculated with ΔTCOD) was 98% ± 35% and 87% ± 13% at HRT 4 day and 8 day, respectively. When the calculation is based on ΔSCOD, CE values during the 4 day HRT phase were over 150% and the highest CE was 239%. In literature, most of the MEC systems that used acetate as sole carbon/energy source reported CE around 80%: 63-78% (Oh et al., 2004), 65% (Min and Logan, 2004), 10-30% (Liu et al., 2005), 82% (Bond et al., 2002), 76±10% (Jung and Regan, 2011), 71% (Lee et al., 2008b), 70%(Lee et al., 2003), 83% (Zhang et al., 2011), 70±15% (Aelterman et al., 2008), and 86% (Torres et al., 2007). The highest possible CE was obtained by *Geobacter sulfurreducens* using acetate as the substrate, which is 95% (Bond and Lovley, 2003). High CE about 190% to 310% has been reported in a single-chamber MEC where hydrogen gas generated on the cathode was re-oxidized by ARB on the anode (Lee and Rittmann, 2010). In this

study, the re-circulation of hydrogen is unlikely in a dual-chamber MEC because of the existence of AEM. These high CE values imply that most of donor electrons were transferred to the anode, and endogenous decay or utilization of intracellular lipophilic inclusions (e.g., PHA or TAGs) could be the secondary source of electrons (Freguia et al., 2007).

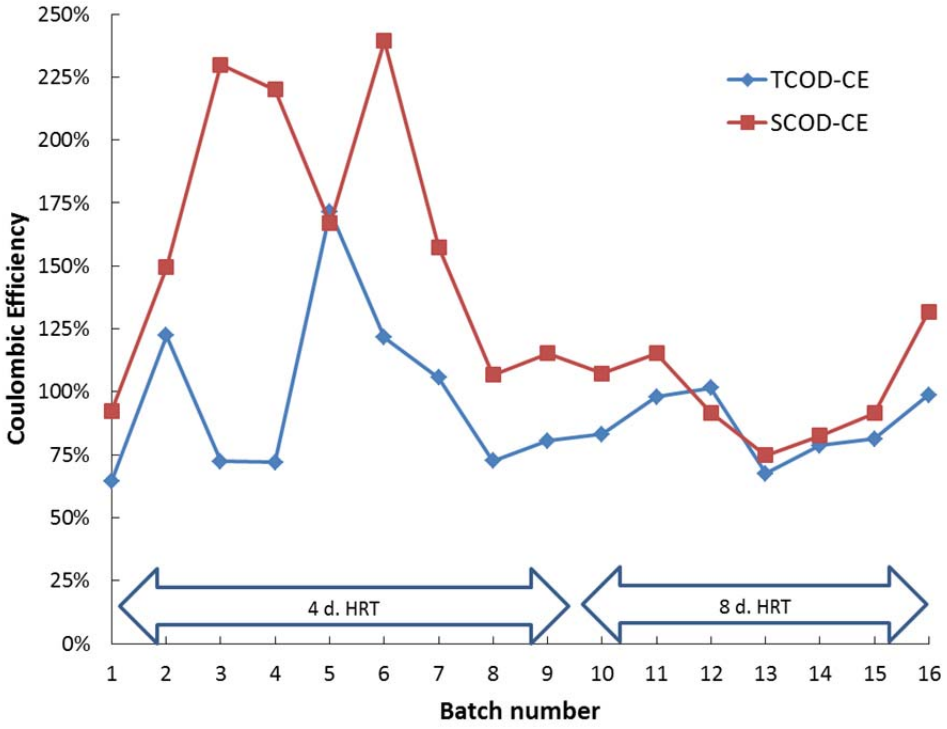

Figure 3–4. Coulombic efficiencies of the microbial electrochemical cell at two different HRTs.

The methane gas production in the headspace of the anode chamber was monitored (batch cycle #13 and #16) to examine whether methane would be a significant electron sink (Figure 3-5). Interestingly, methane was not detected in cycle #13, and it was only 6.85 ml in cycle #16. In addition, dissolved methane in the anolyte was also measured, but its concentration was as small as 8.2 mg CH_4/l in cycle # 16. Hence, total methane in both liquid and gas phases at cycle #16 accounted for 3.42% of ΔTCOD and 4.57% of ΔSCOD (Figure 3-5). Apparently, the decrease of electric current

at longer HRT cannot be solely attributed to an increasing activity of methanogens. High CE and trivial methane accumulation indicate that ARB would have syntrophic partners, such as fermenters and H_2-consumers, besides hydrogenotrophic methanogens, for degrading particulate and fermentable substrates in the anode chamber.

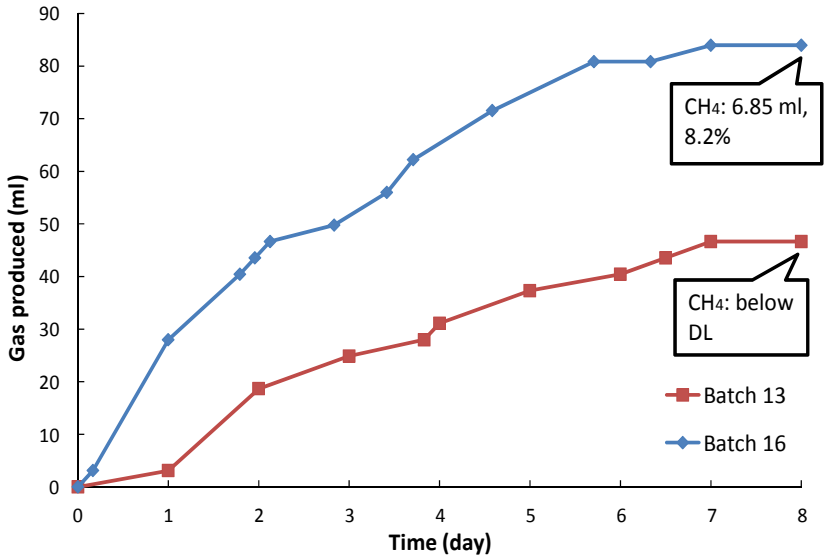

Figure 3–5. Biogas production in batch cycles 13 and 16. The volume of biogas produced from anode chamber was recorded with a gas meter (Ritter, MilliGas Counter, Germany).

3.3.3 Molecular biology analyses of anode biofilm and suspension from the microbial electrochemical cell

Totally 21,311 pyrosequences were analyzed to assess the bacterial community composition associated with the digestate, MEC effluent, and anode biofilm samples. Bacterial compositions in the digestate were completely changed after being treated by the MEC. Excluding unclassified sequences and rare members (less than 4 sequences), 27 bacterial genera were represented in the 16S rRNA gene amplicon libraries for the digestate under HRT 4 day and 8 day, whereas the libraries in MEC effluent showed more diverse bacterial community (47 genera, Table 3-2). In the digestate, members of *Tolumonas* (33%) and *Dysgonomonas* (63%) genera were the numerically most abundant bacteria in HRT 4 day and 8 day samples, respectively. In contrast, relatively low numbers of sequences of those bacteria were observed in MEC effluents. The bacterial community in MEC effluent at HRT 4 day was mostly composed of *Treponema* (28%), *Kosmotoga* (23%), *Pontibacter* (17%), *Arcobacter* (6.6%) and *Thermanaerovibrio* (5.7%). No study clearly has shown that *Kosmotoga* species can ferment propionate to acetate and hydrogen gas, but they can grow on pyruvate (Nunoura et al., 2010). *Arcobacter* species would be one of ARB members (Toh et al., 2011), but they were not detected in anode biofilm (Table 3-2). *Treponema* species are homoacetogens capable of reducing carbon dioxide to acetate using hydrogen gas as electron donor (Graber and Breznak, 2004). In addition, another major detected genus, *Thermanaerovibrio* species, are fermenters capable of using simple acids and hydrogen gas according to the genome sequence study (Sieber et al., 2012). Thus, it is suspected that *Thermanaerovibrio* species could be syntrophic partners of ARB like homoacetogens or H_2-utilizing organism. The substantial increase of sequences affiliated with homoacetogens and fermenters implies the significance of syntrophic

interactions among fermentative bacteria, homoacetogens, and ARB in the MEC, facilitating VFAs (e.g., propionate) fermentation in the MEC. In comparison, limited quantity of hydrogenotrophic methanogens from the domain of Archaea were detected in the HRT 4 day samples (Table 3-3), in agreement with negligible methane accumulation in the MEC. These results clearly demonstrate that homoacetogens or potentially H_2-utilizing ARB mainly scavenged hydrogen gas generated during VFAs fermentation.

For HRT 8 day, species four genera, *Kosmotoga* (24%), *Thermanaerovibrio* (29%), *Rhodococcus* (8.5%) and *Acholeplasma* (4.9%), were dominant in MEC effluent. The abundance of *Thermanaerovibrio* species implies their diverse functions as fermenters and H_2-consumers. *Kosmotoga* species were consistently dominant in MEC effluent, confirming their importance in VFAs fermentation or hydrolysis of particulate matters. *Rhodococcus* species could be ARB (Catal et al., 2008, Torres et al., 2009) but they were not found in biofilm anode. Hydrogenotrophic methanogens were still trivial (i.e., one of 45 clones in Table 3-3, cloning and Sanger sequencing), and this result reconfirms the significance of homoacetogens, or H_2-utilizing ARB in utilizing the hydrogen gas during fermentation.

Table 3-2. Distribution of bacterial 16S rRNA genes by pyrosequencing.

Class	Genus	AD(4)* (n=2,300)	MEC(4)* (n=6,192)	AD(8)* (n=4,589)	MEC(8)* (n=2,877)	MEC-Biofilm# (n=5,353)
Actinobacteria	*Actinomyces*	-	-	-	114 (3.9%)	6
	Corynebacterium	-	-	-	-	20
	Georgenia	-	-	-	31	-
	Mycobacterium	-	-	21	-	-
	Propionibacterium	-	-	-	21	-
	Rhodococcus	12	26	-	245 (8.5%)	51
	Saccharopolyspora	-	16	-	76	-
	Streptomyces	11	191 (3.1%)	26	80	27

Alpha-Proteobacteria	*Bradyrhizobium*	-	-	-	8	17
	Caulobacter	-	-	16	17	-
	Magnetococcus	-	11	-	-	-
	Ochrobactrum	-	-	12	-	-
	Sphingopyxis	-	-	-	9	-
Beta-Proteobacteria	*Acidovorax*	-	-	18	16	-
	Azoarcus	-	-	-	56	-
	Ralstonia	-	-	5	-	-
Delta-Proteobacteria	*Desulfococcus*	-	-	-	-	26
	Geobacter	-	-	-	-	243 (4.5%)
	Syntrophobacter	-	-	-	24	306 (5.7%)
	Syntrophus	-	-	-	-	9
Epsilon-Proteobacteria	*Arcobacter*	5	406 (6.6%)	-	26	-
	Sulfuricurvum	-	15	-	-	-
	Sulfurosirillum	-	-	-	12	-
	Sulfurovum	5	10	-	-	-
Gamma-Proteobacteria	*Stenotrophomonas*	-	-	32	30	-
	Tolumonas	768 (33%)	-	16	-	-
Bacilli	*Brevibacillus*	-	-	-	11	32
	Exiguobacterium	-	-	-	5	5
	Lactobacillus	18	-	-	-	-
	Macrococcus	-	-	11	-	-
	Trichococcus	70	53	-	9	6
Bacteroidia	*Alistipes*	-	10	-	-	5
	Dysgonomonas	130 (5.7%)	228 (3.7%)	2,903 (63%)	62	394 (7.4%)
	Parabacteroides	-	77	-	13	12
	Prevotella	-	10	-	-	-
	Tannerella	-	14	-	-	26
Chlorobia	*Chlorobaculum*	-	-	-	-	7
	Prosthecochloris	-	162 (2.6%)	-	11	-
Clostridia	*Alkaliphilus*	-	23	-	-	-
	Caldicellulosiruptor	-	-	-	-	6
	Clostridium	-	5	-	12	-
	Desulfosporosinus	-	-	53	-	-
	Ethanoligenens	-	5	-	4	40
	Eubacterium	-	7	-	-	4
	Faecalibacterium	-	5	-	34	18
Cytophagia	*Flammeovirga*	-	-	5	4	-
	Flexithrix	-	-	-	-	5
	Pontibacter	478 (21%)	1,074 (17%)	34	7	14
Deinococci	*Thermus*	-	-	-	5	17
Flavobacteria	*Dokdonia*	-	-	-	5	92
	Flavobacterium	62	139 (2.2%)	6	73	550 (10%)
	Krokinobacter	-	5	-	4	7
Mollicutes	*Acholeplasma*	-	5	-	142 (4.9%)	49
Negativicutes	*Acidaminococcus*	-	-	16	-	-
	Desulfosporomusa	-	-	545 (12%)	7	-
	Veillonella	-	6	-	-	-
Sphingobacteria	*Chitinophaga*	-	-	9	-	-
	Pedobacter	-	-	-	-	8
	Sphingobacterium	7	-	-	-	-
Spirochaetes	*Spirochaeta*	-	-	-	5	8
	Treponema	76	1,708 (28%)	47	76	150 (2.8%)
Synergistia	*Jonquetella*	14	128 (2.1%)	16	4	6
	Thermanaerovibrio	160 (7.0%)	352 (5.7%)	194 (4.2%)	840 (29%)	766 (14%)
Thermotogae	*Fervidobacterium*	8	25	-	-	-
	Kosmotoga	446 (19%)	1,411 (23%)	514 (11%)	698 (24%)	2,331 (44%)

"-": not found or less than 4 sequences; *effluent from AD or MEC (HRT in days); # biofilm was collected from the MEC at the end of operation.

In the biofilm library, *Kosmotoga* was the most abundant bacteria (44%), followed by *Thermanaerovibrio* (14%), *Flavobacterium* (10%), *Dysgonomonas* (7.4%), *Syntrophobacter* (5.7%), *Geobacter* (4.5%), and *Treponema* (2.8%). Steady enrichment of *Kosmotoga* in planktonic and biofilm phases demonstrates that these bacteria were mainly responsible for fermentation or hydrolysis of complex substances in the MEC. *Geobacter* species, which was solely detected in the anode biofilm, indicated the requirement of anode biofilm environment for these bacteria to conduct EET-dependent metabolism. In addition, the enrichment of *Geobacter* species in biofilm anode indirectly supports the prediction that acetate was the primary electron donor for ARB in the MEC. Proliferation of *Dysgonomonas* species in biofilm anode suggests that they would be ARB, along with *Geobacter* species on the anode surface, as consolidated by their ability to respire on the anode using shuttle compounds (e.g., 2-hydroxy-1,4-naphtoquinone) (Kodama et al., 2012). The presence of the genera *Syntrophobacter* and *Flavobacterium* together with ARB in biofilm anode suggests possible syntrophic interactions between fermenters and ARB as *Syntrophobacter* species are known to ferment propionate down to acetate and butyrate (Liu et al., 1999). Enrichment of *Treponema* and *Thermanaerovibrio* species in biofilm anode manifests the significance of hydrogen gas consumption by homoacetogens or other H_2-utilizing bacteria, which are essential for bridging propionate fermenters with ARB in the MEC.

Table 3-3. Distribution of archaeal 16S rRNA genes by cloning and Sanger sequencing.

Class	Genus	AD* (HRT4d) (n=56)	MEC* (HRT4d) (n=95)	AD* (HRT8d) (n=45)	MEC* (HRT8d) (n=45)	MEC-Biofilm# (n=87)
Methonomicrobia	*Methanocorpusculum*	0	0	0	1	1
	Methanosaeta	54	94	45	28	79
	Methanosarcina	0	1	0	0	0
Thermoplasmata	*Thermogymnomonas*	2	0	0	13	6
Thermoprotei	*Thermofilum*	0	0	0	0	1
Unclassified Euryarchaeota		0	0	0	3	0

*the effluent from either AD or MEC at HRT of 4d or 8d
#the biofilm was collected at the end of experiments

3.4 The hypothesis of a syntrophic interaction in anode biofilm

Previous studies have shown significant methane accumulation in the anode chambers of MECs fed with fermentable substrates; the proliferation of hydrogenotrophic methanogens seems inevitable in these MECs (Freguia et al., 2007, Pant et al., 2010). In this study, however, negligible methane accumulation was observed, and high current density was maintained during the experiment. In parallel, molecular biology studies showed a small number of clones affiliated with hydrogenotrophic methanogens in both the biofilm and planktonic samples but a large number of sequences affiliated with homoacetogens and fermentative bacteria. Collectively, these evidences indicate that syntrophic interactions among fermenters, homoacetogens, and ARB could suppress the conventional syntrophy between fermenters and acetoclastic and/or hydrogenotrophic methanogens in MECs. As shown in Table 3-4, ARB can outcompete acetoclastic methanogens for acetate due to its lower half saturation constant (Ks) (Lee and Rittmann, 2010); however, hydrogenotrophic methanogens normally outgrow H_2-utilizing ARB (Lee et al., 2009b) or homoacetogens (Peters et al., 1998) because of the kinetic and thermodynamic

advantages in hydrogen metabolism: lower H_2 threshold concentrations, higher maximum growth rate (μ_{max}), and lower Michaelis constant (K_m) (Table 3-4). In this study, the negligible growth of the methanogens in the MEC might be explained by low numbers of hydrogenotrophic methanogens in digestate (Table 3-3), but a significant enrichment of hydrogenotrophic methanogens has been observed in single-chamber MECs inoculated with return activated sludge containing trivial numbers of the methanogens (Lee et al., 2009b, Cusick et al., 2011). This observation implies that instead of low quantities of hydrogenotrophic methanogens in the digestate, other important factors could have facilitated the growth of homoacetogens in the current MEC. Some of the possible reasons are discussed here. A large surface area of anode was provided for ARB growth (1,600 m^2 of anode surface area/m^3 anode volume, which allows high concentration of ARB in the MEC. In contrast, previous studies that showed methane accumulation via hydrogenotrophic methanogenesis employed relatively small specific anode surface area (anode surface area/anode volume from 8.3 to 280 m^2/m^3) (Ren et al., 2012). Besides, a biofilm environment with acetate-loving ARB may allow a quick adaptation of homoacetogens-and-fermenters combination, and thus they can compete with hydrogenotrophic methanogens and fermenters or even outcompete them for hydrogen gas (Lopez et al., 1999, Parameswaran et al., 2012). Low hydrogen gas concentration ranging from 2.3 to 9.3 Pa in steady-state anaerobic digesters (Peters et al., 1998) favors hydrogenotrophic methanogens over homoacetogens; however, the local concentration of hydrogen gas in our anode biofilm could be high enough to encourage the growth of homoacetogens. Last but not least, although there is still the possibility that H_2-oxidizing ARB could drive propionate fermentation without the involvement of homoacetogens, a number of sequences affiliated with homoacetogens were found in biofilm anode, along with fermenters and ARB, supporting the hypothesis that

fermenters, homoacetogens, and ARB are in syntrophy and proliferate with fermentable substrates in biofilm anode.

Table 3-4. Kinetics parameters of ARB, methanogens, and homoacetogens compiled from literature.

Substrate	Microorganism	q_{max} (g COD/g VSS-d)	μ_{max} (d^{-1})	K_s(mg COD/L)	Threshold H_2 concentration (Pa)	Reference
Acetate	*Geobacter sulfurreducens*	22.7	2.4	0.64	-	(Esteve-Núñez et al., 2005)
	ARB	22.3	~3.2	119	-	(Lee et al., 2009a)
	Acetoclastic methanogens	7.6	0.28	180-430	-	(Lee et al., 2010)
Hydrogen	ARB	-	-	-	3	(Bond and Lovley, 2003)
	Hydrogenotrophic methanogens	4.7 g H_2 /g VSS-d	0.77	0.006-1.4 (K_m)	2.3-9.3	(Peters et al., 1998, Stams et al., 2003, Lee et al., 2010)
	Homoacetogens	-	0.576	0.065-3.87 (K_m)	48.9-89.2	(Kotsyurbenko et al., 2001, Stams et al., 2003)

"-": not found

3.5 Conclusions

An MEC fed with digestate showed a high electric current density of 14.6 A/m^2 and a high COD removal percentage of 96%, which are the highest up to now. VFAs were negligible in the MEC effluent, and accumulated methane only accounted for 3.42% of removed COD. The comparison of two HRT conditions accompanied by molecular biology analyses of the anode biofilm and planktonic cells indicated that syntrophic interactions among fermenters (*Kosmotoga* species), homoacetogens (*Treponema* species), and ARB (*Geobacter* species and *Dysgonomonas* species) were established to degrade VFAs and generate high current density. The results showed that MECs can efficiently recover the electrons from VFAs accumulated from complex wastewater containing methanogens (e.g., anaerobic digestion effluent) via unconventional syntrophic pathways.

Chapter 4 Syntrophy between anode-respiring bacteria and lipid-storing bacteria

4.1 Introduction

To survive harsh environment, microorganisms have evolved the mechanisms for synthesizing and storing biopolymers as intracellular storage reserves for carbon and energy when food sources are not available. Polyhydroxyalkanoates (PHAs), glycogen, triacylglycerols (TAGs), polyphosphate, elemental sulfur, and wax esters are the most common cell inclusions for prokaryotes (Garton et al., 2002, Stahl, 2010). Each of these inclusions serves a distinct function during cellular metabolism. PHAs, commonly known lipid inclusions, are synthesized when excessive organic matter is available and are decomposed for metabolic needs. Polyphosphate, on the other hand, is usually stored as a source of phosphate for nucleic acid and phospholipid biosynthesis. Since their discovery, microorganisms capable of synthesizing inclusions have been engineered and the storage behaviors have been exploited for wastewater treatment, such as biological phosphorus removal. When organic source is in excess, polyphosphate-accumulating organisms (PAOs) and glycogen-accumulating organisms (GAOs) can store PHA in anaerobic conditions and subsequently consume the stored biopolymer as food source in aerobic conditions. These traits have been tailored for COD, nitrogen and phosphorus removal during wastewater treatment (Beun et al., 2002, Sakai et al., 2015).

The synthesis of PHA can be induced by the intermittent supply of oxygen to a system, which causes the temporal and spatial separation of electron donors and electron acceptors during a wastewater treatment process (Salehizadeh and Van

Loosdrecht, 2004). Besides, nitrogen- or phosphate-limiting condition, alternate feast and famine condition can all stimulate massive accumulation of PHA (Bengtsson et al., 2008). The accumulation of PHA by activated sludge has been evaluated in various studies. For instance, in a study of PHA production from a mixed municipal and industrial wastewater (COD of 60-130 mg/L and an acetate concentration of 0-20 mg/L), over 20% of sludge dry weight was recovered as PHA in a sequencing batch reactor (Chua et al., 2003). Since the intracellular PHA contains magnificent amount of reducing power, the potential of coupling PHA accumulation with an oxidizing reaction has been intensively explored. One of such kind of research is the coupled denitrification and PHA oxidation (Zeng et al., 2003, Krasnits et al., 2013). When municipal wastewater was examined in three-stage denitrifying process (anaerobic stabilization-aerobic nitrification-denitrification), around 0.36 to 0.48 of the total COD can be converted into PHA in the initial anaerobic phase; nitrate removal of 65-87.7% was achieved at the end of the denitrifying stage (Krasnits et al., 2013). Another study shows that polyhydroxybutyrate (PHB) accumulation, nitrification, and denitrification can sequentially occur in a sequencing batch reactor (Third et al., 2003). In that study, 65% of acetate was preserved as PHB during the initial aerobic phase, and nitrification occurs after acetate was depleted; PHB was then used as the electron donor for denitrification, up to 78%, in the last phase when the dissolved oxygen was around 0.5 mg/L. Such inclusions might be useful for other biological processes, such as microbial fuel cells (MFCs) that marry microbial metabolism with electrochemistry.

Small-sized MFCs are considered a promising power source to electronics or sensors after recognizing the limitation of small power from large-scale MFCs. Recent studies revealed that current and power density were improved to 170 $\mu A/cm^2$ and 3700 W/m^3, respectively (Chen et al., 2012, Choi and Chae, 2013), which is enough to power small electronic/diagnostic devices. There are, however, substantial challenges

to be addressed when using small-sized MFCs as portable power sources, as the ARB in the MFCs must perform their catalytic function in a consistent and reliable manner. Moreover, an MFC, like a battery, would be utilized in a discontinuous rather than continuous manner as portable power source. In this case, the metabolic activity of ARB could be significantly suppressed because of an intermittent starvation or open circuit. The number of active ARB would substantially decrease as a result of endogenous decay during starvation. To allow small-sized MFCs to be used as portable power source, the metabolic activity of the ARB should be maintained at a level sufficient to provide usable ranges of current/power density when needed.

Since microorganisms capable of synthesizing lipid inclusions can store intracellular carbon and energy reserves and thus demonstrate better resistance to the fluctuation of food source, the current work attempts to investigate the possibilities of enriching lipid-accumulating microorganisms together with ARB on an anode surface. The enriched lipid-accumulating microorganisms are expected to preserve carbon and energy source when an exogenous substrate is available and to provide food source to ARB during starvation. The goal of this study was to demonstrate that lipid-storing microorganisms can be coupled with ARB for current/power generation in discontinuously fed MFCs. The proposed research is expected to drive the commercialization of small-sized MFCs as portable power sources.

4.2 Methods and materials

4.2.1 Reactor configuration, acclimation, and operation

A sandwich-type MEC was employed for experiments, and the details of the MEC can be found in Section 3.3.1. The MEC was inoculated with the effluent from another

MEC that had been fed with dissolved methane gas as the sole carbon and energy source. Then, the anode biofilm was acclimated in fed-batch mode with 25 mmol/l of acetate medium (Section 3.3.1). The PBS concentration was set to 50 mmol/l. At the end of the biofilm acclimation, digestate from a lab-scale anaerobic digester was fed as substrate into the anode chamber. The major component of the digestate was acetate and propionate (acetate 793±178 mg COD/l, propionate 1107±292mg COD/l, TCOD 3,610±460 mg/l; SCOD 2,780±400 mg/l). After around 5 months of operation with digestate, the feed was switched back to acetate medium.

At the end of a fed-batch cycle with acetate as feed, when there was no detectable acetate in the anolyte and the residual current was stable around 1.5 A/m^2, a series of three injections of acetate medium was applied to demonstrate that the anode biofilm can generate a substantial electric current from intracellular lipids without exogenous electron donor of acetate. Different volumes of acetate medium were injected to test the robustness of the anode biofilm with 15 ml in the first injection (instant acetate concentration 1.34 mmol/l) and 32.5 ml in the second and third injection (instant acetate concentration 2.90 mmol/l). Every time before injection, the same amount of anolyte was withdrawn from the reactor. The pressure was balanced by a one liter gas sampling bag (nitrogen gas, 99.999% Praxair, Canada) connected to the outlet. The anolyte was sampled at various time points to show that the baseline current was a result of the endogenous decay of biofilm polymers (Figure 4-1).

4.2.2 Calculations

Coulombic efficiency (CE) was calculated using equation (4-1) (Lee et al., 2009b):

$$Coulombic\ efficiency = \frac{e^-_{transferred}}{e^-_{donor}} \times 100\% \qquad (4\text{-}1)$$

where $e^-_{transferred}$ is accumulated electrons obtained from the record of electric current, and e^-_{donor} is the electron equivalents of the consumed organic electron-donor.

Current density (A/m^2) was calculated using equation (4-2):

$$Current\ density = I/A \qquad (4\text{-}2)$$

where I is electric current (A), and A is the geometric surface area of the ion-exchange membrane (m^2).

4.2.3 Starvation-substrate spiking tests in a microbial fuel cell

A two-chamber air-cathode microbial fuel cell (MFC) was assembled by using membrane-cathode assembly (MCA). The MFC was made of Plexiglas® in the Engineering Machine Shop at the University of Waterloo, and the anode working volume was 45 ml. The MCA was composed of proton exchange membrane (PEM) (Nafion® NAF NR212, Dupont, USA) and Pt/C-coated carbon cloth (40% Platinum on vulcan XC-72, BASF Fuel cell, USA) of 0.5 mg Pt/cm^2. The PEM was sequentially pretreated in 3 wt.% H_2O_2 , 3wt.% H_2SO_4 , and deionized water for 1 hr in each solution to oxidize contaminants and to protonate all acidic sites. The anode configuration of the MFC, except for the size, was the same to the MEC described in Section 4.2.1. MCA was directly exposed to atmosphere for passive oxygen diffusion to the cathode. The projected area of the cathode and ion-exchange membrane was

9.6 cm^2. The MFC was inoculated with the anolyte from the MEC mentioned in the last section. The anode potential of the MFC was poised at -0.4 V using the potentiostat during acclimation. Acetate medium (25mM, Section 4.2.1) was fed into the anode chamber using a peristaltic pump (Masterflex, Model 7523-80, USA) at a flow rate of 0.25 ml/min during acclimation. The anolyte was mixed with a magnetic stirrer during experiments. The current-voltage (I-V) curve was obtained by changing an external resistor from 9.5 Ω to 42.6 kΩ. Finally, an external resistor of 32.5 Ω was chosen because it yielded the maximum power density, 65 $\mu W/cm^2$ (working voltage: 0.143 V, current density: 4.26 A/m^2). Acetate spiking tests were conducted when 32.5 Ω resistor was the load.

Before the starvation test, fresh mineral medium was pumped into the anode chamber of the MFC for 3 days (day 0 to 3 in Figure 4-4) with a peristaltic pump. After confirming the absence of acetate in the anolyte, acetate medium, 0.98±0.03 mmol/l, was injected into the anode. Three consecutive starvation-spiking tests, denoted as (a), (b), and (c) in Figure 4-4 were run. Longer starvation, 7 days, was applied for another three consecutive starvation-spiking tests. The absence of acetate in the anolyte was confirmed with the GC-FID (Section 4.2.3) during the experiment (day 0, 4, 7, 10, 17, 25, and 32). During starvation/spiking tests, closed circuit voltage in the MFC was monitored every 1 min using a multimeter (Keithly 2700, Keithley Instruments, Inc. USA). Current density of the MFC was computed according to the geometrical area of the MCA (Section 4.2.1).

4.2.4 Chemical analyses

Volatile fatty acids were quantified using the GC-FID equipped with Nukol fused-silica capillary column (15 m, 0.53 mm, Sigma–Aldrich Co. LLC., Canada). Detailed

operation can be found in Section 3.3.5.1. Chemical oxygen demand (COD) concentrations were measured with Hach method (20–1500 mg/l COD vials, Hach, Canada). Total suspended solids (TSS) and volatile suspended solids (VSS) concentrations were quantified according to Standard Methods (Clesceri et al., 1999).

4.2.5 Molecular biology study

The bacterial diversity in planktonic and biofilm cells in the anode of the MEC was examined with cloning targeting 16S rRNA genes. Biofilm was collected at the end of experiments. After the MEC was disassembled, the whole anode fiber was cut into pieces for biofilm collection. A pair of sterilized scissors was used for cutting. The short pieces of carbon fiber were suspended in PBS in a 50 ml falcon tube. The tube was vortex mixed for 5 min at the highest speed in order to detach the biofilm. Next, the fibers were transferred to another falcon tube for a second extraction while the liquid from the first falcon tube was centrifuged. For better recovery of cells, the suspension was distributed into multiple 1.5 ml microcentrifuge tubes and centrifuged at 10,000 g for 3 min (Eppendorf 5424, Germany). Maximum three extractions were conducted, depending on the amount of cell pellets recovered from the second extraction. For these cells used for subsequent inoculation, equal volume of deoxygenated glycerol solution (30%) was mixed with the sample, and the mixture was stored in a freezer (-80 ^{o}C). The detailed information on DNA extraction can be found in Section 3.3.5.

For PCR, the universal bacterial primers 8F (5'-AGAGTTTGATCCTGGCTCAG-3') and 787R (5'-GGACTACCAGGGTATCTAAT-3') were used to amplify 16S rRNA gene of the domain bacteria as described elsewhere (Ley et al., 2008, Ryu et al., 2012).

PCR amplifications were performed (25 µl reaction volume) using the polymerase TaKaRa Ex Taq™ (Takara Bio Inc.) in a Bio-Rad Tetrad Peltier Thermal Cycler (Bio-Rad, Hercules, CA) under the following cycling conditions: one initial denaturation step at 95°C for 5 min and 30 cycles of 1 min at 95°C, 1 min at 56°C, and 1 min at 72°C with a final extension step of 12 min at 72°C. PCR products were visualized in 1.5% agarose gels using GelStar Nucleic Acid gel stain (Lonza, Rockland, ME, USA). Selected PCR products were cloned into pCR®4 TOPO® vector and transformed to TOPO10 chemically competent *E. coli* cells as described by the manufacturer (Invitrogen, Carlsbad, CA, USA). Individual *E. coli* clones were then sub-cultured into 300 µl of Luria Broth containing 50 µg/ml ampicillin and screened for inserts using M13 PCR. The PCR products were submitted to the Children's Hospital DNA Core Facility (Cincinnati, OH, USA) for sequencing using an Applied Biosystems Prism 3730XL DNA analyzer. Raw sequences were processed using Sequencher 4.10.1 software (Gene Codes, Ann Arbor, MI, USA). Chimeric sequences detected by Bellerophon (Huber et al., 2004) were not included in further analyses. The clone libraries were compared using Naive Bayesian rRNA Classifier version 2.5 of Ribosomal Database Project (RDP) with 95% confidence threshold (Wang et al., 2007).

4.2.6 Biofilm imaging

Anode biofilm was collected from the anode fibers and centrifuged to form cell pellets at 12,000 rpm for 1 min using a centrifuge (5254, Eppendorf, Canada). The cell pellet was then re-suspended in 0.5 ml PBS solution (8.5 g/L KH_2PO_4, 21.75 g/L K_2HPO_4, 33.4 g/l Na_2HPO_4-$7H_2O$, and 1.7 g/l NH_4Cl). For staining, cell suspension (40 µl) was transferred to a slide, and 30 µl of Nile Red solution (N3013, Sigma Aldrich Canada) was mixed with the sample using a sterilized pipette tip; the reaction time was set to 1

min. Nile Red stock solution was prepared in ethanol to make a final concentration of 1 mg/l. The slide was first dried in atmosphere for around 5 min to let the ethanol evaporate, and then fixed with flame. A fluorescence microscope equipped with QImaging Retiga EXi CCD camera and FluArc mercury lamp was used to observe intracellular lipophilic inclusions in cells. Red/yellow-gold fluorescence signals in samples stained with Nile Red were observed using the Zeiss filter set 15.

4.3 Results and discussion

4.3.1 Electric current generation from endogenous decay and consumption of lipids inclusions

Overall, the electric current profiles demonstrate that significant amount of electrons other than the acetate injected into the anolyte, potentially from lipid-inclusions, is available for ARB during anode respiration. Figure 4-1 presents steady current density of 1.5±0.1 A/m^2 in the sandwich-type dual-chamber MEC for over four days without exogenous electron donor (no acetate detected from day 0, 1, 2, and 4). After four days, fresh medium (15 ml of 25 mmol/l acetate medium) was injected into the anode chamber of the MEC (instant acetate concentration in the anode: 1.34 mmol/l). The current density sharply increased up to 4.2 A/m^2 and then decreased to 1.4 A/m^2 with time and finally maintained at 1.7±0.1 A/m^2 for additional three days; again, acetate was not detected on day 8 (the 2nd green arrow in Figure 4-1). The same acetate medium was spiked at around day 8 and day 11 (2nd and 3rd red arrows in Figure 4-1). The same pattern with the first spiking test was observed: a sharp increase and subsequently gradual decrease of current density followed by a steady residual current, along with undetected acetate (the 3rd and 4th green arrows in Figure 4-1).

The absence of acetate in the fourth sampling clearly supports the fact that no acetate when the current reaches the baseline; the variation of steady state current density in the MEC is relatively larger than these reported by the others, and it could be attributed to the large number of carbon fibers used as the anode (24,000 fibers in a bundle) and high frequency of data acquisition.

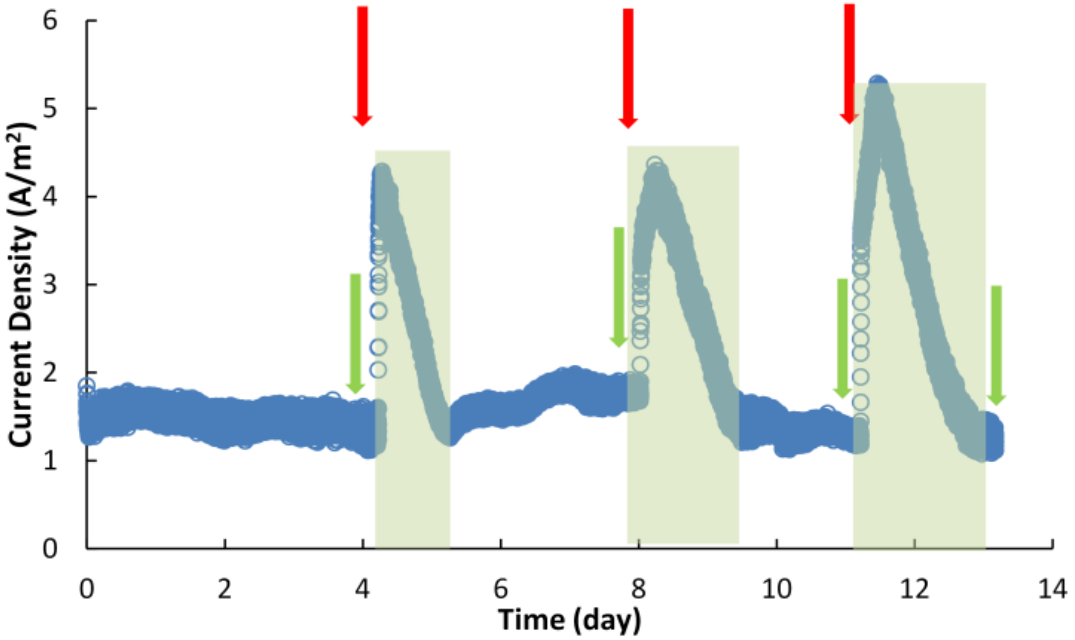

Figure 4–1. Current recovery tests after 2–4 days of starvation. The red arrows denote acetate spiking and the green arrows denote the points of anolyte sampling for acetate quantification. The cumulative Coulombs from the shaded regions under the current density were used to compute the coulombic efficiencies (Table 4-1).

Current generation at substrate-depleted condition and the unusually high CEs of the three spiking tests, which are all around 200% (Table 4-1), lead to the speculation that intracellular energy sources were available for anode respiration. Since intracellular lipids can be synthesized from volatile fatty acids, Nile red was used to probe any lipid compounds in the biofilm. Observations with a fluorescence microscopy show that the biofilm anode accumulated lipid compounds (Figure 4-2B and D).

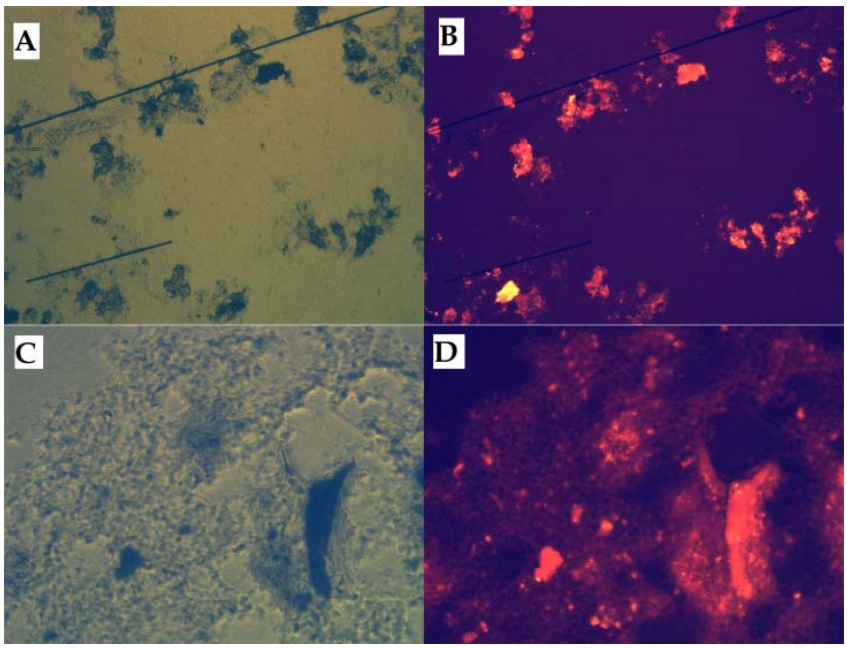

Figure 4–2. Fluorescence microscopy images of anode biofilm stained with Nile red. A, C) without fluorescence, B, D) with fluorescence, before (A and B) and after 5 months of operation (C and D). All photos show 200X magnifications. The dark lines in A), the inoculum, are carbon fibers, which have a diameter of 7 μm.

Theoretically, Nile red is effective for labelling long chain fatty acids, polyesters, lipid-rich lipoprotein, triacylglycerols, and cholesteryl ester (Greenspan et al., 1985, Palatsi et al., 2012). In this study, however, no further analysis of the composition of the cellular lipids was carried out so the identity of the lipid is unknown. Only one study reported similar result of lipid accumulation in an anode biofilm that was subjected to starvation with intermittent supply of glucose; however, no analysis of the lipid component is available (Freguia et al., 2007). Lipids or fats are high energy compounds commonly observed in wastewater. Most of the energy stored in lipids is from the long chain fatty acids, which are available for biodegradation, the β-oxidation and anaerobic tricarboxylic acid cycle, after the hydrolysis of lipids. Previous research shows that lipids can be biodegraded in methanogenic environment with acetate or hydrogen as the end products, which then serve as the feed to methanogenesis (Cirne et al., 2007, Hatamoto et al., 2007). Similarly, biological polyesters, such as PHAs, are also carbon- and energy-rich compounds, and biodegradation of them has been shown to occur in methanogenic environment with VFAs and/or hydrogen gas as the electron carriers (Reischwitz et al., 1997). In this study, the CEs during the three spiking tests are so high that methanogenesis must be inactive. Since ARB are also able to oxidize acetate and hydrogen gas during anode respiration, it is possible that ARB and these lipid-accumulating microorganisms may have synergistically/syntrophically degraded the lipid inclusions when exogenous substrate was not available in the MEC.

Table 4-1. Coulombic efficiencies, calculated from the shaded current density regions in Figure 4-1.

Sampling	Accumulated Coulombs [mol electrons]	Acetate [mol electrons]	Coulombic efficiency
1	0.00651	0.003	217.0%
2	0.01286	0.0065	197.8%
3	0.01319	0.0065	207.5%

4.3.2 Molecular biology studies of the anode biofilm

Cloning and Sanger sequencing of the bacterial community of biofilm shows that the species from the genus *Acholeplasma* account for 53% of the total clones (Figure 4-3). *Acholeplasma laidlawii* are able to incorporate a significant amount of exogenous fatty acids into their membrane and they can accumulate nonbilayer associated lipid aggregates (Al-Shammari and Smith, 1979, Wieslander et al., 1995). It is possible that *Acholeplasma* species is responsible for the lipid accumulation in the anode biofilm. In addition, *Geobacter* and *Kosmotoga* species were enriched in the biofilm anode, along with various species from *Syntrophobacter*, unclassified *Porphyromonadaceae*, *Treponema*, unclassified *Sphingobacteriales*, and *Aminiphilus*. Previous research on the microbial community in anaerobic digesters shows that *Treponema* and unclassified *Sphingobacteriales* are homoacetogens or fermenters (Graber et al., 2004). The proliferation of the two bacteria in the anode chamber is reasonable because digestate was used as feed to the MEC before acetate was used for the current recovery tests (Figure 4-1). In addition to *Acholeplasma* species, *Kosmotoga* and *Treponema* species have enzymes that potentially catalyze the production of lipophilic inclusions (Tucci and Martin, 2007, Swithers et al., 2011). The detection of *Geobacter* species on the

anode has been frequently reported in literature as *Geobacter* species are one of the most common ARB (Logan, 2009, Lovley, 2012, Okamoto et al., 2014). None of the published research clearly shows that *Geobacter* species can synthesize ILIs (intracellular lipophilic inclusions), so the possibility of self-supporting anode respiration is not likely to be true.

In the planktonic phase, species from *Treponema*, unclassified *Sphingobacteriales* and *Aminiphilus* were abundant. The role of *Sphingobacteriales* species are not clear but they have been reported to proliferate in sewage water contaminated river (Korajkic et al., 2015). A species, *Aminiphilus circumscriptus*, is able to ferment a variety of VFAs, amino acids, and even branched-chain fatty acids (Díaz et al., 2007). Therefore, these species in the planktonic phase may have only carried out the fermentation of certain intermediate compounds during anode-respiration. About archaea, *Methanosaeta*, a common acetoclastic methanogen, is the most abundant species in the biofilm, which accounted for around 91% of the total clones. The dominance of *Methanosaeta* supports the reasoning that acetate would be a major product during lipid degradation.

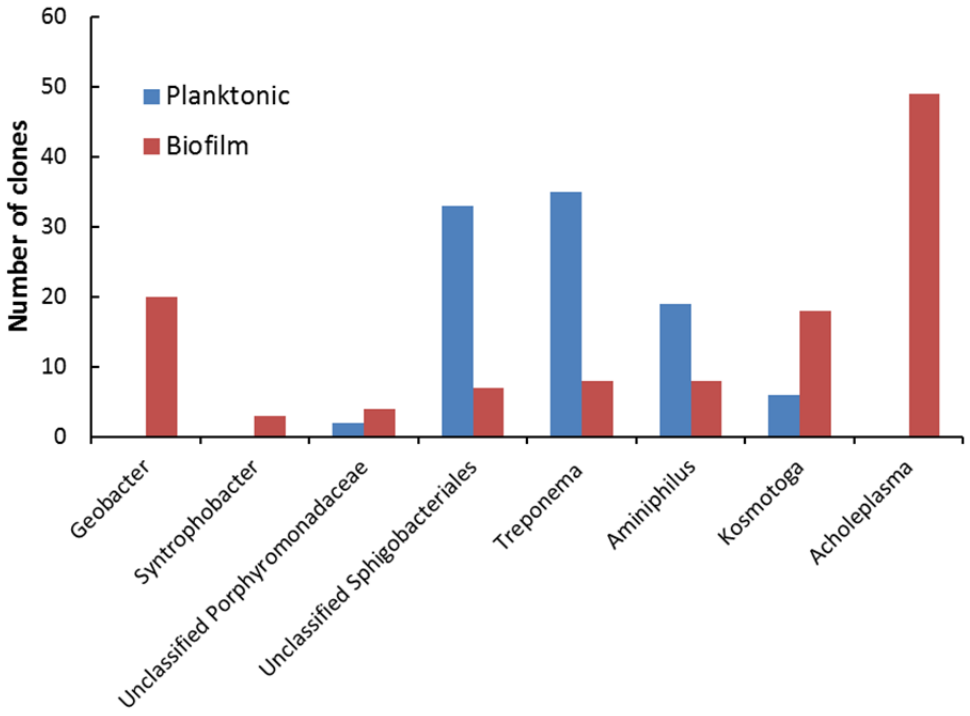

Figure 4–3. Microbial community structures of biofilm and planktonic cells. The planktonic and biofilm cells were sampled at the end of experiments, and a total of 89 and 92 clone sequences, respectively, excluding low quality and chimeric sequences, were analyzed.

4.3.3 Demonstration of the syntrophy between anode-respiring and lipid-storing bacteria in a microbial fuel cell operated under intermittent feeding conditions

As can be seen from Figure 4-4, when the MFC was subjected to starvation, the electric current gradually dropped to around 0.01 A/m^2 until it finally leveled off around 0.005 A/m^2 after 30 days. The experiment with an MFC confirmed current recovery after starvation up to 7 days. The current density was consistently recovered at 1.36±0.22 A/m^2 in six starvation/spiking cycles. In a normal *Geobacter*-dominant MFC, starvation causes a lag phase prior to the recovery of current or a decrease in power production (Chang et al., 2004, Oh and Logan, 2007). The recovery of current density in the current MFC reveals that the activity of ARB was maintained without

exogenous electron donor for a week, due to the syntrophy with lipid-storing bacteria in biofilm anode. Current density in the MFC was lower than that in the MEC, which is common due to the different configuration of reactors. Two potential reasons for the low current could be (1) the fast evaporation of water from the cathode due to a lack of a hydrophobic diffusion layer on the surface of the air-cathode (Cheng et al., 2006) and (2) oxygen intrusion from the atmosphere into the anode chamber by diffusion through Nafion membrane (Liu and Logan, 2004). Some other reasons, such as the existence of high ohmic resistances and cathodic limitations, in an MFC mode can also lower the current.

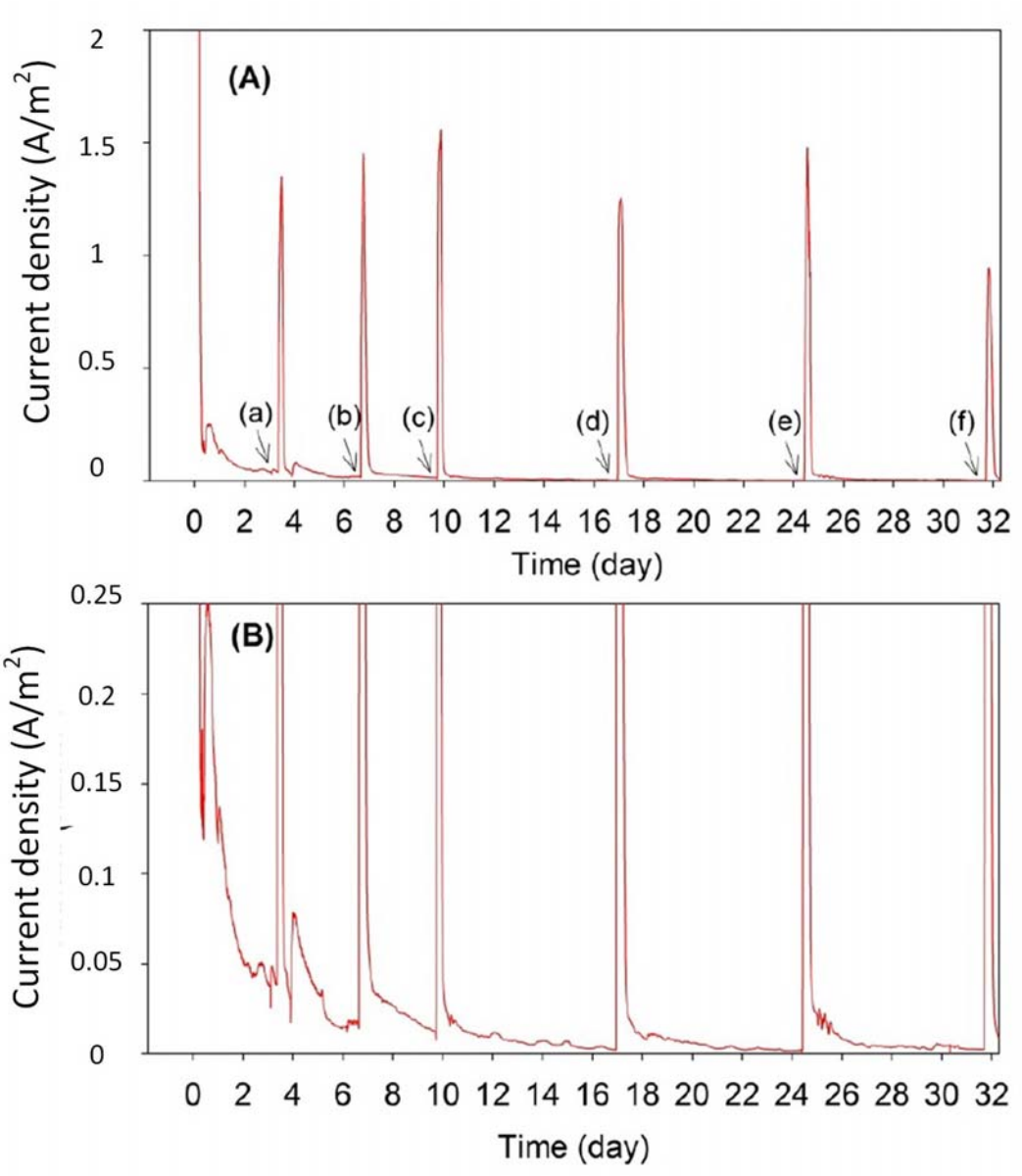

Figure 4–4. The recovery of current density in six sets of starvation/spiking experiments. Arrows (a), (b), and (c) indicate the end of 3 day starvation. Arrows (d), (e), and (f) indicate the end of 7 day starvation. (B) magnifies the lower range of (A).

4.4 Conclusions

The MEC inoculated by the anolyte of a methane-oxidizing MEC was acclimated with acetate and then digestate for over five months. Residual current around 1.5 to 2 A/m^2 was observed when acetate was under the detection limit. When acetate was spiked into the anolyte, extremely high CEs around 200% were achieved; since acetate was almost completely utilized, the high CE values indicate the availability of additional electron donors in the anode biofilm. Nile red staining revealed that lipid inclusions were produced in the anode biofilm. Molecular biology study and information collected from literature search showed that species from *Acholeplasma*, *Kosmotoga* and *Treponema* may be responsible for the production of lipid inclusions in the anode biofilm. *Geobacter* should be the major ARB. Starvation/spiking experiments in the MFC clearly supports that the syntrophic interaction between ARB and lipid-storing bacteria allows MFCs to work in discontinuous feeding manners. In summary, the results from this study imply that the syntrophic relationship between lipid-accumulating bacteria and ARB holds the potential for upgrading MFCs as portable power sources with intermittent substrate provision, which is crucial for the practical application of MFCs for self-sustained current production.

Chapter 5 The syntrophy between *Geobacter* and *Methanobacterium* for anaerobic oxidation of methane

5.1 Introduction

Methane gas is a potent greenhouse gas, and its global warming potential is 25 times higher than that of carbon dioxide (US-EPA, 2012). Apart from geochemical formation of methane gas, the major fraction of methane gas in the atmosphere is a result of microbial activities (US-EPA, 2010). Two counter-acting biological processes determine the net methane emission into the atmosphere. One is methanogenesis and the other is methanotrophy. Methanogenesis is the reaction during which methane molecules are produced from CO_2 or simple organics (e.g., acetate) by methanogens. In comparison, methanotrophy denotes methane consumption reactions conducted by methanotrophs. Aerobic methanotrophs are well known and characterized, but anaerobic methanotrophic microorganisms are relatively new. Martens and Berner (1974) first reported anaerobic oxidation of methane (AOM) coupled to sulfate reduction in marine sediment environment. Recent studies have commonly claimed that AOM would be significant for the methane cycle on earth (Caldwell, 2008). It is estimated that AOM would consume around 100 Tg CH_4/year, which accounts for over 90% of the methane produced in the ocean and 7-25% of methane produced globally (Knittel and Boetius, 2009a).

Due to the abundance of sulfate ion in marine sediment, most of the early studies and discoveries on AOM and anaerobic methanotrophic (ANME) archaea are from sulfate-driven AOM. According to phylogenetic analyses of the microbial

consortia for sulfate-driven AOM, ANME archaea have been grouped into three lineages, i.e. ANME-1, ANME-2, and ANME-3. ANME-2 and ANME-3 are close to *Methanosarcinales* and ANME-1 is classified as a distinct group (Knittel and Boetius, 2009b, Milucka et al., 2012). Two mechanisms of initial methane activation by ANME archaea have been proposed during the study of sulfate-reduction-coupled AOM: (1) reverse methanogenesis and (2) acetogenesis. Recent studies showed that the reverse methanogenesis followed by the consumption of an intermediate derived from methane by sulfate-reducing bacteria can better explain observed laboratory and field results. For example, Kruger *et al*. (2003) found a nickel-based enzyme that could catalyze methane activation in a reverse terminal methyl-coenzyme M reductase reaction. Moreover, gene sequencing analysis further supported the hypothesis that methyl-coenzyme M reductase has participated in the AOM process (Shima et al., 2012). A recent model to elucidate sulfate-driven AOM proposes that ANME archaea conduct both methane oxidation and the reduction of sulfate in syntrophy with their bacterial partner (*Desulfosarcina*/*Desulfococcus* cluster) recycling disulfide to sulfate (Milucka et al., 2012).

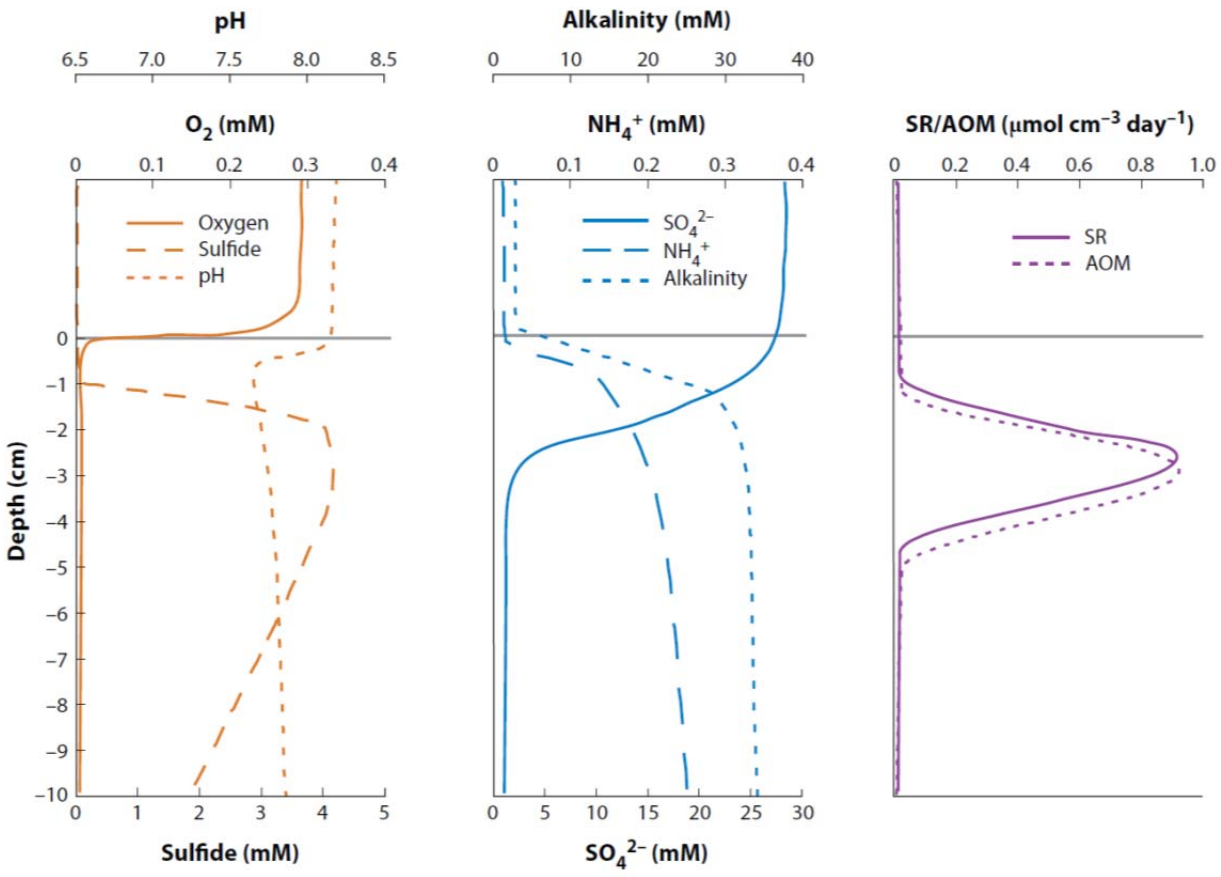

Figure 5–1. Depth concentration profiles of oxygen, sulfate, and sulfide together with the rate of sulfate reduction (SR) and anaerobic oxidation of methane (AOM) in the AOM zone above hydrates. Extracted from (Knittel and Boetius, 2009a).

Although these ANME archaea have never been detected in methanogenic environment, the oxidation of methane by methanogens has been proposed a few decades ago (Zehnder, 1979) and also recently (Blazewicz et al., 2012). Based on an assumption that methanogenesis is a reversible reaction, the oxidation of methane by methanogens could be due to the shift of the reaction from the forward methanogenesis to the backward direction when the electron donors are not available. A number of studies indicate that AOM could be a pervasive bio-reaction in nature as AOM activity has been also detected in lake sediment and wetlands (Shoemaker and

Schrag, 2010, Borrel et al., 2011). Successful cultivation of AOM consortia from freshwater sediment and wastewater stream has also been reported in which nitrite and nitrate serve as the electron acceptors (Ettwig et al., 2010, Haroon et al., 2013). In addition to soluble electron acceptors-driven AOM, metal oxides, especially iron oxide, driven AOM in both freshwater and marine systems have been reported, though this AOM has not been fully understood (Beal, 2009, Borrel et al., 2011, Amos et al., 2012, Segarra et al., 2013). Like sulfate-driven AOM, these studies showed that AOM coupled to metal oxide reduction might also be a syntrophy between ANME archaea/methanogens and bacteria. For instance, when manganese oxide was provided, metal reducing proteobacteria were enriched together with ANME-3; the analysis of the 16S rRNA genes showed that ANME-1 and ANME-3 accounted for around 5% of the total in enrichment culture (Beal, 2009). In another study on crude oil contaminated aquifer, where *Geobacter* species were abundant in the presence of methanogens, $\delta^{13}C\text{-}CH_4$ increased above the reference level, which indicated a preference for $^{12}C\text{-}CH_4$ oxidation by microorganisms during iron reduction (Amos et al., 2012).

Metal-reducing bacteria, such as *Geobacter* species and *Shewanella* species, have been enriched on the anodes in MECs (Logan et al., 2006). For instance, they are able to anaerobically oxidize acetate to carbon dioxide via anaerobic citric acid cycle and transfer electrons from acetate to the anode through extracellular electron transfer (EET) (Logan, 2009); these metal-reducing bacteria are generally called anode-respiring bacteria (ARB) in MECs (Lee et al., 2008a). The AOM coupled to metal-reducing bacteria observed in nature implies that ARB could be coupled to ANME archaea/methanogens for AOM; no studies have demonstrated AOM by dissimilatory metal reducing bacteria using EET in MECs. Thus, it is hypothesized that ANME archaea assisted by ARB could form an AOM consortium on electrode surfaces, and

MECs could oxidize methane anaerobically. To demonstrate this syntrophic AOM interaction, MECs that had been inoculated with recycle activated sludge and enriched by acetate medium were operated with methane molecules as the sole electron donor. The goal of this chapter was fivefold. The first was to examine current generation exclusively from AOM in the MECs. The second was to identify dominant microorganisms responsible for AOM in biofilm anode with pyrosequencing. The third was to confirm AOM and identify AOM microorganisms in biofilm anode using stable-isotope probing (SIP) techniques integrated with denaturing gradient gel electrophoresis (DGGE). The fourth was to visualize the physical structure of the AOM consortium on anode surfaces with fluorescence *in situ* hybridization (*FISH*). The final was to quantify the rate of AOM in MECs.

5.2 Methods and materials

5.2.1 Inoculum and start-up of microbial electrochemical cells

The configuration of the sandwich-type MECs used in this study was the same to the one used in Section 3.3.1 except for a smaller anodic volume (280 ml). Figure 5-2 summarized the research goals of individual MECs, operating conditions, and operation period and other important features. Briefly describing, MEC 1 was operated for the start-up, phase I, and phase II. MEC 2 and 3 were run for the second SIP and isotope tests (Phase III). Finally, two H-type MECs were operated to measure AOM rate. Return activated sludge (10 ml, volatile suspended solids (VSS) concentration 3,050 mg/l) sampled from a local wastewater treatment plant was used as the inoculum to MEC 1. Acetate medium was fed to the MEC during initial acclimation (start-up in Figure 5-2). The composition of the acetate medium can be

found elsewhere (Torres et al., 2008b), except for a lower phosphate buffer saline (PBS) concentration of 50 mmol/l. The medium pH was around 7.30. After inoculation, the anode chamber was purged with N_2/CO_2 (80%/20%) for 30 minutes.

In the early stage (start-up and Phase I in Figure 5-2) of operation, the cathode chamber was filled with tap water. Mineral medium with the same composition of the anolyte was used as catholyte in the rest of this study. The catholyte was maintained in anaerobic condition by regularly purging with nitrogen or helium gas (99.999%, Praxair Canada). The catholyte was refreshed when the pH exceeded 10.

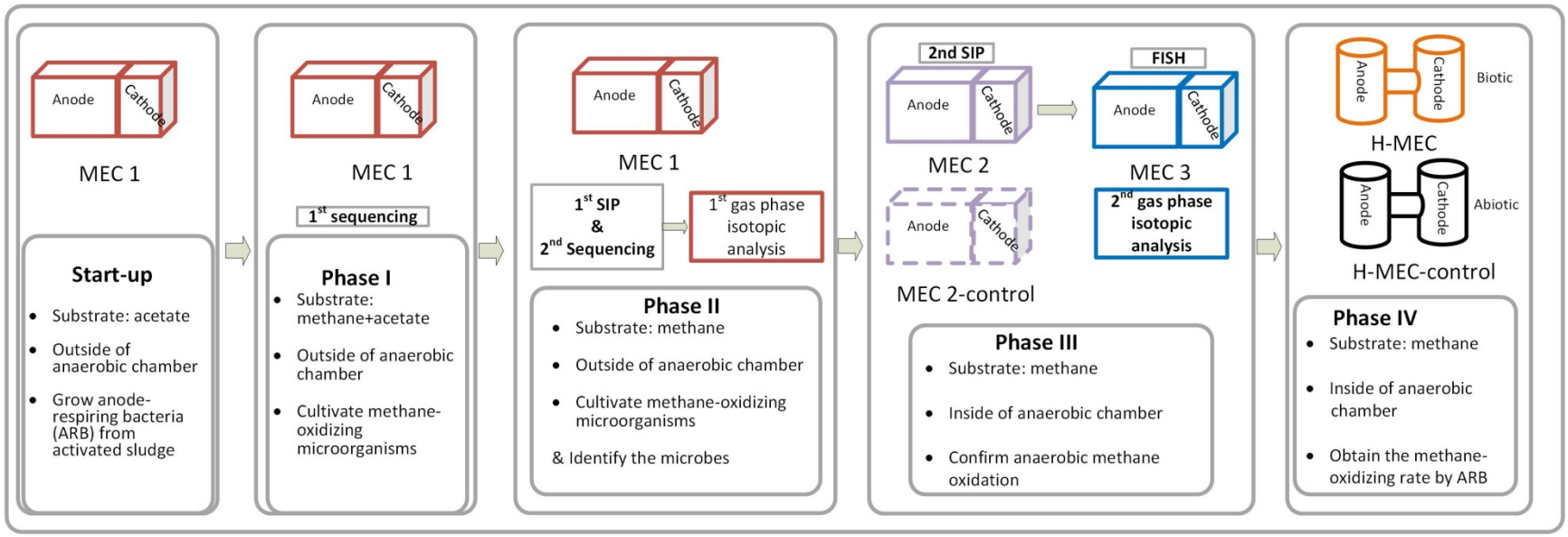

Figure 5-2. Organization of the MECs mentioned in this chapter. MECs with the same color and the same line type are the same reactor. MECs in dash lines were inoculated by the anolyte of the solid-line MEC with the same color. The change of color of the MECs indicates a biofilm transfer and re-inoculation with biofilm cell pellet. SIP stands for stable-isotope probing. All sequencing and SIP tests were conducted in between biofilm transfers. Two isotopic analyses of the head space gas (CO_2 and CH_4) are highlighted.

5.2.2 Cultivation strategy for enriching a methane-oxidizing consortium in microbial electrochemical cells

Overall, the acclimation of methane-oxidizing and anode-respiring microorganisms comprises three phases (Figure 5-2). The objective of the start-up step was to acclimate a regular anode biofilm using acetate medium (Figure 5-3). During phase I, acetate was fed together with methane so that the anode-respiring activity can be sustained while a major organic source was methane; in phase II and III, methane was the sole carbon and energy source. The only difference between phase II and phase III was that the MECs were operated in oxygen-free environment (inside an anaerobic chamber) during phase III to completely exclude O_2 permeation to the MECs.

During the start-up step, acetate (25 mmol/l) was used as the substrate until steady-state current density was achieved (the highest current density was 7.8 A/m^2 and 3.4 A/m^2, in fed-batch and continuous mode, respectively). The anode potential was poised at -0.4 V vs Ag/AgCl (RE-5B, BASi, USA) with a potentiostat (VSP-Biologic, Snowhouse Solutions, Canada) during the experiment. After four months of acclimation, the acetate medium was switched with methane-saturated medium to acclimate AOM-biofilm anode (Phase I in Figure 5-2). To stimulate ARB growth, acetate was intermittently injected to MEC 1 to reach acetate concentrations of 0.16 to 0.42 mmol/l. Acetate was only injected after the current was below 0.02-0.05 A/m^2. After confirming the AOM activity in phase I, the intermittent supply of acetate was stopped and the phase II operation started: methane molecules became the sole electron donor for microorganisms from phase II. In phase I and earlier phase II

(~day 200 to day 310), methane was supplied to the anode chamber using a gas re-circulation loop (Appendix, Figure A3). During the latter part of phase II (day 320 to day 670), methane gas was directly supplied to the MEC 1 with a methane gas cylinder (99.97%, Praxair Canada).

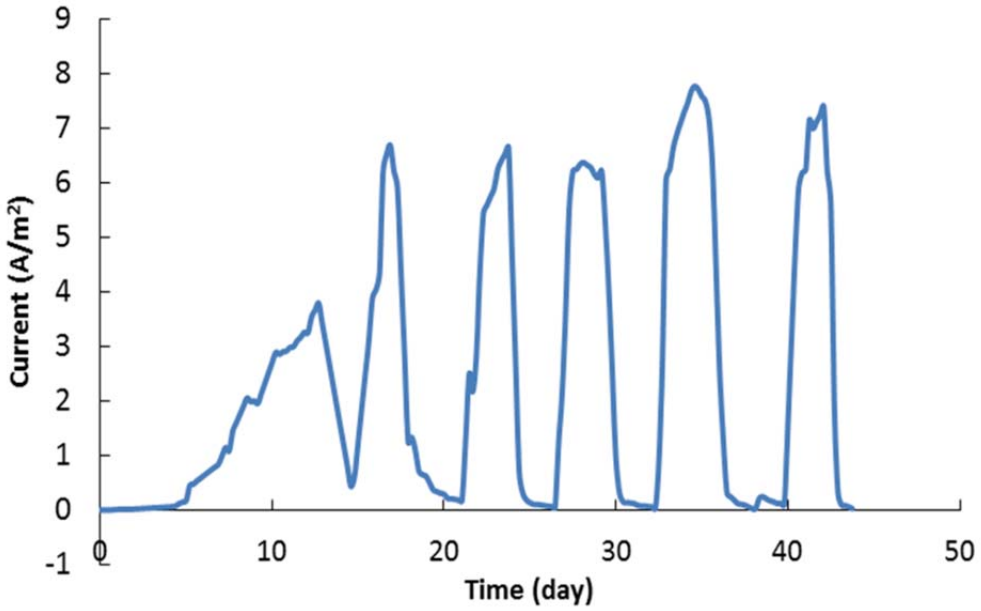

Figure 5–3. Current density of microbial electrochemical cell-1 during the start-up (Figure 5-2). The reactor was operated in fed-batch mode with 25 mmol/l acetate as substrate.

5.2.3 Demonstration of anaerobic oxidation of methane in microbial electrochemical cells (Phase I and Phase II)

To confirm that the electric current from MEC 1 is exclusively generated from AOM, two tests were designed: one in phase I (test 1) and the other in phase II (test 2). The electric current collected without dissolved methane in the anode chamber serves as the background signal, which should be smaller than the current with dissolved methane, provided that AOM occurs on the anode surfaces.

Test 1 was conducted by supplying liquid medium with and without dissolved methane into the anode chamber of MEC 1. At the beginning of the test, the catholyte and anolyte were conditioned by purging with methane gas (99.97%, Praxair Canada) for over half an hour. The reactor was then closed until the electric current was stable. After a stable current was obtained, methane-free mineral medium was anaerobically supplied into the anode chamber at a hydraulic retention time (HRT) of 4 hrs. To avoid oxygen contamination, this medium was continuously purged by nitrogen gas during feeding. When the electric current leveled off, the pump was turned off and nitrogen gas was switched to methane gas so that the medium gradually became methane-saturated. After over nine hours of purging with methane, the medium was supplied into the anode chamber again at the same HRT.

Test 2 was designed to show the electric current generation when methane gas and nitrogen gas supply were alternated while the anolyte was not exchanged during this experiment; this experiment was conducted in phase II. Methane gas had been continuously bubbled into the anolyte at flow rates of 6.7 to 8.3 ml/min for a few weeks until a stable electric current was achieved. Then, methane gas was switched to nitrogen gas, which allowed dissolved methane in the anolyte to decrease gradually. The supply of nitrogen gas was controlled at a similar flow rate of methane gas. When current was close to zero or negative values, methane supply was resumed to confirm current generation in MEC 1. Background current density without biofilm (~1.6 mA/m^2, Figure A7) was subtracted from the steady state current density to report the intrinsic current density from AOM. When volumetric reaction rate is reported, the unit is converted based on the volume of the anolyte (280 ml).

5.2.4 Biomass collection, DNA extraction, Sanger sequencing, and pyrosequencing (Phase I)

Before sequencing analyses, biofilm on the anode and in the anolyte was collected from MEC 1 (Phase I). Since the amount of biomass on the anode was minimal, the whole anode was sacrificed for biofilm collection. A pair of sterilized scissors was used for cutting the anode fiber. The short pieces of carbon fiber were re-suspended in PBS in a 50 ml falcon tube. The tube was shaken with a vortex mixer for 2 min at the highest speed to detach the biofilm. Next, the fibers were transferred to another falcon tube for a second extraction while the suspension from the first falcon tube was centrifuged. Maximum three extractions were conducted, depending on the amount of cell pellets recovered from the second extraction. For a better recovery of cells, the suspension was distributed into multiple 1.5 ml microcentrifuge tubes and centrifuged at 10,000 g for 3 min (Eppendorf 5424, Germany). To collect the planktonic cells, the anolyte was centrifuged in 1.5 ml microcentrifuge tubes at 10,000 g for 3 min (Eppendorf 5424, Germany). The cell pellets were then stored at -80˚C prior to further processing.

The DNA from cell pellets was extracted from both the biofilms and planktonic samples using MoBio PowerSoil kit (MO BIO Laboratories, USA), according to the manufacturer's protocol. The DNA concentrations were measured using a UV fluorometer (Qubit® 2.0 Fluorometer, Life Tech., USA). The DNA extracts were stored at -20°C before further analysis.

For cloning and Sanger sequencing, the universal bacterial primers 8F (5'-AGAGTTTGATCCTGGCTCAG-3') and 787R (5'-GGACTACCAGGGTATCTAAT-3') were used to amplify 16S rRNA gene of bacteria as described elsewhere (Ley et al., 2008, Ryu et al., 2012). PCR (25 μl reaction volume) were performed using the polymerase TaKaRa Ex Taq™ (Takara Bio Inc.) in a Bio-Rad Tetrad 2 Peltier Thermal Cycler (Bio-Rad, Hercules, CA) under the following cycling conditions: 1 initial denaturation step at 95°C for 5 min and 30 cycles of 1 min at 95°C, 1 min at 56°C, and 1 min at 72°C with a final extension step of 12 min at 72°C. PCR products were visualized in 1.5% agarose gels using GelStar Nucleic Acid gel stain (Lonza, Rockland, ME, USA). Selected PCR products were cloned into pCR®4 TOPO® vector and transformed to TOPO10 chemically competent *E. coli* cells as described by the manufacturer (Invitrogen, CA). Individual *E. coli* clones were then sub-cultured into 300 μl of Luria Broth containing 50 μg/ml ampicillin and screened for inserts using M13 PCR. The PCR products were submitted to the Children's Hospital DNA Core Facility (Cincinnati, OH) for sequencing using an Applied Biosystems Prism 3730XL DNA analyzer. Raw sequences were processed using Sequencher 4.10.1 software (Gene Codes, Ann Arbor, MI). Chimeric sequences detected using Bellerophon (Huber et al., 2004) were not included in further analyses. The clone libraries were compared using Naive Bayesian rRNA Classifier version 2.5 of Ribosomal Database Project (RDP) with 95% confidence threshold (Wang et al., 2007).

In addition to Sanger sequencing, bacterial diversity was assessed using 16S rRNA gene pyrosequencing analysis. Each sample was differentiated by using different barcodes or pyrotags linked to the universal primer 28F (GAGTTTGATCNTGGCTCAG) and coupled with 519R (GTNTTACNGCGGCKGCTG) as described by Dowd *et al* (2008). Barcoded libraries

and sequencing were performed at the Molecular Research Laboratory (Shallowater, TX, USA). These primers cover the V1, V2, and V3 hypervariable regions of the 16S rRNA and generate approximately 500 bases (*E. coli* position 28-519).

Raw sequences were processed using Sequencher 4.10.1 software (Gene Codes, USA). Chimeric sequences detected using UCHIME (Edgar et al., 2011) were not included in further analyses. The clone libraries were compared using Naive Bayesian rRNA Classifier version 10 of Ribosomal Database Project (RDP) with 95% confidence threshold (Cole et al., 2009). For 16S rRNA gene sequences, homology searches of DNA sequences in the GenBank (NR) database were undertaken with the National Center for Biotechnology Information (NCBI) BLAST (http://www.ncbi.nlm.nih.gov/BLAST/) (Altschul et al., 1997). The sequencing work was carried out by Dr. Hodon Ryu at USEPA. The data are not included in this thesis.

5.2.5 Stable-isotope probing of DNA and DGGE (Phase II and III)

During the whole AOM study, two SIP tests were conducted; one in phase II and the other in phase III, as indicated in Figure 5-2. The first DNA-SIP was conducted in the middle of phase II, and the second DNA-SIP was carried out in latter phase III with MEC 2. The incubation time with 99% $^{13}CH_4$ (Cambridge Isotope Laboratories, Inc., USA) was 9 days in the first SIP and 24 days in the second SIP. Cloning and Sanger sequencing was only applied during the first SIP.

The extracted DNA was separated in CsCl solution by ultracentrifugation (Beckman Coulter, VTi 65.2 rotor) at 177,000 g and 20 ^{o}C under vacuum for around 36 to 40 hrs. Based on the difference in the buoyant density, DNA molecules were separated along the CsCl density gradient with ^{13}C-containing molecules occupying

lower levels in the centrifuge tube. The separated DNA molecules were retrieved by gradient fractionation afterwards. During the gradient fractionation, mineral oil was pumped from the top of the centrifuge tube and 12 fractions of the DNA samples were collected from the open bottom. The 16S rRNA genes of bacteria and archaea in all fractions were amplified by PCR. For bacterial sequencing, the V3 region of the 16S rRNA gene was amplified using modified 341F and 518R primers (Bartram et al., 2011). Primer sets 958r and 109f and SA1fgc/SA2fgc and PARCH519r were used for amplifying archaeal genes. The fractionated sections were subsequently analyzed by DGGE. The DGGE gel contained 10% acrylamide and bis-acrylamide (37.5:1) with a denaturing gradient from 30-70%. The 100% denaturant is 7 mmol/l urea and 40% of deionized formamide. The amount of samples loaded to each well was 5 μl. The samples were loaded sequentially so that in the final DGGE profiles, the left and middle lanes correspond to the lower and middle part of the fractions in the centrifugation tube. The gels were run at 85 V for 840 min (14 hrs). After the electrophoresis, the gels were stained by SYBR green stain (Molecular Probes, USA) for 2 hrs and then visualized on a Typhoon scanner (Amersham Biosciences, USA). For agarose gel electrophoresis, 1 to 1.5% agarose in Tris-acetate buffer (TAE) was used. The electrophoresis was run at 85 V for 20 or 30 min.

5.2.6 Isotopic analyses of carbon dioxide from anaerobic oxidation of methane in microbial electrochemical cells (Phase II and III)

To further confirm AOM in MECs, the isotopic composition of the carbon dioxide was analyzed for the headspace of MEC-1 and -3 operated with a gas re-circulation loop (Figure A3). Totally two isotopic analyses were conducted, one in phase II and the other in phase III (Figure 5-2). The first isotopic analysis of the carbon dioxide

from AOM was conducted 5 months after the first SIP. The duration of incubation or gas collection was 8.9 days; the second isotope analysis was done around 2 months after the second DNA-SIP with 9 day incubation.

To increase the headspace volume, a gas re-circulation loop with a 250 ml gas sampling bulb (Supelco, Sigma-Aldrich Canada) was used to collect the gas. Before the batch incubation, the anolyte was thoroughly purged with regular methane gas, and the loop was filled with methane gas as well. A digital pump (Masterflex, L/S, Cole-Parmer Canada) was used to maintain a gas recirculation rate of 7 ml/min. The pH of the anolyte was measured before and after the incubation. The gas composition was monitored with a GC-TCD method (Section 5.2.10). The extraction of carbon dioxide and analysis of isotopic composition were carried out by the University of Waterloo-Environmental Isotope Laboratory (uwEILAB). Methane gas (99.97%, Praxair Canada) was sent to the same lab for ^{13}C analysis.

The fractionation factor of carbon was calculated based on equation 5-1 (Mackenzie and Lerman, 2006). Raw data can be found in Appendix Section D.

$$\propto_{CH4/CO2} = \left(\frac{^{13}C}{^{12}C}\right)_{methane} / \left(\frac{^{13}C}{^{12}C}\right)_{carbon\ dioxide} \qquad (5\text{-}1)$$

The ratio of ^{13}C to ^{12}C can be calculated with equation 5-2 (Mackenzie and Lerman, 2006).

$$\left(\frac{^{13}C}{^{12}C}\right)_{sample} = (\delta^{13}C \times 1000 + 1) / \left(\frac{^{13}C}{^{12}C}\right)_{standard} \qquad (5\text{-}2)$$

Where the standard carbon isotope atomic ratios are $\left(\frac{^{13}C}{^{12}C}\right)_{standard,PDB}$=0.01122 and $\left(\frac{^{13}C}{^{12}C}\right)_{standard,VPDB}$=0.011056.

5.2.7 Fluorescence *in situ* hybridization of the anode biofilm (Phase III)

The 16S rRNA-targeted oligonucleotide probes used in this study are listed in Table 5-1. These probes comprised domain-specific ones for bacteria and archaea (Raskin et al., 1994, Richter et al., 2007); family-specific probes for *methanobacterium* (Raskin et al., 1994); and a genus-specific probe for *Geobacter* (Richter et al., 2007). For *in situ* hybridization, the probes for general archaea and *Methanobacteriaceae* were labeled with fluorescein (green fluorescence) and the probes for general bacteria and *Geobacter* species were labeled with TAMARA (red fluorescence). All the probes were purchased from Life Technologies Inc., Canada.

The cell suspension or anode fibers were fixed for one hour with 2% paraformaldehyde, washed with PBS and then fixed on glass slides. Serial ethanol solution (50%, 80% and 96%) was used to dehydrate the samples. Hybridizations were performed at 46°C for 5 hrs with hybridization buffer (0.9 mol/l NaCl, 20 mmol/L Tris-HCl [pH 7.2], 0.01% sodium dodecyl sulfate) containing 5 ng of each labeled probe per ml. The hybridization stringency was adjusted by adding formamide to the hybridization buffer (5% for EUB338; 35% for ARC915, MB1174, and 30% for Geo3 a, b, and c). The washing step was done at 48°C for 30 min with washing buffer containing the same components as the hybridization buffer except for the probes. The hybridized samples were observed via a Zeiss Axiovert 200 microscope equipped with a Zeiss LSM510-Meta confocal module and a Zeiss epifluorescence microscope (Axio Scope.A1) (Figure 5-10 and Figure A8).

Table 5-1. Fluorescently labeled oligonucleotide probes used in this study.

Probe name	Generic name	Target	Sequences (5′ to 3′)	Reference
ARC915	S-D-Arch-0915-a-A-20	General archaea	GTGCTCCCCCGCCAATTCCT	(Raskin et al., 1994)
EB338	S-D-Bact-0338-a-A-18	General bacteria	GCTGCCTCCCGTAGGAGT	(Richter et al., 2007)
MB1174	S-F-Mbac-1174-a-A-22	Methanobacteriaceae	TACCGTCGTCCACTCCTTCCTC	(Raskin et al., 1994)
Geo3 a, b, and c	S-G-Geob-0818-a-A-21	Geobacter cluster*	CCGCAACACCTAGTACTCATC	(Richter et al., 2007)
	S-G-Geob-0818-b-A-21		CCGCAACACCTAGTTCTCATC	
	S-G-Geob-0818-c-A-21		CCGCAACACCTGGTTCTCATC	

*the three probes were evenly mixed to give the maximum coverage of the cluster

5.2.8 UV-Vis spectrum and nuclear magnetic resonance spectroscopy (Phase III)

To qualify shuttling compounds associated with EET, the UV-Vis spectra of the biofilm suspension were measured with a spectrophotometer (Genesys™ 10S, Thermo Sci. Canada). Sodium dithionite (85%, Sigma-Aldrich Canada) was used for

cytochrome reduction. All solutions were deoxygenated before they were moved into an anaerobic chamber. While inside of the chamber, 1 ml of sodium dithionite solution (final concentration 10 mmol/l) and 1 ml of biofilm suspension were mixed in an UV quartz cuvette. The cuvette was sealed with its stopper and then taped for better protection against air. The mixture was left on a rack for 1 min so that the reaction can be completed. A full scan (190 nm to 1100 nm) was done on all the samples.

Nuclear magnetic resonance (NMR) analysis was carried out to qualify intermediate compounds from AOM in biofilm anode. D_2O (Deuterium oxide, 99.9% D, Aldrich Canada) was added (10%, vol/vol) to the supernatant from biofilm suspension in order to provide a lock signal. High resolution magic angle spinning (HRMAS) was performed. The proton NMR was obtained on a 600 MHz NMR (Utrashield, Bruker, USA) with proton resonating at 600.13 MHz. Since the signal from water molecules was enormous and affected signals from other compounds, water suppression in controlled gradient was applied to reduce the signal from water. The NMR was run at 298 K and at 128 scans with a one second delay. NMR analyses were carried out by Janet Venne from the Department of Chemistry.

5.2.9 Estimation of the rate of anaerobic oxidation of methane in microbial electrochemical cells (Phase IV)

In phase IV, two H-type MECs made up of glass (Adams & Chittenden Scientific Glass, USA) were used, one MEC was operated as a bioreactor (H-MEC) and the other was an abiotic control (H-MEC-control, Figure 5-2). Graphite bars (McMaster Carr, Canada) were used as the anode. The graphite bars were connected to copper

wire with silver filled ink (Techspray, Trace Technologies Conductive Pen, USA) and silicone sealant. A day later, the connection was examined by measuring the resistance of the electrodes (179 digital multimeter, Fluke Corporation, USA), which had almost the same value of a piece of graphite bar (~0.3 Ω). The two electrodes were thoroughly dried at room temperature for over a week before any experiments. Stainless steel was used as the cathode. An Ag/AgCl reference electrode (RE-5B, BASi, USA) was installed in the H-MEC to monitor electrode potential. AEM was used to separate the anode chamber from the cathode chamber. Anode potential was fixed at -0.25 V using the potentiostat during the experiments. The same mineral medium (mentioned in the last section) was used. Septa (Hamilton High Temperature Septa, PTFE/silicone, Canada) were equipped in the inlet and outlet parts of the H-MECs, for easy sampling and venting.

The liquid volume inside of the anode chamber was 263 ml, leaving around 88 ml of headspace. The mineral medium inside anode was purged by methane (99.97%, Praxair Canada) after inoculation. The reactor was then moved into an anaerobic chamber. During the acclimation of the H-MEC, methane was supplied as the sole substrate. The medium was replaced after the first batch cycle of current generation, which demonstrated a successful attachment of AOM-ARB biofilm. Methane-dependent current generation was tested thereafter. Methane gas (17 L cylinder, 99.8%, Praxair Canada) was purged into the anolyte every time when the electric current dropped below zero. To avoid vacuum inside of the reactor, sampling only occurred at the end of tests before gas purging. Dissolved methane was measured with a GC-FID (gas chromatography-flame ionization detector) method.

To quantify the loss of methane due to diffusion through septa and the AEM, an abiotic control reactor (H-MEC-control, Figure 5-2) was operated. The same control test was repeated for six times. MilliQ water, instead of mineral medium, was

used in control study. Methane was purged into the anode chamber for 1-2 hrs, and the dissolved methane concentration was measured. The reactor was then sealed. After a certain time, the dissolved methane was measured again. The mass transfer of methane through the septa and the AEM was characterized by a mass transfer equation (equation 5-3). Loss of methane via diffusion was excluded from the AOM rates reported in the following sections. The electric current and results from the abiotic control study can be found in Appendix Section E.

$$-\frac{dvC}{dt} = Ak(C - C_g/H) \qquad (5\text{-}3)$$

Where v is the volume of the liquid inside of the H-MEC (l); A is the effective surface area of the septa and AEM (cm^2); C and C_g are the concentration of methane in liquid and the hypothetical concentration of methane in the atmosphere, respectively (mg/l); H is Henry's law constant; k is the overall mass transfer coefficient of methane through septa and AEM (cm/day). In this study, C_g is assumed to be zero.

5.2.10 Quantification of acetate and dissolved methane

Acetate quantification can be found in Section 3.3.5.1. During the course of this study, two dissolved methane quantification methods were developed. The first method relies on a GC (SRI 310C, SRI Instruments, USA) with a thermal conductivity detector (TCD). For details of this method, refer to Section 3.3.5.2. The method developed on the GC-TCD was mainly used during the start-up step and phase I (Figure 5-2). Since frequent dissolved methane quantification became necessary after phase I, the volume of liquid sample cannot be as large as over 10 ml. Hence, a method on GC-FID was developed, which only required 2 ml of liquid sample for each measurement. From phase II, dissolved methane was measured with the GC-FID method.

The GC-FID was equipped with a six feet Poraqak Q column (1/8 2 mm 80/100 Ni, Agilent Technologies, VWR Canada). Calibration curves were built with dilute methane-saturated water (0.25%, 0.5%, 5%, 10%, 80%, and 100% of saturation, all gases were from Praxair Canada). A Varian 8200 autosampler was used for sampling. Hexane and methanol were the solvent for syringe cleaning. Each vial was quantified for three to four times, and triplicate or quadruplicate sampling was applied each time. The temperature of the inlet, detector and oven was set at 220 ^{o}C, 250 ^{o}C, and 110 ^{o}C, respectively. Samples were not filtered.

5.3 Results and discussion

5.3.1 Electric current profiles (Phase I to III)

Figure 5-4 plots the current density during this study and the time points of major tests and analyses in corresponding phases. In phase I, the current density ranged from 12 to 242 mA/m^2 (all current densities reported here excluded the background current, which can be found in Appendix Section F), which is deemed as a compound value caused by acetate oxidation and methane oxidation (Figure 5-4A, Phase I). After a month of growth with methane as the sole substrate (Figure 5-4B, Phase II), the electric current dropped to around 2.5 mA/m^2 (day 330 in Figure 5-4B), an order of magnitude lower than that in phase I. When the current density became stable, a gas purging test (Test 2 in Section 5.2.3) was designed to confirm the current production was from AOM. The electric current became zero or negative when nitrogen gas (99.999%, Praxair Canada) was continuously supplied. The drop of current implies that AOM occurs in the MEC. On the resumption of methane supply, the current recovered rapidly (day 381 to 383 in Figure 5-4B, Phase II); on day 423,

the biofilm on the anode was sampled for sequencing (Figure 5-4B, Phase II, the first SIP), and a new biofilm anode was cultivated with methane-medium (Figure 5-4, day 580 to day 670). Following the growth of a new biofilm anode, the current density reached a higher level, ranged from 7.9 to 8.4 mA/m^2 (Figure 5-4B, Phase II, day 580-590).

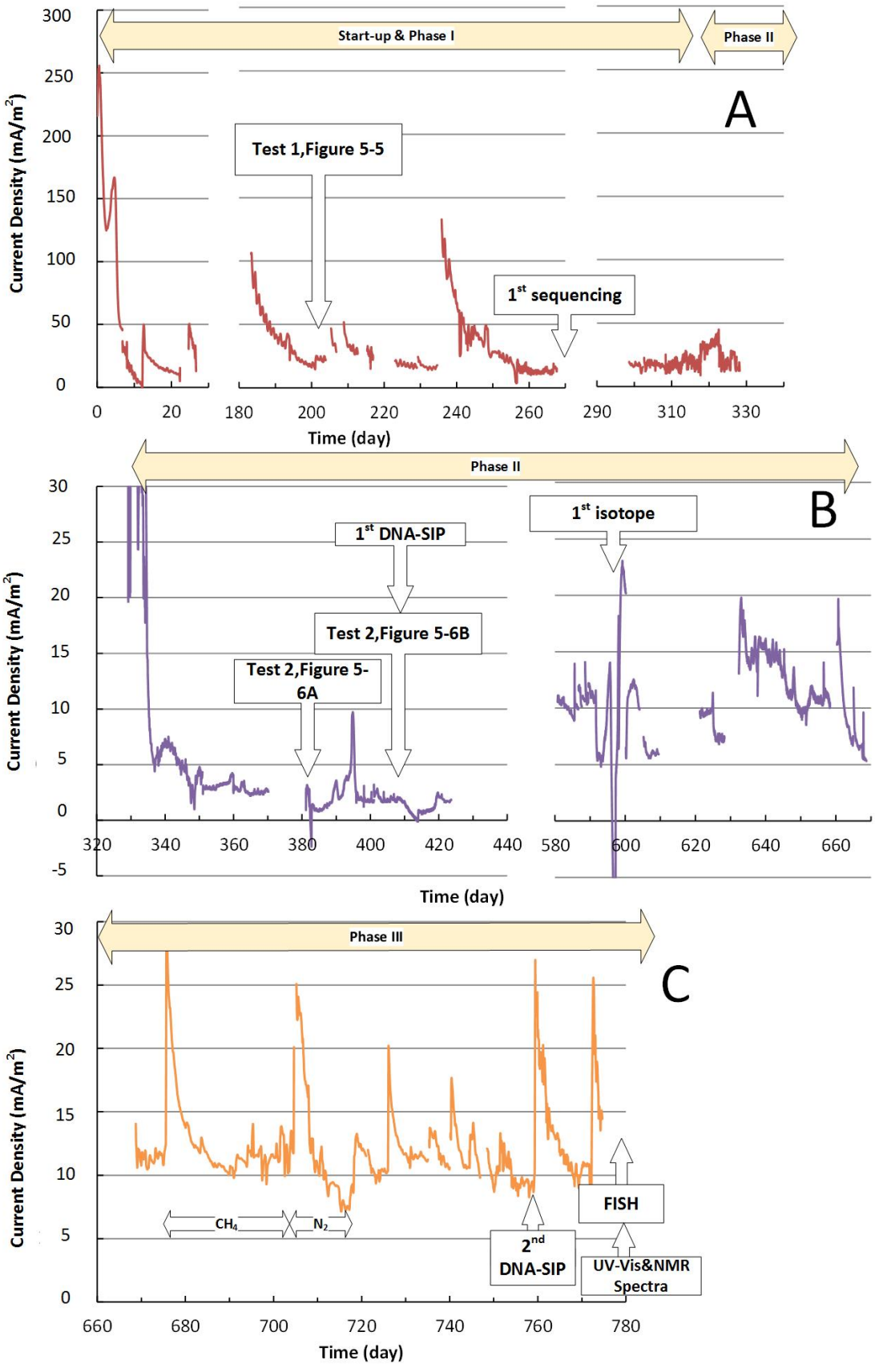
Start-up & Phase I
Phase II
A
Test 1,Figure 5-5
1st sequencing
Current Density (mA/m2)
Time (day)
Phase II
B
1st DNA-SIP
Test 2,Figure 5-6B
Test 2,Figure 5-6A
1st isotope
Current Density (mA/m2)
Time (day)
Phase III
C
CH4
N2
2nd DNA-SIP
FISH
UV-Vis&NMR Spectra
Current Density (mA/m2)
Time (day)

Figure 5–4. Electric current profiles from the main anaerobic methane oxidizing-microbial electrochemical cell. A shows the current during the acclimation phase when acetate and methane co-existed (phase I); B shows the current when only methane was supplied as carbon and energy source (phase II); C shows the current profile when the microbial electrochemical cell was operated inside of an anaerobic chamber (phase III). The second isotopic analysis of carbon dioxide was done with microbial electrochemical cell-3 and not highlighted in this figure. The current spikes in C are mainly caused by the electric charge accumulation in biofilm anode, the capacitance effect, when the microbial electrochemical cell is disconnected from the potentiostat.

Although MEC 1 (Phase I and II) was sealed and methane gas was continuously supplied into the anolyte, oxygen permeation through tubing lines, rubber gaskets, or even Plexiglas® could create micro-aerobic conditions in the anode chamber of MEC-1, which might cause aerobic methane oxidation. To rule out oxygen contamination and create absolute anaerobic conditions, MEC 2 and MEC 3 were operated inside the anaerobic chamber (Phase III). Figure 5-4 C shows the current generation for MEC 3 run inside the anaerobic chamber. Except for peak current densities, the average of steady-state current density was 11 mA/m^2. This result evidently shows that AOM coupled to EET generated current in MEC 3.

To reconfirm AOM in the MEC, a gas re-circulation loop with a 500 ml glass bottle in the anaerobic chamber was initiated: alternate gas supply of CH_4 and N_2 on day 675 to day 720 (Figure 5-4C, highlighted by double arrows). A current density of around of 10.4 mA/m^2 was achieved (day 680 to day 700 in Figure 5-4C). On day 705 the methane gas in the 500 ml glass bottle was replaced by nitrogen gas (99.999%, Praxair Canada), and current density decreased by 2.9 mA/m^2 as shown in Figure 5-4 C. A decline of current reconfirmed anaerobic methane oxidation coupled to EET in MEC 3. When mineral medium was being refreshed, MEC 3 was switched from closed circuit mode to open circuit mode for around 30 min to 1 hour. The current

spikes in the current density profile were repetitively observed at every open-closed circuit switch (Figure 5-4 C), which supports the capacitance effect of anode biofilm (Uría et al., 2011). Under open circuit mode, ARB metabolism continues for a while and hence the oxidized forms of intracellular and extracellular electron carriers associated with EET are temporarily reduced–electrons storage in biofilm anode or the capacitance effect. Charged biofilm anode will transfer to the electrons to the anode as soon as the anode is re-connected to the cathode (i.e., closed-circuit mode), leading to an instant sharp increase of current density (Uría et al., 2011, Bonanni et al., 2012). Literature reported that the total accumulated charges usually increase with increasing open-circuit time, ranged from several mC to 177 C in a few minutes to around two hours (Uría et al., 2011, Deeke et al., 2012). In this study, significant amount of electric charges from 0.2 C to 11 C was observed at the moments of open and closed circuit switch, which is within a normal range as reported in literature. The accumulation of charges also demonstrates that the ARB were metabolically active with dissolved methane as the carbon/energy source.

5.3.2 Demonstration of methane-dependent current production

5.3.2.1 Current production with and without dissolved methane (Phase I and II)

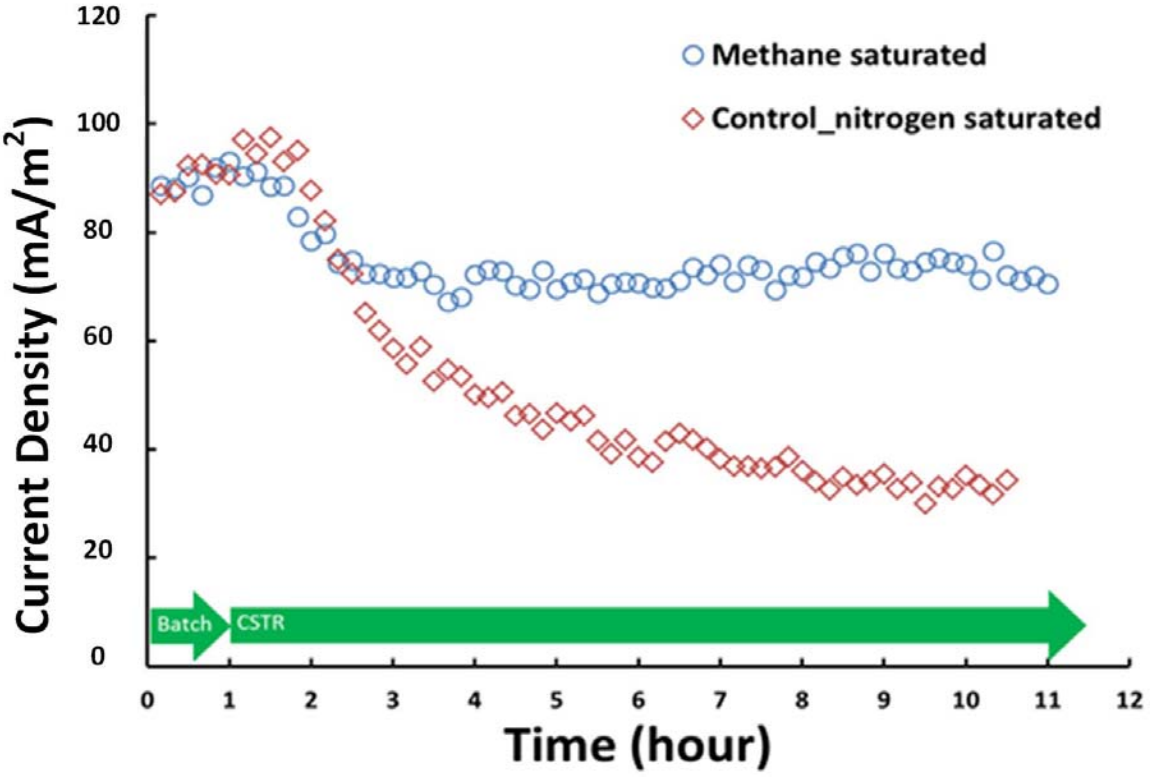

Figure 5–5. Electric current profile of control test and test with continuous supply of methane-saturated mineral medium (both with 10 mmol/L sodium bicarbonate as additional carbon source) in microbial electrochemical cell-1 (Phase I, Figure 5-2). After one hour, the microbial electrochemical cell was switched from batch mode to continuous mode as indicated by the arrows. The area in between two curves is attributed to dissolved methane oxidation. HRT=3 hrs.

Theoretically, the observed electric current originates from endogenous decay in anode biofilm and movement of ions through the membrane when no electron donors are available. This background current can serve as a control signal so that a higher electric current in the presence of dissolved methane can be a proof of AOM coupled to EET. Based on this reasoning, two qualitative tests were designed to demonstrate this anaerobic methane oxidation by the acclimated anode biofilm (refer to Section 5.2.3). Figure 5-5 shows the results for the first test using MEC 1 (Phase I). The current densities from O_2-free mineral medium and CH_4-saturated mineral medium were plotted together for comparison. When methane was absent, the electric current gradually decreased with time and then leveled off. Stable background current density of 33.0±1.7 mA/m^2 (9.5 hour to 10.5 hour) was detected after eight hours of feeding, which can be attributed to the endogenous decay of microorganisms and the trans-membrane movement of ions. When the same mineral medium was saturated with methane, a higher current density of 72.0±2.2 mA/m^2 was obtained. Stable and higher current density in the presence of dissolved methane clearly indicates that AOM is coupled to EET for current production in MEC 1.

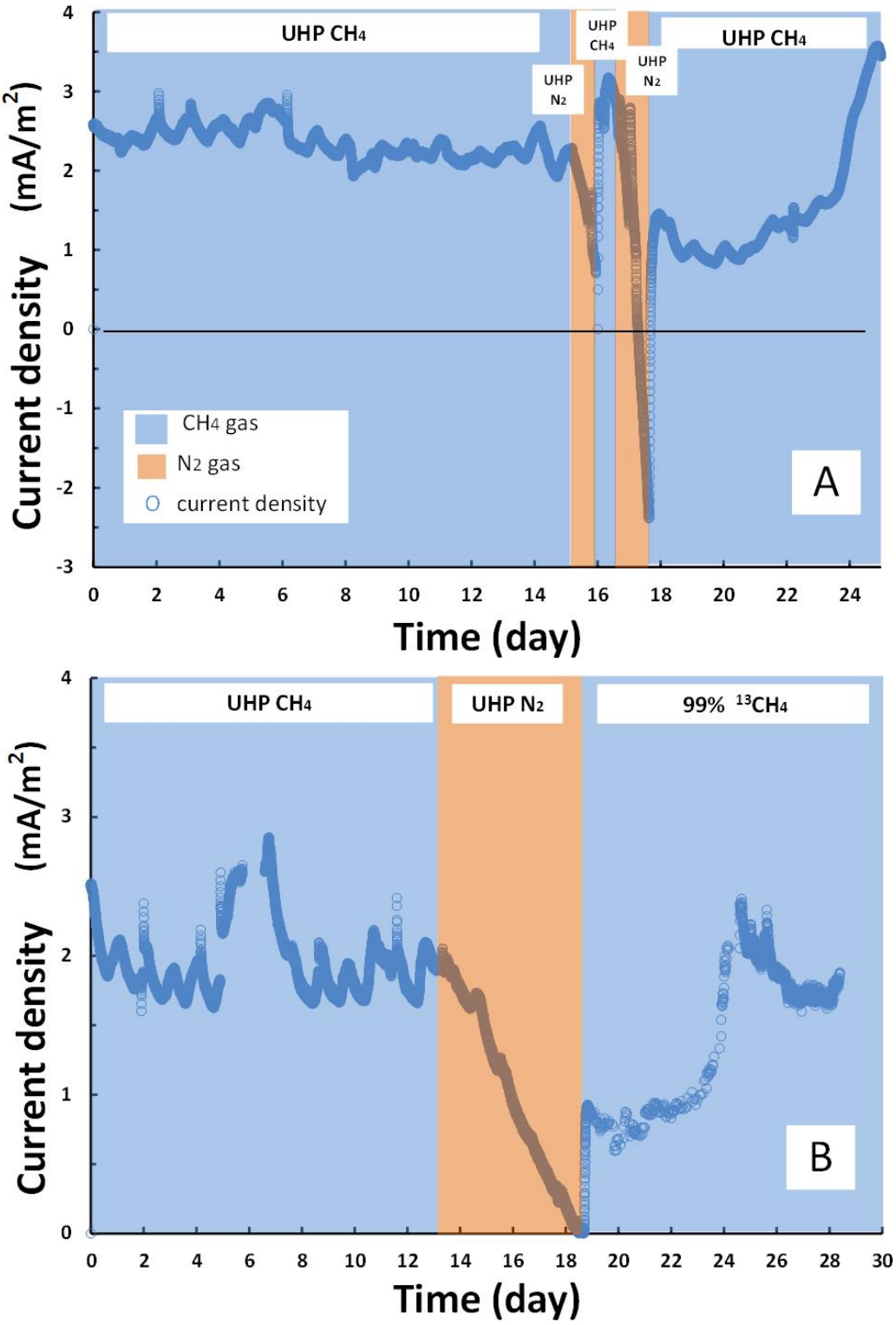

Figure 5–6. Methane-dependent electric current generation in microbial electrochemical cell-1 (Phase II): A shows alternate continuous methane and nitrogen

supply; B shows the electric current profile before and after the first DNA-SIP incubation.

To demonstrate a quick response of the anode biofilm to changes in dissolved methane concentration, a second test was designed. Figure 5-6 shows the results of gas purging tests with MEC 1 (Phase I). Nitrogen (99.999%, Praxair Canada) was continuously purged into the anode chamber, which had been saturated with methane before; under this condition, dissolved methane concentration gradually decreased with time. After the first drop of current down to 0 mA/m^2 in Figure 5-6A, methane gas supply was resumed and the current density immediately recovered to 3.2 mA/m^2. After around a day of methane supply, nitrogen was supplied into the MEC again but for over 20 hours. As shown in Figure 5-6A, the current density dramatically dropped to -2.5 mA/m^2 when nitrogen gas was sparged into the anode chamber. Upon the resumption of methane supply, current density increased by 3.8 mA/m^2 within 8 hours. Figure 5-6B shows the same pattern of current density to nitrogen/methane gas supplies: gradual drop of current density with N_2 sparging and the fast recovery of current density with methane gas provision. These results clearly show that current is generated via AOM.

5.3.2.2 Isotopic analyses of the headspace gas (Phase II and III)

In the first analysis (Phase II), the final $\delta^{13}C$ of carbon dioxide accumulated in 8.9 days are -56.4 and -58.4 (duplication). The fractionation factors (substrate/product) from these two duplications are 1.020 and 1.023 (CH_4/CO_2), respectively, which are close to those commonly observed in AOM environment (Holler et al., 2009). In the second analysis (Phase III), the $\delta^{13}C$ of carbon dioxide is +4.110, which indicates ^{13}C has been enriched in the carbon dioxide. Since this $\delta^{13}C$ value is much higher than the

background values, -37.14 and -37.23, which belong to the methane used as the feed, it is concluded that the $^{13}CH_4$ (99% $^{13}CH_4$) supplied during the incubation phase for the second DNA-SIP had been consumed and the heavy carbon was further oxidized to carbon dioxide.

With regard to oxygen in carbon dioxide, the $\delta^{18}O$ (-11.355) in carbon dioxide is a little lower than $\delta^{18}O$ (-10.19 and -10.11) in water, and these numbers are in a typical range of $\delta^{18}O$ of surface water. The slightly lower $\delta^{18}O$ of the oxygen from carbon dioxide indicates that water might be a source of oxygen in carbon dioxide. However, the $\delta^{18}O$ data are not be solid enough to bolster the speculation that H_2O is an oxygen source for CO_2. To extract oxygen atom from water molecules is energy-intensive, which means that exogenous energy is essential for this oxygen extraction process. According to the Gibbs' free energy change of AOM in MECs at pH 7 (Table A5), -38.6 kJ/mol CH_4, the microorganisms that conduct AOM coupled to EET in biofilm anode are living close to thermodynamic limits, and these microorganisms would not prefer to invest considerable energy for cleaving H_2O molecules for oxygen molecules. Therefore, oxygen elements in intracellular or extracellular substances (e.g., acids, alcohols, or ethers) formed during endogenous decay may serve as an oxygen source of carbon dioxide in AOM-EET. Future study is necessary to elucidate the source of oxygen for AOM-EET.

5.3.3 Quantification of the rate of anaerobic oxidation of methane coupled to extra-cellular electron transfer (Phase IV)

The AOM rates in the H-MEC ranged from 0.012 to 0.027 μmole e^-/hr/cm^3, which are one order of magnitude higher than that in the sandwich-type MEC (0.00083-0.0053 μmole e^-/hr/cm^3). The higher methane oxidation rate in the H-MEC supports that

graphite bars could be more efficient than carbon fibers and carbon felt for ARB growth and current generation (Torres et al., 2008a, Zhou et al., 2011). Table 5-2 compares AOM rates coupled with various electron acceptors, including sulfate, nitrite, nitrate, metal oxides, and conductive solids. The rates of AOM coupled with sulfate, nitrite, or nitrate generally falls in the range of 0.0475 to 76.6 μmole e^-/hr/cm^3. In comparison, the rates of AOM with solid electron acceptors (metal oxides) are one to three orders of magnitude lower than the AOM rates using soluble electron acceptors, ranging from 0.008 to 0.0128 μmole e^-/hr/cm^3. The AOM rates in the H-type MEC are in between these AOM rates from metal-oxide electron acceptors and soluble electron acceptors. This comparison indicates that AOM on electrodes is comparable to and even faster than the AOM coupled to solid metal oxides.

In general, the low methane oxidizing rates indicate that the initial activation of methane would be a rate-limiting step in all AOM reactions since (1) the reduction of sulfate or nitrate with other organic substrates, such as acetate, is approximately 40-200 times faster (Elferink et al., 1998, Tugtas and Pavlostathis, 2007) and (2) anode respiration in a *Geobacter*-dominant MEC with acetate as the substrate usually generates a few A/m^2 of electric current, which are at least three orders of magnitude higher than AOM in MECs. Researchers (Caldwell, 2008, Knittel and Boetius, 2009b, Scheller et al., 2010) usually attribute the observed low AOM rates to (1) the high activation energy required to break the first C-H bond in methane molecule, which is 439 kJ/mol CH_4 and (2) the thermodynamic constraint of AOM reactions, a $\Delta G^{0\prime}$ of -34.4 kJ/mol CH_4 using sulfate as an electron acceptor. However, the dissociation of a C-O bond in acetate by Coenzyme A (CoA) is in a similar range, 452 kJ/mol acetate (Darwent, 1970) and sulfate-driven acetate oxidation has a similar $\Delta G^{0\prime}$ of -52.4 kJ/mol acetate when H_2S and HS^- are the reduced forms of sulfate. In MECs fed with acetate, the $\Delta G^{0\prime}$ is -69.5 kJ/mol acetate when the anode is poised at -0.4 V vs Ag/AgCl

reference electrode. Therefore, low Gibbs free energy gain and high C-H bond energy of methane cannot satisfyingly explain the low AOM rates. A possible reason of the low AOM rates could be the nonpolar structure of methane, which causes low solubility in water (1.4 mmol/l at room temperature and 1 atm) compared with acetate (15 mol/l of sodium acetate at room temperature). Furthermore, the different molecular structure may also cause different behaviors of the enzymatic reactions. For example, study on the enzymatic activities of CoA in activating acetate shows a rate of 40 μmol/min/mg (Glasemacher et al., 1997), whereas methyl-coenzyme M reductase (MCR), the enzyme responsible for activating methane in reverse methanogenesis, only has a rate from 11.4-70 nmol/min/mg (Scheller et al., 2010). These values are in accord with the reported reaction rates in sulfate and nitrate-driven acetate oxidation (Elferink et al., 1998, Tugtas and Pavlostathis, 2007) and common AOM rates compiled in Table 5-2, which confirm the reasoning that the inherent characteristics in the biochemical aspect of the methane activation reaction lead to slow AOM rates.

Table 5-2. Summary of commonly observed rates of anaerobic oxidation of methane in literature and the observed methane oxidizing rates in this study with the corresponding details.

Bioreactor and inoculum	Rate of AOM (μmole e^-/hr/cm^3)	Concentration of dissolved methane (mg CH_4/L)	Growth rate, day^{-1}	Residual methane, mg/L	Doubling time, months	Electron acceptors
Incubated methane seep sediment (Beal, 2009)	0.0475	24 (calculated based on Henry's law)	N/A	N/A	N/A	Sulfate
	0.0128					Manganese
	0.00548					Ferric iron
Continuous bioreactor with inoculum from anoxic methane cold seep sediment (Girguis, 2003)	0.00274±0.00116	24	N/A	N/A	N/A	Electron acceptors in filtered seawater

The same as above (Girguis et al., 2005)	0.09223±0.00768		<0.01	N/A	>3	sulfate
Sediment from a Fjord (Hansen, 1998)	~ 0.005	~ 6.4 – 21	N/A	N/A	N/A	N/A
Sediment cores collected near gas hydrate (Joye, 2004)	~ 0.167 (peak value, Figure 6B)	~24	N/A	N/A	N/A	sulfate
sediment sample collected at the southern hydrate ridge, north-east Pacific (Nauhaus et al., 2007)	76.6 μmole e^-/hr/g dry sediment	336	0.003	N/A	7.5	sulfate
Enriched culture from Ooijpolder ditch sediment (Ettwig et al., 2010)	0.315-0.52	1.67-2.54 or higher	N/A	1.3-2.2 mg/L	N/A	nitrite
Sediments from Dover Bluff and Hammersmith Creek (Segarra et al., 2013)	~3.3×10^{-5}-0.0089	N/A, headspace is 100% methane	N/A	N/A	N/A	sulfate
	~8.3×10^{-5}-0.0013					nitrate
	~8.3×10^{-5}-0.0042					Ferric iron
	~8.3×10^{-5}-0.0008					manganese
sediment from the Twentekanaal, a canal in the Netherlands (Raghoebarsing, 2006)	0.107±0.01	0.95 of saturated value at 25 °C			Several weeks	Nitrite and nitrate
Inoculated by RAS from Waterloo Wastewater Treatment Plant (this study)	0.012-0.027	4.9-9.3	N/A	0.17-1.0	N/A	Graphite bars
	0.00083-0.0053	6.2-22.4		<detection limit of GC-TCD		Carbon fibers

5.3.4 Stable-isotope probing of DNA and DGGE profiles of the anode microbial communities (Phase II and III)

In regard to bacteria, the overall number of species decreased from the first to the second analysis (bacteria in Figure 5-7 and Figure 5-8). The decreasing diversity implies that an absolute anaerobic condition can selectively enrich a small number of bacteria. In both analyses, *Geobacter* species dominated the community. Two methanotrophs (*Methylomicrobium* and *Methylomonas*) were labeled by heavy carbon in the first analysis (Phase II). Noticeably, the aerobic methanotroph, *Methylomonas*, disappeared after enrichment in absolute anaerobic condition (Phase III), which means they were not involved in the AOM. In contrast, *Methylomicrobium* species were still present when oxygen was absent. Since *Methylomicrobium* species were reported to inhabit in marine sediment (Jensen et al., 2008), they might be able to respire on other electron acceptors besides oxygen. *Bradyrhizobium* species, which was abundant in the first analysis, faded in the second analysis. Species from this genus are known to be nitrogen fixers ($N_2 + 8H^+ + 8e^- \rightarrow 2NH_3 + H_2$) (Kaneko et al., 2002). Since nitrogen gas was used to create oxygen-free condition during the course of this study, the dissolved nitrogen gas might be used by *Bradyrhizobium* species as a nitrogen source. Another species, *Aminiphilus*, also faded in the second analysis. Species from this genus are able to ferment common volatile fatty acids (e.g., acetate, propionate, and butyrate), ethanol and methanol (Díaz et al., 2007), and their role in AOM is unknown.

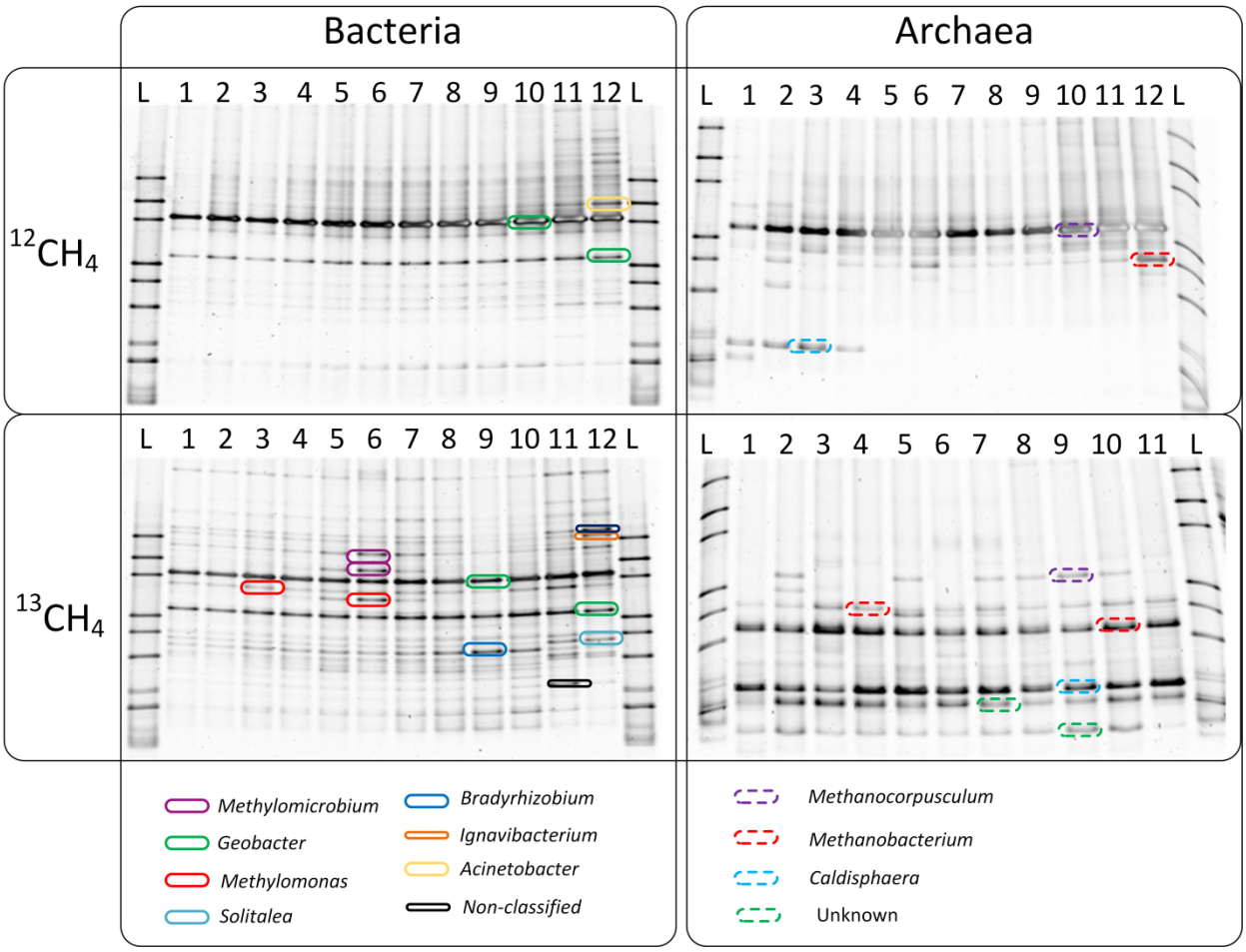

Figure 5–7. DGGE profiles of all 12 PCR amplified fractions from the first DNA-SIP with MEC 1 (Phase II). The control sample was prepared during the operation of MEC 1, and the actual sample labeled by heavy carbon was prepared at the end of the first SIP. Lanes labeled by "L" show the DGGE profiles of a standard.

About archaea, the shift of the microbial community was less dramatic (archaea in Figure 5-7 and Figure 5-8). Overall, the diversity of archaeal species increased in the second analysis (Phase III), which suggests the absolute anaerobic condition preferably enriched some archaea. Although the newly emerged species were not identified, their relative low abundance indicates that they may not be responsible for methane oxidation. Two methanogens, *Methanobacterium* and *Methanocorpusculum,* were detected during the first analysis. The latter species were

much more abundant in MEC 2-control. In the second analysis, *Methanocorpusculum* species almost disappeared, and *Methanobacterium* species became dominant. This shift of methanogens implies that both methanogens might have the ability to anaerobically oxidize methane but *Methanobacterium* species can better adapt to the MEC environment. The potential attribute of *Methanobacterium* species in EET may have given them advantages over *Methanocorpusculum* species (Siegert et al., 2014). Another significant difference from the first to the second analysis is that the number of *Caldisphaera* species (Itoh et al., 2003), heterotrophs, greatly decreased with prolonged operation inside an anaerobic chamber.

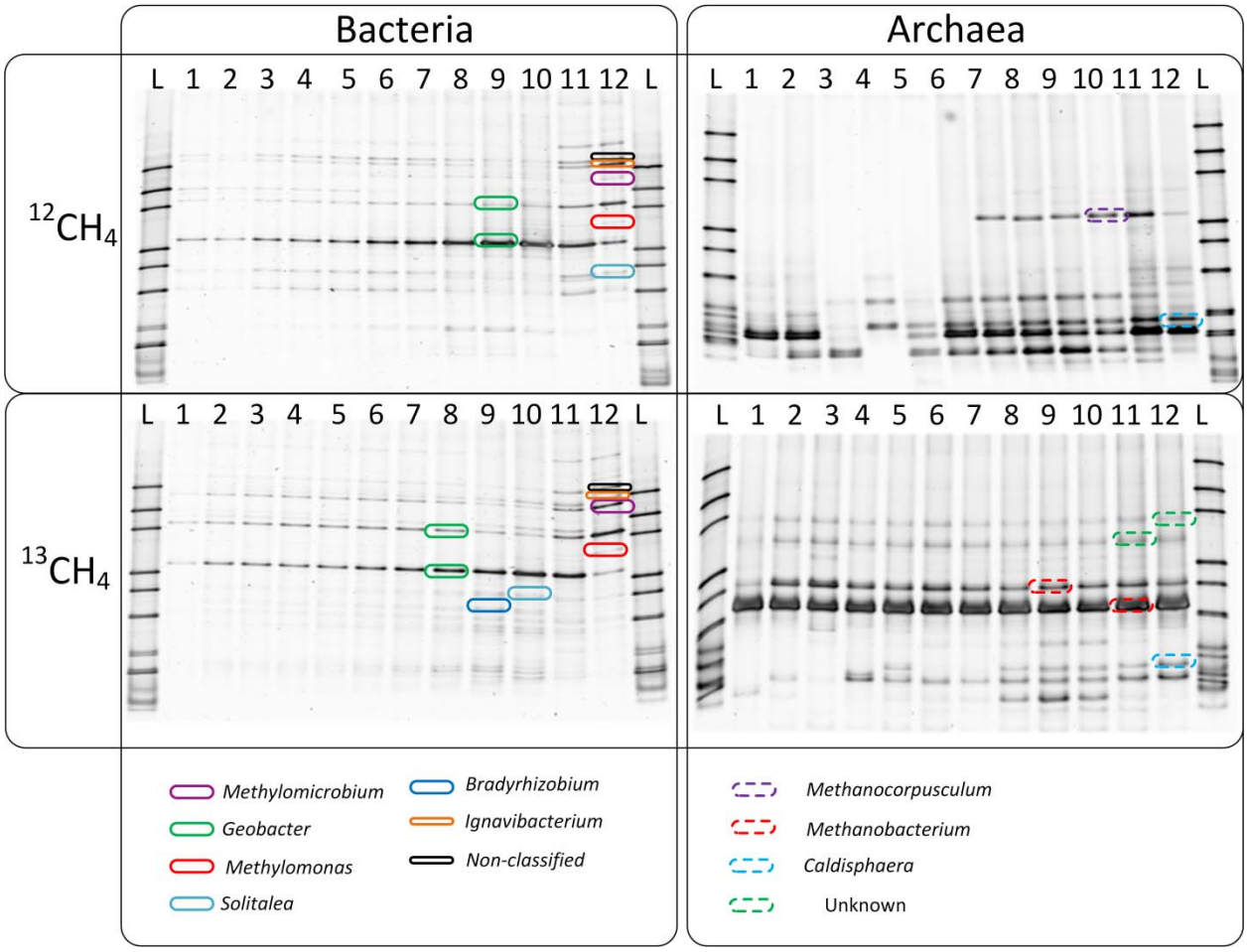

Figure 5–8. DGGE profiles of all 12 PCR amplified fractions from the second DNA-SIP with microbial electrochemical cell-2 and microbial electrochemical cell-2-control (Phase III). Lanes labeled by "L" show the DGGE profiles of a standard.

Unlike previous studies where distinct or separate species emerge from the comparison of the data from a control reactor (MEC 2-control) and a functional reactor (MEC 2), a similar comparison cannot be done in this study because the fractionated DNA from control and working samples showed inconsistency in archaeal structure (refer to Appendix Section C for details). Hence, the non-fractionated DNA originally extracted from the biofilms of the functional reactor was analyzed by DGGE, as shown in Figure 5-9. Apparently, the diversity of bacterial species decreased from day 425 to day 780 with *Geobacter* species becoming the most

abundant species. In the domain of archaea, *Methanobacterium* species were enriched together with two other unknown archaeal species. The results after long term enrichment and growth with dissolved methane suggest that *Geobacter* species and *Methanobacterium* species play crucial roles in the AOM on anode surfaces.

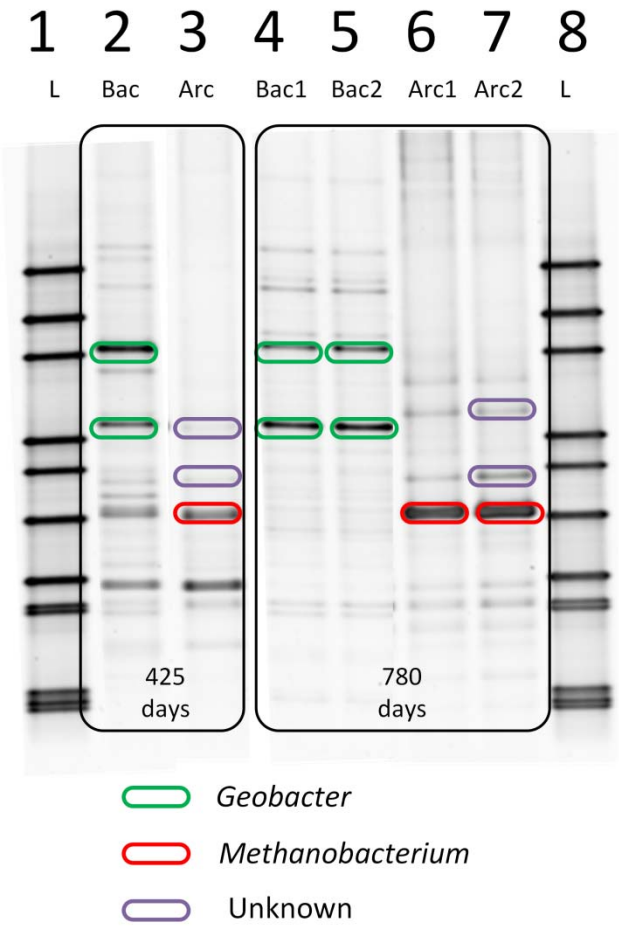

Figure 5–9. DGGE profiles of extracted non-fractionated DNA during the two DNA-SIP (MEC 1 and MEC 2). Duplicate analysis was done for the 780 days samples. Lanes labeled by "L" show the DGGE profiles of a standard.

5.3.5 Fluorescence *in situ* hybridization of the anode biofilm of microbial electrochemical cell-3 (Phase III)

The aforementioned DGGE profiles all confirmed the fact that a long term acclimation and enrichment with methane inside the anaerobic chamber resulted in *Geobacter* and *Methanobacterium* as the two dominant species on the anode. To reveal the spatial organization of this AOM consortium on the surface of the carbon fibers, intact anode biofilm was visualized with fluorescence *in situ* hybridization (*FISH*). The images from a confocal microscope show that *Geobacter* species and *Methanobacterium* species (as represented by the family *Methanobacteriaceae*) formed aggregates on the surface of the carbon fibers (Figure 5-10). It can be seen from Figure 5-10 A & B that neither of the two species dominated the biofilm, and they all closely attached to the carbon fibers. The association on carbon fibers is similar to the randomly mixed aggregate of ANME-1/sulfate-reducing *Desulfosarcina* aggregate (Figure 2-1D), rather than these monospecies aggregates as shown in Figure 2-1A, B, & G and these loosely formed aggregate as shown in Figure 2-1F. In a sulfate-driven AOM syntrophy, ANME-1 archaea are often discovered in the absence of any bacterial partners, which means they can anaerobically oxidized methane alone (Orphan et al., 2002). Instead, the intermixed colonies of *Geobacter* and *Methanobacterium* species on carbon fibers suggest that the two species collaboratively oxidized methane in MECs.

Moreover, the three-dimensional images of intact biofilm showed that the biofilm thickness was from around ~5 to 20 μm, which is close to the thickness of *Geobacter sulfurreducens* biofilm on carbon fibers with acetate as the substrate (Nevin

et al., 2008). In contrast, when solid graphite electrodes are the anode, commonly reported ARB biofilm are usually much thicker, about 50 μm to a few hundred μm when acetate was the substrate (Lee et al., 2009c, Babauta et al., 2011). The thin AOM biofilm on the carbon fiber may be caused by the inherent characteristics of the carbon fiber on one hand. On the other hand, this thin biofilm reflects the low energy generation from AOM coupled to EET on anode, which can limit biofilm growth (Table A5). Given that energy losses are negligible in EET to the anode, the Gibbs free energy gain is computed at -38.6 kJ/mol CH_4 in the AOM-EET reaction (measured values of CO_2=0.003187 atm, CH_4=0.135 atm at pH=7.4). The thin biofilm also indicates that low AOM rates in MECs should not be caused by the diffusion limitation commonly observed in thick biofilm environment (Lee et al., 2009a).

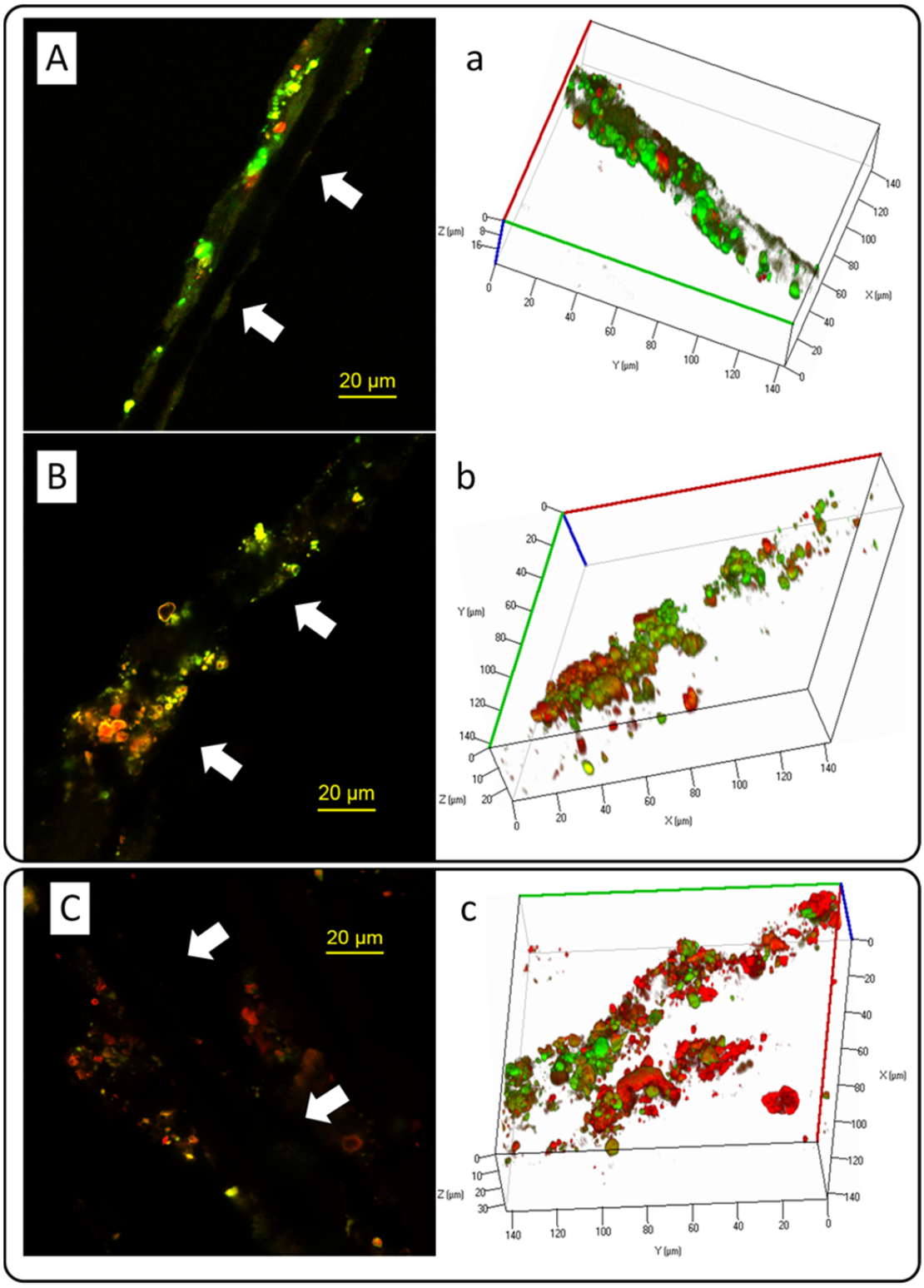

Figure 5–10. Confocal microscopy images of *FISH* of intact biofilms on carbon fibers from MEC 3 (Phase III). A+a and B+b show the distribution of archaea (green) and bacteria (red) from two different spots on the surface of carbon fiber. C+c shows the

distribution of *Methanobacterium* (green) and *Geobacter* (red) on the surface of carbon fiber. Arrows are perpendicular to anode fibers.

5.3.6 Analyses of potential intermediate compounds during anaerobic oxidation of methane (Phase III)

Overall, the DNA-SIP-DGGE revealed that *Geobacter* and *Methanobacterium* could have collaborated in AOM on anode surfaces since their genes were all labeled by heavy carbon (Figure 5-7 and 5-8). The labelling indicates that the two species shared the carbon from methane oxidation. In other words, the two species would share an intermediate compound during AOM-EET on the anode, instead of solely relying on the direct transfer of electrons from *Methanobacterium* to *Geobacter*, finally to the anode.

In order to gain a better understanding of the AOM process on the anode, biofilm suspension was analyzed for potential electron mediators. As shown in Figure 5-11, the biofilm suspension of AOM consortium shared the attribute of a pure *Geobacter* culture, which means that microbial cells bearing outer membrane cytochromes were abundant in the AOM biofilm (Hartshorne et al., 2009, Liu and Bond, 2012). The Soret peak shifted from 406 nm for the air-oxidized sample to around 420 nm upon the reduction by sodium dithionite. The β and α peaks are visible at 523 nm and 552 nm. When the suspension was exposed to air for a sufficiently long time, the cell suspension and the supernatant showed no characteristic peaks associated with quinone-like compounds (peak around 244 nm) (Gulaboski et al., 2013) nor did any peaks associated with flavin compounds (266, 370, and 445 nm) were discovered (Suzuki et al., 2010).

For its straightforward operation and accurate determination of certain compounds, UV-Vis spectrophotometer has been frequently employed for qualitative analysis of common electron mediators such as phenazine (Rabaey et al., 2004), quinones (Nevin and Lovley, 2002), cytochromes and flavin compounds (Marsili et al., 2008); however, UV-Vis spectrophotometry usually is not suitable for detecting single bond compounds, and a keto group shows little absorption at wavelength over 160 nm. Therefore, NMR spectroscopy was introduced as a complementary technique. NMR is suited to determining the molecular structure of an unknown chemical, and the technique has been used in both qualitative and quantitative analysis of electron mediating compounds and metabolic intermediates in biofilm systems (Sugnaux et al., 2013, Yeom et al., 2013). When proton NMR spectroscopy was applied (Figure 5-12), no characteristic peaks of aromatic compounds, such as flavin or quinone compounds, were identified so they would not exist in the biofilm or their concentrations were negligible. Characteristic peak of ethanol (except that -OH peak cannot be seen because it is diminished together with the water peak) or dimethyl ether and/or its derivative were identified. This result indicates that an ethanol- or ether-like compound might be an intermediate in AOM via methanotrophic archaea (i.e., *Methanobacterium*), and *Geobacter* might use it for current generation.

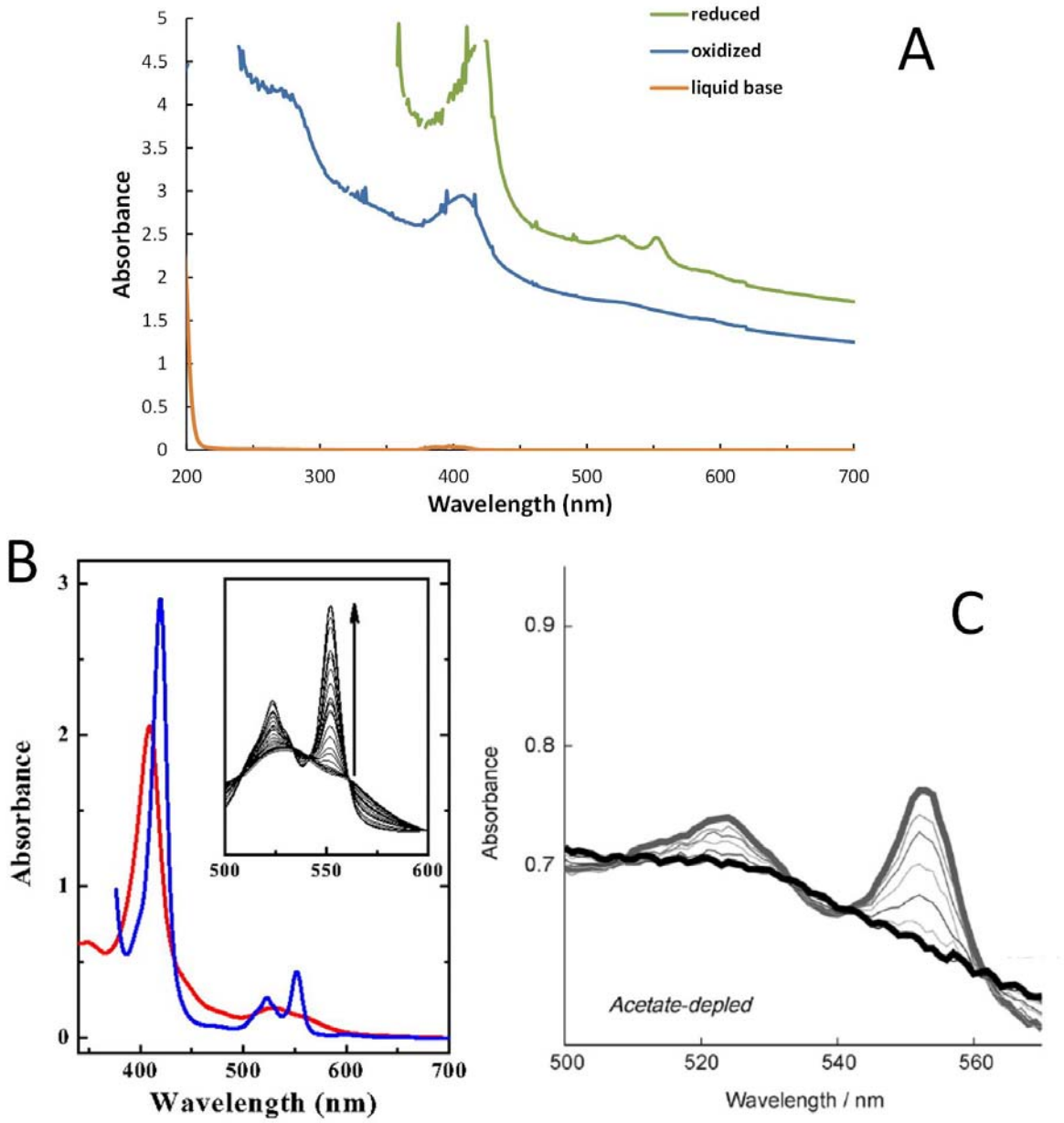

Figure 5–11. UV-Vis spectra of cell suspensions and the corresponding supernatant from microbial electrochemical cell-2 (Phase III) (A); B shows the spectra of the transmembrane proteins in their oxidized (red spectrum) and reduced (blue spectrum) forms from *Shewanella oneidensis* MR-1 (Hartshorne et al., 2009); C shows the spectra of *Geobacter sulfurreducens* biofilm in oxidized (black) and reduced (grey) conditions (Liu and Bond, 2012).

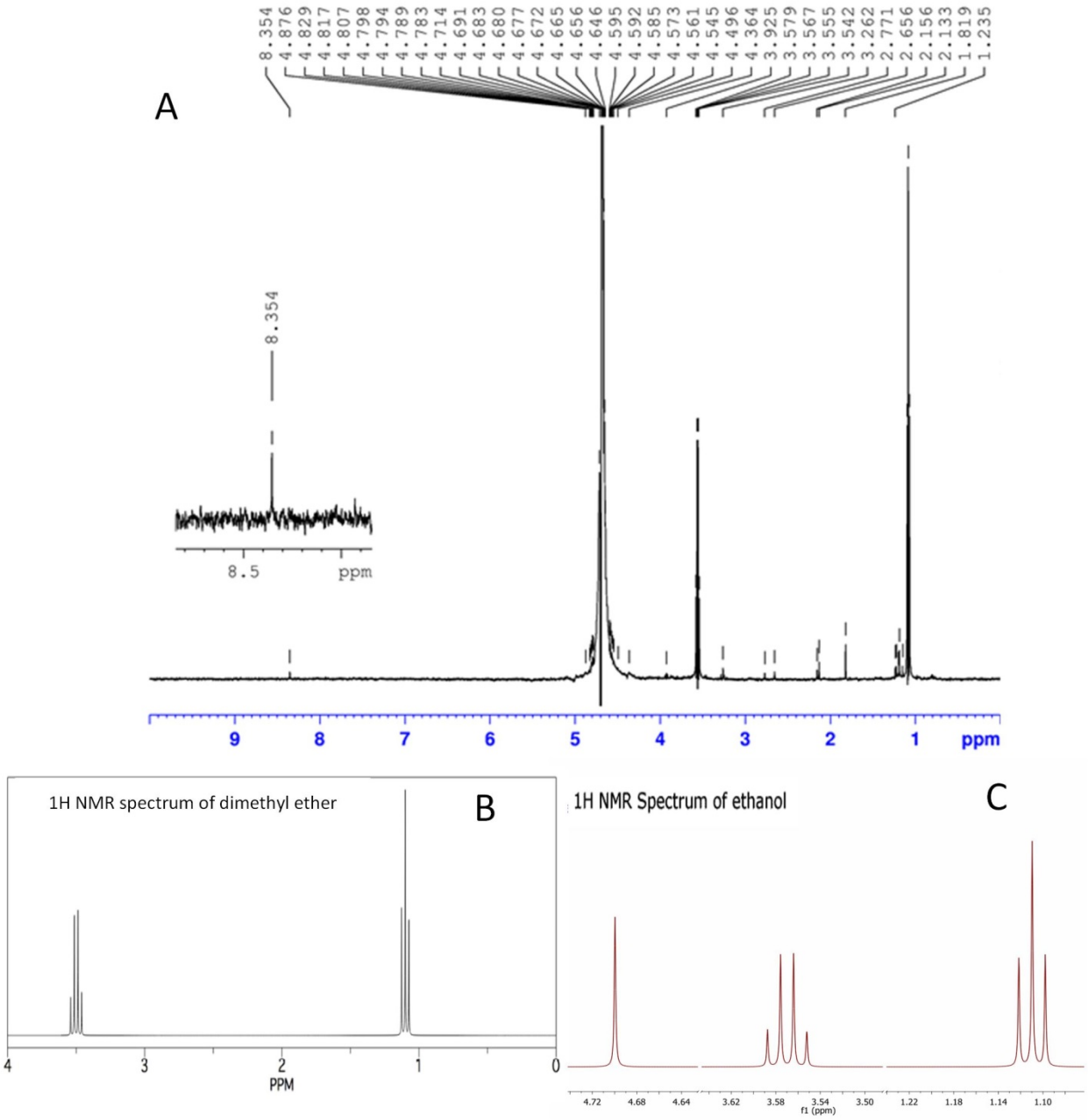

Figure 5–12. NMR spectrum of the supernatant of biofilm suspension from microbial electrochemical cell-2 (Phase III) (A). B and C show the spectra of ethanol and dimethyl ether, respectively (Sources: http://www.chem.ucla.edu/harding/IGOC/IGOC.html and Mestrelab Research 1H NMR Analysis: Common Myths and Misconceptions).

5.3.7 Summary of a new syntrophy

Based on the evidences of AOM ($CH_4 \rightarrow CO_2$), the aforementioned results from DGGE profiles and the close physical interaction of *Geobacter* and *Methanobacterium* species, a syntrophic interaction between *Geobacter* species and *Methanobacterium* species is proposed. Since (1) the available studies on genomes do not support that *Geobacter* species can oxidize methane (Methé et al., 2003, Aklujkar et al., 2009) and (2) some methanogens are proposed to carry out reverse methanogenesis (Zehnder, 1979, Blazewicz et al., 2012), it is speculated that *Methanobacterium* species oxidized methane through the backward reactions of methanogenesis like ANME while *Geobacter* species conducted anode respiration. The detection of heavy carbon labeled genes from both *Geobacter* and *Methanobacterium* species in SIP tests indicates that the two species utilized or shared organic carbon compounds generated from AOM. Thus, the two members could form a syntrophy by sharing an intermediate (i.e., ethanol- or ether-like compounds).

Additionally, direct electron transfer between the two species might have occurred in the consortium, along with intermediate-dependent syntrophy. For example, the syntrophic interaction with direct electron transfer between methanogen and *Geobacter* species was suggested: transfer of electrons embedded in ethanol or acetate by *Geobacter* species to methanogens through conductive metal oxide was proposed to explain the improved methanogenesis (Kato et al., 2012). Another study claimed that two *Geobacter* species, *Geobacter metallireducens* and *Geobacter sulfurreducens* are able to directly share electrons with the assistance of their conductive pili or "nanowire" (Shrestha et al., 2013). Rotaru *et al*. (2014) recently reported a syntrophic interaction between *Geobacter metallireducens* and *Methanosaeta harundinacea* in a microcosm degrading ethanol in which "conductive pili" could serve as a conduit for direct electron transfer. Thus, a direct transfer of electrons from

Methanobacterium to *Geobacter* might be another channel for the AOM coupled to EET in MECs. In this study, the SIP experiments clearly demonstrated that Geo*bacter* and *Methanobacterium* species shared organic carbons, which supports that the two members share intermediates during the AOM-EET.

5.4 Conclusions

The acclimation of methane-oxidizing microorganisms on conductive surfaces in MECs was successful. The methane oxidation rate ranged from 0.00083 to 0.027 μmole e^-/hr/cm^3. Sequencing of the anode microbial community showed that *Geobacter* species from the domain bacteria and *Methanobacterium* species from the domain archaea were the two dominant species after ~800 days of enrichment. No common electron mediators found in biofilm anode were detected in the AOM-MEC, likely because they were rapidly consumed during the anode respiration or their concentrations were too low; instead, an ethanol- or dimethyl ether-like compound was detected. *FISH* images showed that species from both bacteria and archaea (i.e., *Geobacter* and *Methanobacterium*) were randomly mixed on the surface of anode in close proximity to each other; the results suggest that the two species closely interact with each other during AOM. Since *Geobacter* species lack the ability to oxidize methane but some methanogens have been reported to conduct reverse methanogenesis, a syntrophic interaction between *Geobacter* and *Methanobacterium* is proposed with *Methanobacterium* conducting reverse methanogenesis for methane oxidation and *Geobacter* conducting the EET on the anode with intermediates from AOM. SIP tests showed that the two species shared reducing carbon sources from

methane oxidation but more studies are necessary to elucidate the role of direct electron transfer in this new syntrophy.

Chapter 6 Conclusions and recommendations

6.1 Conclusions

Understanding syntrophic interactions between ARB and non-ARB is significant for improving MEC performance in wastewater treatment and expanding MEC applications as renewable and sustainable sensors. The present study explored the potentials of establishing three syntrophic interactions that can catalyze the application of MECs to (1) sustainable anaerobic wastewater treatment, (2) portable power sources and (3) biosensors for methane or methanogenesis. The key conclusions drawn from this study are summarized below.

Serial acclimation of a biofilm anode with acetate and digestate enriched ARB (*Geobacter* species and *Dysgonomonas* species), fermentative bacteria (*Kosmotoga* species), and homoacetogens (*Treponema* species) in an MEC; a high electric current density of 14.6 A/m^2 and a high COD removal percentage of 96% were achieved when digestate was used as feed: the highest current density and COD removal in MECs treating digestate up to now. Unlike previous studies, methane only accounted for 3.42% of removed COD in MEC effluent. SMP (soluble microbial products) and VFAs in digestate were further degraded in MECs. A syntrophy among ARB, fermentative bacteria and homoacetogens is proposed to explain these observations. The results revealed that MECs can efficiently recover the electrons from digester effluent in which VFAs and methanogens are accumulated.

Lipid-accumulating bacteria (*Acholeplasma* and *Kosmotoga*) and ARB (*Geobacter*) predominated in a biofilm anode acclimated from the anolyte of an oligotrophic MEC, which was operated in a feast-and-famine feeding condition. When acetate was depleted and mineral medium was fed into the anode chamber, a residual

current around 1.5 to 2 A/m^2 was observed; when acetate was spiked into the anolyte, nearly complete utilization of acetate and extremely high CEs around 200% were achieved, which indicate the availability of additional electron donors in the biofilm. Nile red staining revealed that abundant lipid compounds were accumulated on the biofilm anode. According to these findings, a syntrophy among lipid-accumulating bacteria, fermentative bacteria and ARB is proposed; in this syntrophy the lipid inclusions of *Acholeplasma* species serve as energy source for *Geobacter* species after exogenous substrate is depleted. The results from this study imply that MFCs would be deployed as portable power sources under discontinuous feeding conditions if the syntrophy between lipid-accumulating bacteria and ARB can be established and sustained in the anode biofilm.

Finally, the acclimation of methane-oxidizing microorganisms, ~800 days, on conductive surfaces in MECs resulted in an anode biofilm that is dominated by *Methanobacterium* species and *Geobacter* species; it is proposed that *Methanobacterium* species conducted reverse methanogenesis for methane oxidation and *Geobacter* species conducted the EET on the anode. The methane oxidation rate from this syntrophy was from 0.00083 to 0.027 μmole e^-/hr/cm^3. No common electron mediators found in biofilm anode were detected; instead, an ethanol- or dimethyl ether-like compound was detected. The microbial consortium on anode surface showed no structural pattern but the species from *Geobacter* and *Methanobacterium* were in close proximity to each other. DNA-SIP tests showed that the two species shared intermediate compounds from methane oxidation because all their genes were labeled by heavy carbon.

6.2 Recommendations

The findings presented in this study add new insights into the potentials of MECs. However, more studies are required to extend the knowledge on how these syntrophy are established and how the syntrophy can be sustained and augmented for real-world applications. For these purposes, some future research topics are identified and listed here.

- Anaerobic digestion usually applies a hydraulic retention time (HRT) of 10-20 days because the feed contains large molecules and suspended organic particles, which cost time to be broken down. The present study examined the biodegradation of digestate in an MEC; at HRT of 4 days only around 60% of particulate matters (TSS and VSS) were reduced, and TCOD and SCOD removals were 56% and 58%, respectively. The MEC in this study used carbon fibers as the anode, and the electrode was located as close as possible to the membrane for a minimal internal resistance, while most of the space in the anodic chamber was filled with liquid. The relatively large ratio of anolyte volume to anode biofilm volume may be limiting the volumetric treatment efficiency of anode biofilm. Future study can investigate a different design of MECs with smaller anolyte volume per unit anode biofilm volume so that the treatment efficiency can be increased at a shorter HRT.
- Future studies from two aspects are recommended for improving performance of small-sized MFCs as portable power suppliers. First, a better designed air cathode and a different ion exchange membrane should be tested to examine the performance of the anode biofilm while cathode limitation is absent and oxygen contamination from cathodic side is decreased. Second, two factors may lead to this special anode biofilm, starvation of the original

inoculum and provision of higher-carbon VFAs, such as propionate and valerate. The stimulating factors of lipid accumulating properties should be investigated so that the function of this special anode biofilm can potentially be sustained.

- High capacitive current was observed from the AOM-MECs; the capacitive current impaired the study of electric current responses from various levels of dissolved methane but it can also be an asset: instead of recording the small electric current, a measurement of the accumulated coulomb during a fixed time interval from various levels of dissolved methane theoretically should yield a linear relationship between concentration of dissolved methane and accumulated coulomb, which would demonstrate that the AOM-MEC can be deployed as a dissolved methane detector. Furthermore, more investigation should be conducted on the oxygen source of the carbon dioxide detected during AOM. Analysis of the isotope composition of the potential oxygen sources (e.g., water, phosphate, and biomass) and application of oxygen isotope tracer (i.e., ^{18}O) in original feed medium can be considered.

Bibliography

1. 1999. Standard Methods for the Examination of Water and Wastewater. 20th ed., the American Public Health Association and the Water Environment Federation, Washington, DC
2. Aelterman, P., Versichele, M., Marzorati, M., Boon, N., Verstraete, W., 2008. Loading rate and external resistance control the electricity generation of microbial fuel cells with different three-dimensional anodes. Bioresource Technology. 99, 8895-8902.
3. Aklujkar, M., Krushkal, J., Dibartolo, G., Lapidus, A., Land, M. L., Lovley, D. R., 2009. The genome sequence of Geobacter metallireducens: Features of metabolism, physiology and regulation common and dissimilar to Geobacter sulfurreducens. BMC Microbiology. 9.
4. Al-Shammari, A. J., Smith, P. F., 1979. Lipid and lipopolysaccharide composition of Acholeplasma oculi. Journal of Bacteriology. 139, 356-361.
5. Alperin, M. J. R., W. S., 1985. Inhibition experiments on anaerobic methane oxidation. Applied and Environmental Microbiology. 50, 940-945.
6. Altschul, S. F., Madden, T. L., Schäffer, A. A., Zhang, J., Zhang, Z., Miller, W., Lipman, D. J., 1997. Gapped BLAST and PSI-BLAST: A new generation of protein database search programs. Nucleic Acids Research. 25, 3389-3402.
7. Amos, R. T., Bekins, B. A., Cozzarelli, I. M., Voytek, M. A., Kirshtein, J. D., Jones, E. J. P., Blowes, D. W., 2012. Evidence for iron-mediated anaerobic methane oxidation in a crude oil-contaminated aquifer. Geobiology. 10, 506-517.
8. Arends, J. B. A., Verstraete, W., 2012. 100 years of microbial electricity production: three concepts for the future. Microbial Biotechnology. 5, 333-346.
9. Babauta, J. T., Nguyen, H. D., Beyenal, H., 2011. Redox and pH Microenvironments within Shewanella oneidensis MR-1 Biofilms Reveal an Electron Transfer Mechanism. Environmental Science & Technology. 45, 6654-6660.
10. Barker, D. J., Mannucchi, G. A., Salvi, S. M. L., Stuckey, D. C., 1999. Characterisation of soluble residual chemical oxygen demand (COD) in anaerobic wastewater treatment effluents. Water Research. 33, 2499-2510.
11. Bartram, A. K., Lynch, M. D. J., Stearns, J. C., Moreno-Hagelsieb, G., Neufeld, J. D., 2011. Generation of Multimillion-Sequence 16S rRNA Gene Libraries from Complex Microbial Communities by Assembling Paired-End Illumina Reads. Applied and Environmental Microbiology. 77, 3846-3852.

12. Beal, E. J., House, C. H., Orphan, V. J., 2009. Manganese- and iron-dependent marine methane oxidation. Science. 325, 184-187.
13. Beal, E. J. H., C. H.; Orphan, V. J., 2009. Manganese and iron dependent marine methane oxidation. Science. 325, 184-187.
14. Bengtsson, S., Werker, A., Christensson, M., Welander, T., 2008. Production of polyhydroxyalkanoates by activated sludge treating a paper mill wastewater. Bioresource Technology. 99, 509-516.
15. Beun, J. J., Dircks, K., Van Loosdrecht, M. C. M., Heijnen, J. J., 2002. Poly-β-hydroxybutyrate metabolism in dynamically fed mixed microbial cultures. Water Research. 36, 1167-1180.
16. Blazewicz, S. J., Petersen, D. G., Waldrop, M. P., Firestone, M. K., 2012. Anaerobic oxidation of methane in tropical and boreal soils: Ecological significance in terrestrial methane cycling. Journal of Geophysical Research: Biogeosciences. 117, G02033.
17. Boetius, A. R., K.; Schubert, C. J. *et al*, 2000. A marine mcirobial consortium apparently mediating anaerobic oxidation of methane. Nature. 407, 623-626.
18. Bonanni, P. S., Schrott, G. D., Robuschi, L., Busalmen, J. P., 2012. Charge accumulation and electron transfer kinetics in Geobacter sulfurreducens biofilms. Energy and Environmental Science. 5, 6188-6195.
19. Bond, D. R., Holmes, D. E., Tender, L. M., Lovley, D. R., 2002. Electrode-reducing microorganisms that harvest energy from marine sediments. Science. 295, 483-485.
20. Bond, D. R., Lovley, D. R., 2003. Electricity production by Geobacter sulfurreducens attached to electrodes. Applied and Environmental Microbiology. 69, 1548-1555.
21. Borrel, G., Jézéquel, D., Biderre-Petit, C., Morel-Desrosiers, N., Morel, J. P., Peyret, P., Fonty, G., Lehours, A. C., 2011. Production and consumption of methane in freshwater lake ecosystems. Research in Microbiology. 162, 833-847.
22. Caldwell, S. L. L., J. R.; Brewer, E. A. *et al*, 2008. Anaerobic oxidation of methane: mechanisms, bioenergetics, and the ecology of associated microorganisms. Environmental Science and Technolgoy. 42, 6791-6799.
23. Call, D., Logan, B. E., 2008. Hydrogen Production in a Single Chamber Microbial Electrolysis Cell Lacking a Membrane. Environmental Science & Technology. 42, 3401-3406.
24. Catal, T., Cysneiros, D., O'Flaherty, V., Leech, D., 2011. Electricity generation in single-chamber microbial fuel cells using a carbon source sampled from anaerobic reactors utilizing grass silage. Bioresource Technology. 102, 404-410.
25. Catal, T., Li, K., Bermek, H., Liu, H., 2008. Electricity production from twelve monosaccharides using microbial fuel cells. Journal of Power Sources. 175, 196-200.

26. Chae, K. J., Choi, M. J., Kim, K. Y., Ajayi, F. F., Park, W., Kim, C. W., Kim, I. S., 2010. Methanogenesis control by employing various environmental stress conditions in two-chambered microbial fuel cells. Bioresource Technology. 101, 5350-5357.
27. Chang, I. S., Jang, J. K., Gil, G. C., Kim, M., Kim, H. J., Cho, B. W., Kim, B. H., 2004. Continuous determination of biochemical oxygen demand using microbial fuel cell type biosensor. Biosensors and Bioelectronics. 19, 607-613.
28. Chen, S., He, G., Liu, Q., Harnisch, F., Zhou, Y., Chen, Y., Hanif, M., Wang, S., Peng, X., Hou, H., Schroder, U., 2012. Layered corrugated electrode macrostructures boost microbial bioelectrocatalysis. Energy and Environmental Science. 5, 9769-9772.
29. Chen, S., Rotaru, A. E., Shrestha, P. M., Malvankar, N. S., Liu, F., Fan, W., Nevin, K. P., Lovley, D. R., 2014. Promoting interspecies electron transfer with biochar. Scientific Reports. 4.
30. Cheng, S., Liu, H., Logan, B. E., 2006. Increased performance of single-chamber microbial fuel cells using an improved cathode structure. Electrochemistry Communications. 8, 489-494.
31. Chernicharo, C. A. L., 2006. Post-treatment options for the anaerobic treatment of domestic wastewater. Reviews in Environmental Science and Biotechnology. 5, 73-92.
32. Choi, J. D. R., Chang, H. N., Han, J. I., 2011. Performance of microbial fuel cell with volatile fatty acids from food wastes. Biotechnology Letters. 33, 705-714.
33. Choi, S., Chae, J., 2013. Optimal biofilm formation and power generation in a micro-sized microbial fuel cell (MFC). Sensors and Actuators A: Physical. 195, 206-212.
34. Chua, A. S. M., Takabatake, H., Satoh, H., Mino, T., 2003. Production of polyhydroxyalkanoates (PHA) by activated sludge treating municipal wastewater: Effect of pH, sludge retention time (SRT), and acetate concentration in influent. Water Research. 37, 3602-3611.
35. Cirne, D. G., Paloumet, X., Björnsson, L., Alves, M. M., Mattiasson, B., 2007. Anaerobic digestion of lipid-rich waste—Effects of lipid concentration. Renewable Energy. 32, 965-975.
36. Clauwaert, P., Aelterman, P., Pham, T. H., De Schamphelaire, L., Carballa, M., Rabaey, K., Verstraete, W., 2008. Minimizing losses in bio-electrochemical systems: The road to applications. Applied Microbiology and Biotechnology. 79, 901-913.
37. Clauwaert, P., Verstraete, W., 2009. Methanogenesis in membraneless microbial electrolysis cells. Applied Microbiology and Biotechnology. 82, 829-836.
38. Clesceri, L. S., Greenberg, A. E., Eaton, A. D., 1999. Standard Methods for the Examination of Water and Wastewater. 20th ed., the American Public Health Association and the Water Environment Federation, Washington, DC
39. Cole, J. R., Wang, Q., Cardenas, E., Fish, J., Chai, B., Farris, R. J., Kulam-Syed-Mohideen, A. S., McGarrell, D. M., Marsh, T., Garrity, G. M., Tiedje, J. M., 2009. The

Ribosomal Database Project: Improved alignments and new tools for rRNA analysis. Nucleic Acids Research. 37, D141-D145.
40. Conrad, R., Bak, F., Seitz, H. J., Thebrath, B., Mayer, H. P., Schütz, H., 1989. Hydrogen turnover by psychrotrophic homoacetogenic and mesophilic methanogenic bacteria in anoxic paddy soil and lake sediment.
41. Cusick, R. D., Bryan, B., Parker, D. S., Merrill, M. D., Mehanna, M., Kiely, P. D., Liu, G., Logan, B. E., 2011. Performance of a pilot-scale continuous flow microbial electrolysis cell fed winery wastewater. Applied Microbiology and Biotechnology. 89, 2053-2063.
42. Darwent, B. d., 1970. Bond dissociation energies in simple molecules. U.S. National Bureau of Standards; for sale by the Supt. of Docs., U.S. Govt. Print. Off., [Washington]
43. Deeke, A., Sleutels, T. H. J. A., Hamelers, H. V. M., Buisman, C. J. N., 2012. Capacitive Bioanodes Enable Renewable Energy Storage in Microbial Fuel Cells. Environmental Science & Technology. 46, 3554-3560.
44. Di Lorenzo, M., Curtis, T. P., Head, I. M., Scott, K., 2009. A single-chamber microbial fuel cell as a biosensor for wastewaters. Water Research. 43, 3145-3154.
45. Díaz, C., Baena, S., Fardeau, M.-L., Patel, B. K. C., 2007. Aminiphilus circumscriptus gen. nov., sp. nov., an anaerobic amino-acid-degrading bacterium from an upflow anaerobic sludge reactor. International Journal of Systematic and Evolutionary Microbiology. 57, 1914-1918.
46. Dowd, S. E., Callaway, T. R., Wolcott, R. D., Sun, Y., McKeehan, T., Hagevoort, R. G., Edrington, T. S., 2008. Evaluation of the bacterial diversity in the feces of cattle using 16S rDNA bacterial tag-encoded FLX amplicon pyrosequencing (bTEFAP). BMC Microbiology. 8, 1-8.
47. Edgar, R. C., Haas, B. J., Clemente, J. C., Quince, C., Knight, R., 2011. UCHIME improves sensitivity and speed of chimera detection. Bioinformatics. 27, 2194-2200.
48. Elferink, S. J. W. H. O., Luppens, S. B. I., Marcelis, C. L. M., Stams, A. J. M., 1998. Kinetics of Acetate Oxidation by Two Sulfate Reducers Isolated from Anaerobic Granular Sludge. Applied and Environmental Microbiology. 64, 2301-2303.
49. Environment_Canada 2010 Municipal Water Use Report: Municipal Water Use, 2006 Statistics, Catalogue no. En11-2/2006E-PDF.
50. EPA, U. *Methane and Nitrous Oxide Emissions From Natural Sources*; 2010.
51. Esteve-Núñez, A., Rothermich, M., Sharma, M., Lovley, D., 2005. Growth of Geobacter sulfurreducens under nutrient-limiting conditions in continuous culture. Environmental Microbiology. 7, 641-648.
52. Ettwig, K. F., Butler, M. K., Le Paslier, D., Pelletier, E., Mangenot, S., Kuypers, M. M. M., Schreiber, F., Dutilh, B. E., Zedelius, J., De Beer, D., Gloerich, J., Wessels, H. J. C. T., Van Alen, T., Luesken, F., Wu, M. L., Van De Pas-Schoonen, K. T., Op Den

Camp, H. J. M., Janssen-Megens, E. M., Francoijs, K. J., Stunnenberg, H., Weissenbach, J., Jetten, M. S. M., Strous, M., 2010. Nitrite-driven anaerobic methane oxidation by oxygenic bacteria. Nature. 464, 543-548.
53. Ettwig, K. F., Shima, S., Van De Pas-Schoonen, K. T., Kahnt, J., Medema, M. H., Op Den Camp, H. J. M., Jetten, M. S. M., Strous, M., 2008. Denitrifying bacteria anaerobically oxidize methane in the absence of Archaea. Environmental Microbiology. 10, 3164-3173.
54. Fornero, J. J., Rosenbaum, M., Angenent, L. T., 2010. Electric Power Generation from Municipal, Food, and Animal Wastewaters Using Microbial Fuel Cells. Electroanalysis. 22, 832-843.
55. Freguia, S., Rabaey, K., Yuan, Z., Keller, J., 2008. Syntrophic processes drive the conversion of glucose in microbial fuel cell anodes. Environmental Science and Technology. 42, 7937-7943.
56. Freguia, S., Rabaey, K., Yuan, Z., Keller, J., 2007. Electron and carbon balances in microbial fuel cells reveal temporary bacterial storage behavior during electricity generation. Environmental Science and Technology. 41, 2915-2921.
57. Freguia, S., Teh, E. H., Boon, N., Leung, K. M., Keller, J., Rabaey, K., 2010. Microbial fuel cells operating on mixed fatty acids. Bioresource Technology. 101, 1233-1238.
58. Garcia, J.-L., Patel, B. K. C., Ollivier, B., 2000. Taxonomic, Phylogenetic, and Ecological Diversity of Methanogenic Archaea. Anaerobe. 6, 205-226.
59. Garton, N. J., Christensen, H., Minnikin, D. E., Adegbola, R. A., Barer, M. R., 2002. Intracellular lipophilic inclusions of mycobacteria in vitro and in sputum. Microbiology. 148, 2951-2958.
60. Ge, Z., Zhang, F., Grimaud, J., Hurst, J., He, Z., 2013. Long-term investigation of microbial fuel cells treating primary sludge or digested sludge. Bioresource Technology. 136, 509-514.
61. Gil, G.-C., Chang, I.-S., Kim, B. H., Kim, M., Jang, J.-K., Park, H. S., Kim, H. J., 2003. Operational parameters affecting the performannce of a mediator-less microbial fuel cell. Biosensors and Bioelectronics. 18, 327-334.
62. Girguis, P. R., Cozen, A. E., DeLong, E. F., 2005. Growth and Population Dynamics of Anaerobic Methane-Oxidizing Archaea and Sulfate-Reducing Bacteria in a Continuous-Flow Bioreactor. Applied and Environmental Microbiology. 71, 3725-3733.
63. Girguis, P. R. O., V. J.; Hallam, S. J. et al, 2003. Growth and Methane Oxidation Rates of Anaerobic Methanotrophic Archaea in a Continuous-Flow Bioreactor. Applied and Environmental Microbiology. 69, 5472–5482.
64. Glasemacher, J., Bock, A.-K., Schmid, R., Schönheit, P., 1997. Purification and Properties of Acetyl-CoA Synthetase (ADP-forming), an Archaeal Enzyme of Acetate

Formation and ATP Synthesis, from the Hyperthermophile Pyrococcus furiosus. European Journal of Biochemistry. 244, 561-567.
65. Gorby, Y. A., Yanina, S., McLean, J. S., Rosso, K. M., Moyles, D., Dohnalkova, A., Beveridge, T. J., Chang, I. S., Kim, B. H., Kim, K. S., Culley, D. E., Reed, S. B., Romine, M. F., Saffarini, D. A., Hill, E. A., Shi, L., Elias, D. A., Kennedy, D. W., Pinchuk, G., Watanabe, K., Ishii, S., Logan, B., Nealson, K. H., Fredrickson, J. K., 2006. Electrically conductive bacterial nanowires produced by Shewanella oneidensis strain MR-1 and other microorganisms. Proceedings of the National Academy of Sciences of the United States of America. 103, 11358-11363.
66. Graber, J. R., Breznak, J. A., 2004. Physiology and Nutrition of *Treponema primitia*, an H_2/CO_2-Acetogenic Spirochete from Termite Hindguts. Applied and Environmental Microbiology. 70, 1307-1314.
67. Graber, J. R., Leadbetter, J. R., Breznak, J. A., 2004. Description of Treponema azotonutricium sp. nov. and Treponema primitia sp. nov., the First Spirochetes Isolated from Termite Guts. Applied and Environmental Microbiology. 70, 1315-1320.
68. Greenspan, P., Mayer, E. P., Fowler, S. D., 1985. Nile red: a selective fluorescent stain for intracellular lipid droplets. The Journal of Cell Biology. 100, 965-973.
69. Gregoire, K. P., Becker, J. G., 2012. Design and characterization of a microbial fuel cell for the conversion of a lignocellulosic crop residue to electricity. Bioresource Technology. 119, 208-215.
70. Grossman, E. L., Cifuentes, L. A., Cozzarelli, I. M., 2002. Anaerobic methane oxidation in a landfill-leachate plume. Environmental Science and Technology. 36, 2436-2442.
71. Gulaboski, R., Bogeski, I., Mirceski, V., Saul, S., Pasieka, B., Haeri, H. H., Stefova, M., Stanoeva, J. P., Mitrev, S., Hoth, M., Kappl, R., 2013. Hydroxylated derivatives of dimethoxy-1,4-benzoquinone as redox switchable earth-alkaline metal ligands and radical scavengers. Sci. Rep. 3.
72. Hansen, L. B. F., K.; Fossing, H. et al, 1998. Anaerobic methane oxidation in sulfate depleted sediments: effects of sulfate and molybdate additions Aquatic Microbial Ecology. 14, 195-204.
73. Harmsen, H. J. M., Van Kuijk, B. L. M., Plugge, C. M., Akkermans, A. D. L., De Vos, W. M., Stams, A. J. M., 1998. Syntrophobacter fumaroxidans sp. nov., a syntrophic propionate-degrading sulfate-reducing bacterium. International Journal of Systematic Bacteriology. 48, 1383-1387.
74. Haroon, M. F., Hu, S., Shi, Y., Imelfort, M., Keller, J., Hugenholtz, P., Yuan, Z., Tyson, G. W., 2013. Anaerobic oxidation of methane coupled to nitrate reduction in a novel archaeal lineage. Nature. 500, 567-570.
75. Hartshorne, R. S., Reardon, C. L., Ross, D., Nuester, J., Clarke, T. A., Gates, A. J., Mills, P. C., Fredrickson, J. K., Zachara, J. M., Shi, L., Beliaev, A. S., Marshall, M. J.,

Tien, M., Brantley, S., Butt, J. N., Richardson, D. J., 2009. Characterization of an electron conduit between bacteria and the extracellular environment. Proceedings of the National Academy of Sciences of the United States of America. 106, 22169-22174.
76. Hatamoto, M., Imachi, H., Ohashi, A., Harada, H., 2007. Identification and Cultivation of Anaerobic, Syntrophic Long-Chain Fatty Acid-Degrading Microbes from Mesophilic and Thermophilic Methanogenic Sludges. Applied and Environmental Microbiology. 73, 1332-1340.
77. He, Z., Kan, J., Mansfeld, F., Angenent, L. T., Nealson, K. H., 2009. Self-Sustained Phototrophic Microbial Fuel Cells Based on the Synergistic Cooperation between Photosynthetic Microorganisms and Heterotrophic Bacteria. Environmental Science & Technology. 43, 1648-1654.
78. He, Z., Minteer, S. D., Angenent, L. T., 2005. Electricity generation from artificial wastewater using an upflow microbial fuel cell. Environmental Science and Technology. 39, 5262-5267.
79. Heidrich, E. S., Curtis, T. P., Dolfing, J., 2011. Determination of the internal chemical energy of wastewater. Environmental Science and Technology. 45, 827-832.
80. Hinrichs, K. U., Hayes, J. M., Sylva, S. P., Brewert, P. G., DeLong, E. F., 1999. Methane-consuming archaebacteria in marine sediments. Nature. 398, 802-805.
81. Holler, T., Wegener, G., Knittel, K., Boetius, A., Brunner, B., Kuypers, M. M. M., Widdel, F., 2009. Substantial 13C/12C and D/H fractionation during anaerobic oxidation of methane by marine consortia enriched in vitro. Environmental Microbiology Reports. 1, 370-376.
82. Hu, H., Fan, Y., Liu, H., 2008. Hydrogen production using single-chamber membrane-free microbial electrolysis cells. Water Research. 42, 4172-4178.
83. Huber, T., Faulkner, G., Hugenholtz, P., 2004. Bellerophon: a program to detect chimeric sequences in multiple sequence alignments. Bioinformatics. 20, 2317-2319.
84. Inoue, K., Ito, T., Kawano, Y., Iguchi, A., Miyahara, M., Suzuki, Y., Watanabe, K., 2013. Electricity generation from cattle manure slurry by cassette-electrode microbial fuel cells. Journal of Bioscience and Bioengineering. 116, 610-615.
85. Itoh, T., Suzuki, K., Sanchez, P. C., Nakase, T., 2003. Caldisphaera lagunensis gen. nov., sp. nov., a novel thermoacidophilic crenarchaeote isolated from a hot spring at Mt Maquiling, Philippines. International Journal of Systematic and Evolutionary Microbiology. 53, 1149-1154.
86. Jensen, S., Neufeld, J. D., Birkeland, N. K., Hovland, M., Murrell, J. C., 2008. Methane assimilation and trophic interactions with marine Methylomicrobium in deep-water coral reef sediment off the coast of Norway. FEMS Microbiology Ecology. 66, 320-330.

87. Joye, S. B. B., A.; Orcutt, B. N. *et al*, 2004. The anaerobic oxidation of methane and sulfate reduction in sediments from Gulf of Mexico cold seeps. Chemical Geology. 205, 219–238.
88. Jung, S., Regan, J. M., 2011. Influence of External Resistance on Electrogenesis, Methanogenesis, and Anode Prokaryotic Communities in Microbial Fuel Cells. Applied and Environmental Microbiology. 77, 564-571.
89. Kaneko, T., Nakamura, Y., Sato, S., Minamisawa, K., Uchiumi, T., Sasamoto, S., Watanabe, A., Idesawa, K., Iriguchi, M., Kawashima, K., Kohara, M., Matsumoto, M., Shimpo, S., Tsuruoka, H., Wada, T., Yamada, M., Tabata, S., 2002. Complete Genomic Sequence of Nitrogen-fixing Symbiotic Bacterium Bradyrhizobium japonicum USDA110. DNA Research. 9, 189-197.
90. Karadagli, F., Rittmann, B. E., 2005. Kinetic Characterization of *Methanobacterium bryantii* M.o.H. Environmental Science and Technology. 39, 4900-4905.
91. Kato, S., Hashimoto, K., Watanabe, K., 2012. Methanogenesis facilitated by electric syntrophy via (semi)conductive iron-oxide minerals. Environmental Microbiology. 14, 1646-1654.
92. Kaur, A., Kim, J. R., Michie, I., Dinsdale, R. M., Guwy, A. J., Premier, G. C., 2013. Microbial fuel cell type biosensor for specific volatile fatty acids using acclimated bacterial communities. Biosensors and Bioelectronics. 47, 50-55.
93. Kim, J. R., Dec, J., Bruns, M. A., Logan, B. E., 2008. Removal of Odors from Swine Wastewater by Using Microbial Fuel Cells. Applied and Environmental Microbiology. 74, 2540-2543.
94. Kim, J. R., Jung, S. H., Regan, J. M., Logan, B. E., 2007. Electricity generation and microbial community analysis of alcohol powered microbial fuel cells. Bioresource Technology. 98, 2568-2577.
95. Knittel, K., Boetius, A., Anaerobic oxidation of methane: Progress with an unknown process. 2009a; Vol. 63, pp 311-334.
96. Knittel, K., Boetius, A., Anaerobic oxidation of methane: Progress with an unknown process. In Annual Review of Microbiology, 2009b; Vol. 63, pp 311-334.
97. Knittel, K., Lösekann, T., Boetius, A., Kort, R., Amann, R., 2005. Diversity and distribution of methanotrophic archaea at cold seeps. Applied and Environmental Microbiology. 71, 467-479.
98. Knittel, K. B., A., 2009. Anaerobic oxidation of methane: Progress with an unknown process. Annual Review of Microbiology. 63, 311-334.
99. Kodama, Y., Shimoyama, T., Watanabe, K., 2012. *Dysgonomonas oryzarvi* sp. nov., isolated from a microbial fuel cell. International Journal of Systematic and Evolutionary Microbiology. 62, 3055-3059.

100. Korajkic, A., Parfrey, L. W., McMinn, B. R., Baeza, Y. V., VanTeuren, W., Knight, R., Shanks, O. C., 2015. Changes in bacterial and eukaryotic communities during sewage decomposition in Mississippi river water. Water Research. 69, 30-39.
101. Kotsyurbenko, O. R., Glagolev, M. V., Nozhevnikova, A. N., Conrad, R., 2001. Competition between homoacetogenic bacteria and methanogenic archaea for hydrogen at low temperature. FEMS Microbiology Ecology. 38, 153-159.
102. Krasnits, E., Beliavsky, M., Tarre, S., Green, M., 2013. PHA based denitrification: Municipal wastewater vs. acetate. Bioresource Technology. 132, 28-37.
103. Kristjansson, J., Schönheit, P., Thauer, R., 1982. Different Ks values for hydrogen of methanogenic bacteria and sulfate reducing bacteria: An explanation for the apparent inhibition of methanogenesis by sulfate. Archives of Microbiology. 131, 278-282.
104. Krüger, M., Meyerdierks, A., Glöckner, F. O., Amann, R., Widdel, F., Kube, M., Reinhardt, R., Kahnt, J., Böcher, R., Thauer, R. K., Shima, S., 2003. A conspicuous nickel protein in microbial mats that oxidize methane anaerobically. Nature. 426, 878-881.
105. Lee, H.-S., Parameswaran, P., Kato-Marcus, A., Torres, C. I., Rittmann, B. E., 2008a. Evaluation of energy-conversion efficiencies in microbial fuel cells (MFCs) utilizing fermentable and non-fermentable substrates. Water Research. 42, 1501-1510.
106. Lee, H.-S., Torres, Ć. I., Rittmann, B. E., 2009a. Effects of substrate diffusion and anode potential on kinetic parameters for anode-respiring bacteria. Environmental Science and Technology. 43, 7571-7577.
107. Lee, H.-S., Vermaas, W. F. J., Rittmann, B. E., 2010. Biological hydrogen production: Prospects and challenges. Trends in Biotechnology. 28, 262-271.
108. Lee, H. S., Parameswaran, P., Kato-Marcus, A., Torres, C. I., Rittmann, B. E., 2008b. Evaluation of energy-conversion efficiencies in microbial fuel cells (MFCs) utilizing fermentable and non-fermentable substrates. Water Research. 42, 1501-1510.
109. Lee, H. S., Rittmann, B. E., 2010. Significance of biological hydrogen oxidation in a continuous single-chamber microbial electrolysis cell. Environmental Science and Technology. 44, 948-954.
110. Lee, H. S., Torres, C. I., Parameswaran, P., Rittmann, B. E., 2009b. Fate of H2 in an upflow single-chamber microbial electrolysis cell using a metal-catalyst-free cathode. Environmental Science and Technology. 43, 7971-7976.
111. Lee, H. S., Torres, Ć. I., Rittmann, B. E., 2009c. Effects of substrate diffusion and anode potential on kinetic parameters for anode-respiring bacteria. Environmental Science and Technology. 43, 7571-7577.
112. Lee, J., Phung, N. T., Chang, I. S., Kim, B. H., Sung, H. C., 2003. Use of acetate for enrichment of electrochemically active microorganisms and their 16S rDNA analyses. FEMS Microbiology Letters. 223, 185-191.

113. Lettinga, G., 1995. Anaerobic digestion and wastewater treatment systems. Antonie van Leeuwenhoek, International Journal of General and Molecular Microbiology. 67, 3-28.
114. Ley, R. E., Hamady, M., Lozupone, C., Turnbaugh, P. J., Ramey, R. R., Bircher, J. S., Schlegel, M. L., Tucker, T. A., Schrenzel, M. D., Knight, R., Gordon, J. I., 2008. Evolution of Mammals and Their Gut Microbes. Science. 320, 1647-1651.
115. Li, W.-W., Yu, H.-Q., He, Z., 2014. Towards sustainable wastewater treatment by using microbial fuel cells-centered technologies. Energy & Environmental Science.
116. Liu, B., Lei, Y., Li, B., 2014. A batch-mode cube microbial fuel cell based "shock" biosensor for wastewater quality monitoring. Biosensors and Bioelectronics. 62, 308-314.
117. Liu, H., Cheng, S., Logan, B. E., 2005. Production of electricity from acetate or butyrate using a single-chamber microbial fuel cell. Environmental Science and Technology. 39, 658-662.
118. Liu, H., Logan, B. E., 2004. Electricity Generation Using an Air-Cathode Single Chamber Microbial Fuel Cell in the Presence and Absence of a Proton Exchange Membrane. Environmental Science & Technology. 38, 4040-4046.
119. Liu, Y., Balkwill, D. L., Aldrich, H. C., Drake, G. R., Boone, D. R., 1999. Characterization of the anaerobic propionate-degrading syntrophs *Smithella propionica* gen. nov., sp. nov. and *Syntrophobacter wolinii*. International Journal of Systematic Bacteriology. 49, 545-556.
120. Liu, Y., Bond, D. R., 2012. Long-distance electron transfer by G. sulfurreducens biofilms results in accumulation of reduced c-type cytochromes. ChemSusChem. 5, 1047-1053.
121. Liu, Z., Liu, J., Zhang, S., Xing, X.-H., Su, Z., 2011. Microbial fuel cell based biosensor for in situ monitoring of anaerobic digestion process. Bioresource Technology. 102, 10221-10229.
122. Logan, B. E., 2004. Extracting Hydrogen and Electricity from Renewable Resources. Environmental Science and Technology. 38, 160A-167A.
123. Logan, B. E., 2009. Exoelectrogenic bacteria that power microbial fuel cells. Nature Reviews Microbiology. 7, 375-381.
124. Logan, B. E., 2012. Essential data and techniques for conducting microbial fuel cell and other types of bioelectrochemical system experiments. ChemSusChem. 5, 988-994.
125. Logan, B. E., Hamelers, B., Rozendal, R., Schröder, U., Keller, J., Freguia, S., Aelterman, P., Verstraete, W., Rabaey, K., 2006. Microbial fuel cells: Methodology and technology. Environmental Science and Technology. 40, 5181-5192.
126. Logan, B. E., Rabaey, K., 2012. Conversion of Wastes into Bioelectricity and Chemicals by Using Microbial Electrochemical Technologies. Science. 337, 686-690.

127. López-Cortés, A., Lanz-Landázuri, A., García-Maldonado, J., 2008. Screening and Isolation of PHB-Producing Bacteria in a Polluted Marine Microbial Mat. Microbial Ecology. 56, 112-120.
128. Lopez, S., McIntosh, F. M., Wallace, R. J., Newbold, C. J., 1999. Effect of adding acetogenic bacteria on methane production by mixed rumen microorganisms. Animal Feed Science and Technology. 78, 1-9.
129. Lovley, D. R., 2012. Electromicrobiology. Annual Review of Microbiology. 66, in press.
130. Lu, L., Xing, D., Ren, N., 2012. Pyrosequencing reveals highly diverse microbial communities in microbial electrolysis cells involved in enhanced H2 production from waste activated sludge. Water Research. 46, 2425-2434.
131. Mackenzie, F. T., Lerman, A., 2006. Carbon in the Geobiosphere: - Earth's Outer Shell Springer Netherlands.
132. Mancinelli, R. L., 1995. The regulation of methane oxidation in soil. Annual Review of Microbiology. 49, 581-605.
133. Marsili, E., Baron, D. B., Shikhare, I. D., Coursolle, D., Gralnick, J. A., Bond, D. R., 2008. Shewanella secretes flavins that mediate extracellular electron transfer. Proceedings of the National Academy of Sciences of the United States of America. 105, 3968-3973.
134. Martens, C. S., Berner, R. A., 1974. Methane Production in the Interstitial Waters of Sulfate-Depleted Marine Sediments. Science. 185, 1167-1169.
135. McCarty, P. L., Bae, J., Kim, J., 2011. Domestic wastewater treatment as a net energy producer-can this be achieved? Environmental Science and Technology. 45, 7100-7106.
136. McCarty, P. L., Smith, D. P., 1986. Anaerobic wastewater treatment. Environmental Science and Technology. 20, 1200-1206.
137. McCormick, A. J., Bombelli, P., Scott, A. M., Philips, A. J., Smith, A. G., Fisher, A. C., Howe, C. J., 2011. Photosynthetic biofilms in pure culture harness solar energy in a mediatorless bio-photovoltaic cell (BPV) system. Energy & Environmental Science. 4, 4699-4709.
138. McInerney, M. J., Bryant, M. P., Hespell, R. B., Costerton, J. W., 1981. Syntrophomonas wolfei gen. nov. sp. nov., an Anaerobic, Syntrophic, Fatty Acid-Oxidizing Bacterium. Applied and Environmental Microbiology. 41, 1029-1039.
139. McInerney, M. J., Sieber, J. R., Gunsalus, R. P., 2009. Syntrophy in Anaerobic Global Carbon Cycles. Current Opinion in Biotechnology. 20, 623-632.
140. Methé, B. A., Nelson, K. E., Eisen, J. A., Paulsen, I. T., Nelson, W., Heidelberg, J. F., Wu, D., Wu, M., Ward, N., Beanan, M. J., Dodson, R. J., Madupu, R., Brinkac, L. M., Daugherty, S. C., DeBoy, R. T., Durkin, A. S., Gwinn, M., Kolonay, J. F., Sullivan, S. A., Haft, D. H., Selengut, J., Davidsen, T. M., Zafar, N., White, O., Tran, B., Romero, C., Forberger, H. A., Weidman, J., Khouri, H., Feldblyum, T. V., Utterback, T. R., Van

Aken, S. E., Lovley, D. R., Fraser, C. M., 2003. Genome of Geobacter sulfurreducens: Metal Reduction in Subsurface Environments. Science. 302, 1967-1969.
141. Milucka, J., Ferdelman, T. G., Polerecky, L., Franzke, D., Wegener, G., Schmid, M., Lieberwirth, I., Wagner, M., Widdel, F., Kuypers, M. M. M., 2012. Zero-valent sulphur is a key intermediate in marine methane oxidation. Nature. 491, 541-546.
142. Min, B., Kim, J., Oh, S., Regan, J. M., Logan, B. E., 2005. Electricity generation from swine wastewater using microbial fuel cells. Water Research. 39, 4961-4968.
143. Min, B., Logan, B. E., 2004. Continuous electricity generation from domestic wastewater and organic substrates in a flat plate microbial fuel cell. Environmental Science and Technology. 38, 5809-5814.
144. Mino, T., Van Loosdrecht, M. C. M., Heijnen, J. J., 1998. Microbiology and biochemistry of the enhanced biological phosphate removal process. Water Research. 32, 3193-3207.
145. Mu, C., Kien, B. L., Liwei, L., 2006. Micromachined microbial and photosynthetic fuel cells. Journal of Micromechanics and Microengineering. 16, 2547.
146. Nauhaus, K., Albrecht, M., Elvert, M., Boetius, A., Widdel, F., 2007. In vitro cell growth of marine archaeal-bacterial consortia during anaerobic oxidation of methane with sulfate. Environmental Microbiology. 9, 187-196.
147. Nauhaus, K., Boetius, A., Krüger, M., Widdel, F., 2002. In vitro demonstration of anaerobic oxidation of methane coupled to sulfate reduction in sediment from a marine gas hydrate area. Environmental Microbiology. 4, 296-305.
148. Nauhaus, K., Treude, T., Boetius, A., Krüger, M., 2005. Environmental regulation of the anaerobic oxidation of methane: A comparison of ANME-I and ANME-II communities. Environmental Microbiology. 7, 98-106.
149. Nevin, K. P., Lovley, D. R., 2002. Mechanisms for Accessing Insoluble Fe(III) Oxide during Dissimilatory Fe(III) Reduction by Geothrix fermentans. Applied and Environmental Microbiology. 68, 2294-2299.
150. Nevin, K. P., Richter, H., Covalla, S. F., Johnson, J. P., Woodard, T. L., Orloff, A. L., Jia, H., Zhang, M., Lovley, D. R., 2008. Power output and columbic efficiencies from biofilms of Geobacter sulfurreducens comparable to mixed community microbial fuel cells. Environmental Microbiology. 10, 2505-2514.
151. Nishio, K., Hashimoto, K., Watanabe, K., 2010. Light/electricity conversion by a self-organized photosynthetic biofilm in a single-chamber reactor. Applied Microbiology and Biotechnology. 86, 957-964.
152. Nunoura, T., Hirai, M., Imachi, H., Miyazaki, M., Makita, H., Hirayama, H., Furushima, Y., Yamamoto, H., Takai, K., 2010. *Kosmotoga arenicorallina* sp. nov. a thermophilic and obligately anaerobic heterotroph isolated from a shallow hydrothermal system occurring within a coral reef, southern part of the Yaeyama Archipelago, Japan, reclassification of *Thermococcoides shengliensis* as *Kosmotoga*

shengliensis comb. nov., and emended description of the genus *Kosmotoga*. Archives of Microbiology. 192, 811-819.
153. Oh, S., Logan, B. E., 2005. Hydrogen and electricity production from a food processing wastewater using fermentation and microbial fuel cell technologies. Water Research. 39, 4673-4682.
154. Oh, S., Min, B., Logan, B. E., 2004. Cathode performance as a factor in electricity generation in microbial fuel cells. Environmental Science and Technology. 38, 4900-4904.
155. Oh, S. E., Logan, B. E., 2007. Voltage reversal during microbial fuel cell stack operation. Journal of Power Sources. 167, 11-17.
156. Okamoto, A., Saito, K., Inoue, K., Nealson, K. H., Hashimoto, K., Nakamura, R., 2014. Uptake of self-secreted flavins as bound cofactors for extracellular electron transfer in Geobacter species. Energy & Environmental Science.
157. Orphan, V. J., House, C. H., Hinrichs, K. U., McKeegan, K. D., DeLong, E. F., 2002. Multiple archaeal groups mediate methane oxidation in anoxic cold seep sediments. Proceedings of the National Academy of Sciences of the United States of America. 99, 7663-7668.
158. Palatsi, J., Affes, R., Fernandez, B., Pereira, M. A., Alves, M. M., Flotats, X., 2012. Influence of adsorption and anaerobic granular sludge characteristics on long chain fatty acids inhibition process. Water Research. 46, 5268-5278.
159. Pant, D., Van Bogaert, G., Diels, L., Vanbroekhoven, K., 2010. A review of the substrates used in microbial fuel cells (MFCs) for sustainable energy production. Bioresource Technology. 101, 1533-1543.
160. Parameswaran, P., Torres, C. I., Kang, D. W., Rittmann, B. E., Krajmalnik-Brown, R., 2012. The role of homoacetogenic bacteria as efficient hydrogen scavengers in microbial electrochemical cells (MXCs). Water Science and Technology. 65, 1-6.
161. Parameswaran, P., Torres, C. I., Lee, H. S., Krajmalnik-Brown, R., Rittmann, B. E., 2009. Syntrophic interactions among anode respiring bacteria (ARB) and non-ARB in a biofilm anode: Electron balances. Biotechnology and Bioengineering. 103, 513-523.
162. Parameswaran, P., Torres, C. I., Lee, H. S., Rittmann, B. E., Krajmalnik-Brown, R., 2011. Hydrogen consumption in microbial electrochemical systems (MXCs): The role of homo-acetogenic bacteria. Bioresource Technology. 102, 263-271.
163. Parameswaran, P., Zhang, H., Torres, C. I., Rittmann, B. E., Krajmalnik-Brown, R., 2010. Microbial community structure in a biofilm anode fed with a fermentable substrate: The significance of hydrogen scavengers. Biotechnology and Bioengineering. 105, 69-78.
164. Patakova, P., Maxa, D., Rychtera, M., Linhova, M., Fribert, P., Muzikova, Z., Lipovsky, J., Paulova, L., Pospisil, M., Sebor, G., Melzoch, K., 2011. Perspectives of

Biobutanol Production and Use, in: Bernardes, M. A. d. S., Ed. Biofuel's Engineering Process Technology.
165. Peters, V., Janssen, P. H., Conrad, R., 1998. Efficiency of hydrogen utilization during unitrophic and mixotrophic growth of *Acetobacterium woodii* on hydrogen and lactate in the chemostat. FEMS Microbiology Ecology. 26, 317-324.
166. Pinchuk, G. E., Hill, E. A., Geydebrekht, O. V., De Ingeniis, J., Zhang, X., Osterman, A., Scott, J. H., Reed, S. B., Romine, M. F., Konopka, A. E., Beliaev, A. S., Fredrickson, J. K., Reed, J. L., 2010. Constraint-Based Model of <italic>Shewanella oneidensis</italic> MR-1 Metabolism: A Tool for Data Analysis and Hypothesis Generation. PLoS Comput Biol. 6, e1000822.
167. Qian, F., Morse, D. E., 2011. Miniaturizing microbial fuel cells. Trends in Biotechnology. 29, 62-69.
168. Rabaey, K., Boon, N., Siciliano, S. D., Verhaege, M., Verstraete, W., 2004. Biofuel cells select for microbial consortia that self-mediate electron transfer. Applied and Environmental Microbiology. 70, 5373-5382.
169. Rabaey, K., Rozendal, R. A., 2010. Microbial electrosynthesis - Revisiting the electrical route for microbial production. Nature Reviews Microbiology. 8, 706-716.
170. Rabaey, K., Verstraete, W., 2005. Microbial fuel cells: Novel biotechnology for energy generation. Trends in Biotechnology. 23, 291-298.
171. Raghoebarsing, A. A. P., A.; van de Pas-Schoonen, K. T. *et al*, 2006. A microbial consortium couples anaerobic methane oxidation to denitrification. Nature. 440, 918-921.
172. Raskin, L., Stromley, J. M., Rittmann, B. E., Stahl, D. A., 1994. Group-specific 16S rRNA hybridization probes to describe natural communities of methanogens. Applied and Environmental Microbiology. 60, 1232-1240.
173. Reischwitz, A., Stoppok, E., Buchholz, K., 1997. Anaerobic degradation of poly-3-hydroxybutyrate and poly-3-hydroxybutyrate-co-3-hydroxyvalerate. Biodegradation. 8, 313-319.
174. Ren, H., Lee, H.-S., Chae, J., 2012. Miniaturizing microbial fuel cells for potential portable power sources: promises and challenges. Microfluid Nanofluid. 13, 353-381.
175. Ren, Z., Ward, T. E., Regan, J. M., 2007. Electricity production from cellulose in a microbial fuel cell using a defined binary culture. Environmental Science and Technology. 41, 4781-4786.
176. Richter, H., Lanthier, M., Nevin, K. P., Lovley, D. R., 2007. Lack of Electricity Production by Pelobacter carbinolicus Indicates that the Capacity for Fe(III) Oxide Reduction Does Not Necessarily Confer Electron Transfer Ability to Fuel Cell Anodes. Applied and Environmental Microbiology. 73, 5347-5353.
177. Rismani-Yazdi, H., Christy, A. D., Dehority, B. A., Morrison, M., Yu, Z., Tuovinen, O. H., 2007. Electricity generation from cellulose by rumen

microorganisms in microbial fuel cells. Biotechnology and Bioengineering. 97, 1398-1407.
178. Rittmann, B., McCarty, P., 2001. Environmental Biotechnology: Principles and Applications. 1st Ed. ed., McGraw-Hill Inc. , Boston
179. Rosenbaum, M., He, Z., Angenent, L. T., 2010. Light energy to bioelectricity: photosynthetic microbial fuel cells. Current Opinion in Biotechnology. 21, 259-264.
180. Rotaru, A. E., Shrestha, P. M., Liu, F., Shrestha, M., Shrestha, D., Embree, M., Zengler, K., Wardman, C., Nevin, K. P., Lovley, D. R., 2014. A new model for electron flow during anaerobic digestion: Direct interspecies electron transfer to Methanosaeta for the reduction of carbon dioxide to methane. Energy and Environmental Science. 7, 408-415.
181. Rozendal, R. A., Hamelers, H. V. M., Rabaey, K., Keller, J., Buisman, C. J. N., 2008. Towards practical implementation of bioelectrochemical wastewater treatment. Trends in Biotechnology. 26, 450-459.
182. Ryu, H., Griffith, J. F., Khan, I. U. H., Hill, S., Edge, T. A., Toledo-Hernandez, C., Gonzalez-Nieves, J., Santo Domingo, J., 2012. Comparison of Gull Feces-Specific Assays Targeting the 16S rRNA Genes of Catellicoccus marimammalium and Streptococcus spp. Applied and Environmental Microbiology. 78, 1909-1916.
183. Sakai, K., Miyake, S., Iwama, K., Inoue, D., Soda, S., Ike, M., 2015. Polyhydroxyalkanoate (PHA) accumulation potential and PHA-accumulating microbial communities in various activated sludge processes of municipal wastewater treatment plants. Journal of Applied Microbiology. 118, 255-266.
184. Salehizadeh, H., Van Loosdrecht, M. C. M., 2004. Production of polyhydroxyalkanoates by mixed culture: Recent trends and biotechnological importance. Biotechnology Advances. 22, 261-279.
185. Scheller, S., Goenrich, M., Boecher, R., Thauer, R. K., Jaun, B., 2010. The key nickel enzyme of methanogenesis catalyses the anaerobic oxidation of methane. Nature. 465, 606-608.
186. Schmitt-Wagner, D., Brune, A., 1999. Hydrogen Profiles and Localization of Methanogenic Activities in the Highly Compartmentalized Hindgut of Soil-Feeding Higher Termites (Cubitermes spp.). Applied and Environmental Microbiology. 65, 4490-4496.
187. Schubert, C. J., Vazquez, F., Lösekann-Behrens, T., Knittel, K., Tonolla, M., Boetius, A., 2011. Evidence for anaerobic oxidation of methane in sediments of a freshwater system (Lago di Cadagno). FEMS Microbiology Ecology. 76, 26-38.
188. Segarra, K. E. A., Comerford, C., Slaughter, J., Joye, S. B., 2013. Impact of electron acceptor availability on the anaerobic oxidation of methane in coastal freshwater and brackish wetland sediments. Geochimica et Cosmochimica Acta. 115, 15-30.

189. Seth, E. C., Taga, M. E., 2014. Nutrient sharing in the microbial world. Frontiers in Microbiology. 5.
190. Shi, Y., Hu, S., Lou, J., Lu, P., Keller, J., Yuan, Z., 2013. Nitrogen removal from wastewater by coupling anammox and methane-dependent denitrification in a membrane biofilm reactor. Environmental Science and Technology. 47, 11577-11583.
191. Shima, S., Krueger, M., Weinert, T., Demmer, U., Kahnt, J., Thauer, R. K., Ermler, U., 2012. Structure of a methyl-coenzyme M reductase from Black Sea mats that oxidize methane anaerobically. Nature. 481, 98-101.
192. Shoemaker, J. K., Schrag, D. P., 2010. Subsurface characterization of methane production and oxidation from a New Hampshire wetland. Geobiology. 8, 234-243.
193. Shoener, B. D., Bradley, I. M., Cusick, R. D., Guest, J. S., 2014. Energy positive domestic wastewater treatment: the roles of anaerobic and phototrophic technologies. Environmental Science: Processes & Impacts. 16, 1204-1222.
194. Shrestha, P. M., Rotaru, A.-E., Summers, Z. M., Shrestha, M., Liu, F., Lovley, D. R., 2013. Transcriptomic and Genetic Analysis of Direct Interspecies Electron Transfer. Applied and Environmental Microbiology. 79, 2397-2404.
195. Sieber, J. R., McInerney, M. J., Gunsalus, R. P., 2012. Genomic insights into syntrophy: The paradigm for anaerobic metabolic cooperation. Annual Review of Microbiology. 66, 429-452.
196. Siegert, M., Li, X.-F., Yates, M. D., Logan, B. E., 2014. The presence of hydrogenotrophic methanogens in the inoculum improves methane gas production in microbial electrolysis cells. Frontiers in Microbiology. 5, 778.
197. Singh, P., Carliell-Marquet, C., Kansal, A., 2012. Energy pattern analysis of a wastewater treatment plant. Appl Water Sci. 2, 221-226.
198. Smemo, K. A. Y., J. B., 2007. Evidence for anaerobic CH_4 oxidation in freshwater peatlands. Geomicrobiology Journal. 24, 583-579.
199. Stahl, M. T. M. J. M. M. D. A., 2010. Brock biology of microorganisms. Benjamin-Cummings Publishing Company.
200. Stams, A. J. M., Elferink, S. J. W. H. O., Westermann, P., 2003. Metabolic Interactions Between Methanogenic Consortia and Anaerobic Respiring Bacteria, in: Ahring, B., Angelidaki, I., Macario, E. C., Gavala, H. N., Hofman-Bang, J., Macario, A. J. L., Elferink, S. J. W. H. O., Raskin, L., Stams, A. J. M., Westermann, P., Zheng, D., Eds. Biomethanation I. Springer Berlin Heidelberg, Vol. 81, pp 31-56.
201. Sugnaux, M., Mermoud, S., da Costa, A. F., Happe, M., Fischer, F., 2013. Probing electron transfer with Escherichia coli: A method to examine exoelectronics in microbial fuel cell type systems. Bioresource Technology. 148, 567-573.
202. Suzuki, M. T., Taylor, L. T., DeLong, E. F., 2000. Quantitative analysis of small-subunit rRNA genes in mixed microbial populations via 5'-nuclease assays. Applied and Environmental Microbiology. 66, 4605-4614.

203. Suzuki, Y., Kitatsuji, Y., Ohnuki, T., Tsujimura, S., 2010. Flavin mononucleotide mediated electron pathway for microbial U(vi) reduction. Physical Chemistry Chemical Physics. 12, 10081-10087.
204. Swithers, K. S., DiPippo, J. L., Bruce, D. C., Detter, C., Tapia, R., Han, S., Goodwin, L. A., Han, J., Woyke, T., Pitluck, S., Pennacchio, L., Nolan, M., Mikhailova, N., Land, M. L., Nesbø, C. L., Gogarten, J. P., Noll, K. M., 2011. Genome Sequence of Kosmotoga olearia Strain TBF 19.5.1, a Thermophilic Bacterium with a Wide Growth Temperature Range, Isolated from the Troll B Oil Platform in the North Sea. Journal of Bacteriology. 193, 5566-5567.
205. Teng, S. X., Tong, Z. H., Li, W. W., Wang, S. G., Sheng, G. P., Shi, X. Y., Liu, X. W., Yu, H. Q., 2010. Electricity generation from mixed volatile fatty acids using microbial fuel cells. Applied Microbiology and Biotechnology. 87, 2365-2372.
206. Thauer, R. K., 2011. Anaerobic oxidation of methane with sulfate: On the reversibility of the reactions that are catalyzed by enzymes also involved in methanogenesis from CO2. Current Opinion in Microbiology. 14, 292-299.
207. Third, K. A., Burnett, N., Cord-Ruwisch, R., 2003. Simultaneous nitrification and denitrification using stored substrate (phb) as the electron donor in an SBR. Biotechnology and Bioengineering. 83, 706-720.
208. Toh, H., Sharma, V. K., Oshima, K., Kondo, S., Hattori, M., Ward, F. B., Free, A., Taylor, T. D., 2011. Complete genome sequences of *Arcobacter butzleri* ED-1 and *Arcobacter* sp. Strain L, both isolated from a microbial fuel cell. Journal of Bacteriology. 193, 6411-6412.
209. Toledo-Hernandez, C., Ryu, H., Gonzalez-Nieves, J., Huertas, E., Toranzos, G. A., Santo Domingo, J. W., 2013. Tracking the primary sources of fecal pollution in a tropical watershed in a one-year study. Applied and Environmental Microbiology. 79, 1689-1696.
210. Torres, C. I., Kato Marcus, A., Rittmann, B. E., 2007. Kinetics of consumption of fermentation products by anode-respiring bacteria. Applied Microbiology and Biotechnology. 77, 689-697.
211. Torres, C. I., Krajmalnik-Brown, R., Parameswaran, P., Marcus, A. K., Wanger, G., Gorby, Y. A., Rittmann, B. E., 2009. Selecting anode-respiring bacteria based on anode potential: Phylogenetic, electrochemical, and microscopic characterization. Environmental Science and Technology. 43, 9519-9524.
212. Torres, C. I., Marcus, A. K., Parameswaran, P., Rittmann, B. E., 2008a. Kinetic experiments for evaluating the nernst-monod model for anode-respiring bacteria (ARB) in a biofilm anode. Environmental Science and Technology. 42, 6593-6597.
213. Torres, C. I., Marcus, A. K., Rittmann, B. E., 2008b. Proton transport inside the biofilm limits electrical current generation by anode-respiring bacteria. Biotechnology and Bioengineering. 100, 872-881.

214. Tront, J. M., Fortner, J. D., Plötze, M., Hughes, J. B., Puzrin, A. M., 2008. Microbial fuel cell biosensor for in situ assessment of microbial activity. Biosensors and Bioelectronics. 24, 586-590.
215. Tucci, S., Martin, W., 2007. A novel prokaryotic trans-2-enoyl-CoA reductase from the spirochete Treponema denticola. FEBS Letters. 581, 1561-1566.
216. Tugtas, A. E., Pavlostathis, S. G., 2007. Electron donor effect on nitrate reduction pathway and kinetics in a mixed methanogenic culture. Biotechnology and Bioengineering. 98, 756-763.
217. Uría, N., Muñoz Berbel, X., Sánchez, O., Muñoz, F. X., Mas, J., 2011. Transient storage of electrical charge in biofilms of Shewanella oneidensis MR-1 growing in a microbial fuel cell. Environmental Science and Technology. 45, 10250-10256.
218. US-EPA, 2010. Methane and Nitrous Oxide Emissions From Natural Sources. EPA 430-R-10-001.
219. US-EPA, 2012. Inventory of U.S. greenhouse gas emissions and sinks: 1990 – 2010.
220. Velasquez-Orta, S., Yu, E., Katuri, K., Head, I., Curtis, T., Scott, K., 2011. Evaluation of hydrolysis and fermentation rates in microbial fuel cells. Applied Microbiology and Biotechnology. 90, 789-798.
221. Walter Anthony, K. M., Anthony, P., Grosse, G., Chanton, J., 2012. Geologic methane seeps along boundaries of Arctic permafrost thaw and melting glaciers. Nature Geoscience. 5, 419-426.
222. Wang, Q., Garrity, G. M., Tiedje, J. M., Cole, J. R., 2007. Naïve Bayesian Classifier for Rapid Assignment of rRNA Sequences into the New Bacterial Taxonomy. Applied and Environmental Microbiology. 73, 5261-5267.
223. Wankel, S. D., Adams, M. M., Johnston, D. T., Hansel, C. M., Joye, S. B., Girguis, P. R., 2012. Anaerobic methane oxidation in metalliferous hydrothermal sediments: influence on carbon flux and decoupling from sulfate reduction. Environmental Microbiology. 14, 2726-2740.
224. Wiegant, W. M., Lettinga, G., 1985. Thermophilic anaerobic digestion of sugars in upflow anaerobic sludge blanket reactors. Biotechnology and Bioengineering. 27, 1603-1607.
225. Wieslander, Å., Nordström, S., Dahlqvist, A., Rilfors, L., Lindblom, G., 1995. Membrane Lipid Composition and Cell Size of Acholeplasma laidlawii Strain A are Strongly Influenced by Lipid Acyl Chain Length. European Journal of Biochemistry. 227, 734-744.
226. Xu, G.-H., Wang, Y.-K., Sheng, G.-P., Mu, Y., Yu, H.-Q., 2014. An MFC-Based Online Monitoring and Alert System for Activated Sludge Process. Sci. Rep. 4.
227. Yeom, J., Shin, J.-H., Yang, J.-Y., Kim, J., Hwang, G.-S., 2013. ¹H NMR-Based Metabolite Profiling of Planktonic and Biofilm Cells in <italic>Acinetobacter baumannii</italic> 1656-2. PLoS ONE. 8, e57730.

228. Yu, J., Park, Y., Cho, H., Chun, J., Seon, J., Cho, S., Lee, T., 2012. Variations of electron flux and microbial community in air-cathode microbial fuel cells fed with different substrates. Water Science and Technology. 66, 748-753.
229. Zehnder, A. J. B., T. D., 1979. Methane formation and methane oxidation by methanogenic bacteria. Journal of Bacteriology. 137, 420-431.
230. Zeng, R. J., Yuan, Z., Keller, J., 2003. Enrichment of denitrifying glycogen-accumulating organisms in anaerobic/anoxic activated sludge system. Biotechnology and Bioengineering. 81, 397-404.
231. Zhang, X., Cheng, S., Liang, P., Huang, X., Logan, B. E., 2011. Scalable air cathode microbial fuel cells using glass fiber separators, plastic mesh supporters, and graphite fiber brush anodes. Bioresource Technology. 102, 372-375.
232. Zhou, M., Chi, M., Luo, J., He, H., Jin, T., 2011. An overview of electrode materials in microbial fuel cells. Journal of Power Sources. 196, 4427-4435.

Appendices

A. Characterization of the inoculum

To characterize the activity of the inoculum, various levels of three common volatile fatty acids (VFAs, e.g., acetate, propionate, and butyrate) were fed into the mother MEC to examine the current responses. During the continuous operation, autoclaved fresh medium with various concentrations of different VFA compounds (Table A1) was continuously pumped into the anode chamber by a peristaltic pump (Masterflex L/S digital pump, Cole-Parmer Canada) at a hydraulic retention time (HRT) of 6 hours. Before each level of VFA provision, the MEC was pre-conditioned in mineral medium until the electric current was below 0.1 mA. The continuous feed was stopped until the electric current reached a plateau. Detailed electric current profiles of the 15 conditions can be found in Figure A2. The concentrations of propionate and butyrate were set to be of the same electron equivalent of the measured concentrations of acetate. UHP nitrogen gas or helium (99.999%, Praxair Canada) was bubbled into the medium bottle during the continuous operation so that oxygen contamination from atmosphere could be avoided. A bacteria air vent (Pall Corporation, VWR Canada) was incorporated into the gas tubing line for better sterilization. The results were plotted in Figure A1.

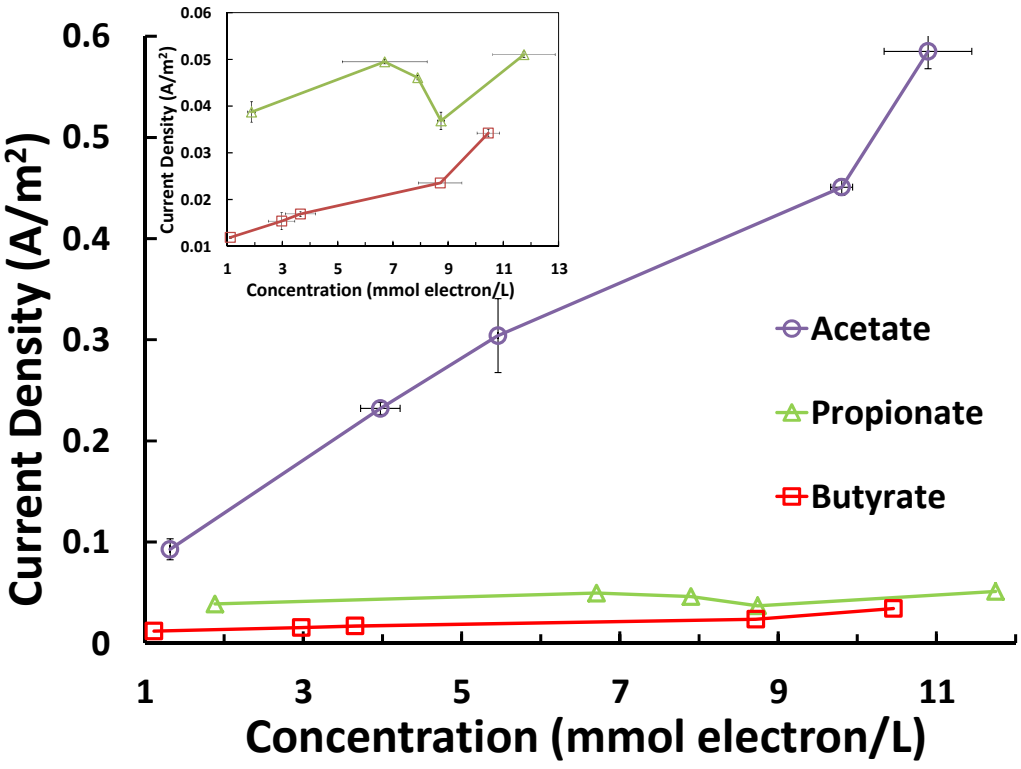

Figure A1. Evaluation of anode biofilm activity of a mother MEC with three common volatile fatty acids. Error bars denote one standard deviation from the means of quadruplicate samples (x-axis) and all data points in the last two hours (y-axis). Original data for creating this plot was shown in Figure A2.

The growth of non-ARB, fermenters and methanogens, in anode biofilm is usually inevitable when an MEC is acclimated with a continuous fed-batch operation. For instance, in an MEC that acclimated by continuous feeding of acetate, 3.6 mmol electron/l of propionate shows comparable performance with 8 mmol electron/l of acetate (Oh and Logan, 2005). Similar consumption rate of propionate and acetate has also been reported elsewhere (Yu et al., 2012). Another study using wastewater-acclimated MECs showed that the consumption rates of propionate and butyrate (~35 mmol electron/l) are similar and both of them are around 1/3 of acetate consumption rate (Kim et al., 2008).

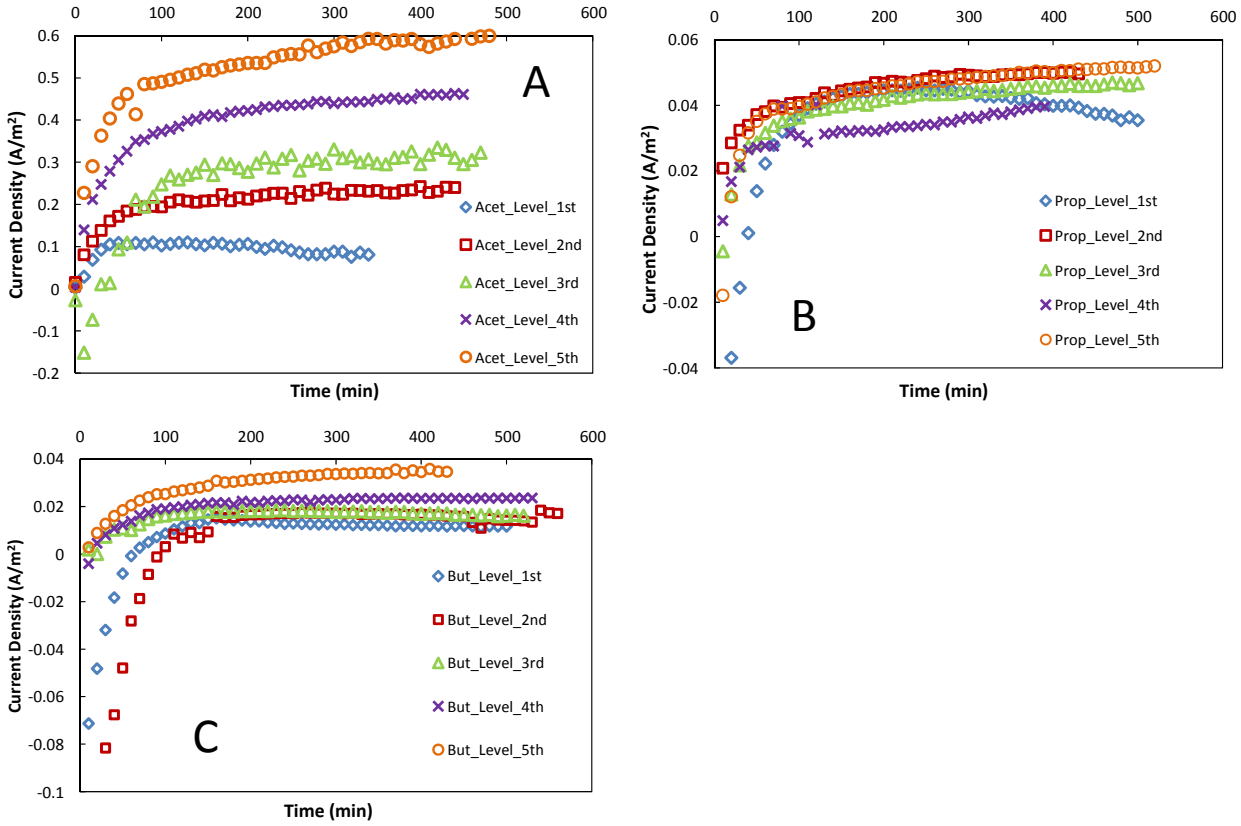

Figure A2. Electric current densities from continuous supply of various levels (Table A1) of three VFAs.

In current study, when all compounds were around 11 mmol electron/L, acetate yielded over 10 times electric current of these from propionate and butyrate. Apparently, the anode biofilm prefers acetate over fermentable substrates, such as propionate and butyrate, which also indicates the inactivity of fermentative bacteria and hydrogenotrophic methanogens in the anode biofilm. The much higher consumption rate of acetate compared with those of propionate and butyrate clearly demonstrates that the electrochemical properties of the MEC system are not the rate-limiting factors for propionate and butyrate utilization. Instead, fermentation or the consumption of the fermentative end-products, such as hydrogen gas, is limiting the current generation using these two fermentable substrates.

Table A1. The concentrations of three volatile fatty acids used in characterizing the anode biofilm in a mother MEC

Acetate (mmol electron/l)	(mg/l*)	Butyrate (mmol electron/l)	(mg/l*)	Propionate (mmol electron/l)	(mg/l*)
1.181	12.112	1.181	6.502	1.181	8.106
4.492	46.062	4.492	24.727	4.492	30.826
5.670	58.140	5.670	31.211	5.670	38.909
8.549	87.654	8.549	47.055	8.549	58.661
11.071	113.522	11.071	60.942	11.071	75.972

*as corresponding sodium salt, anhydrous

B. Detection limits of volatile fatty acids by the GC-FID method

The limitations of detection were determined, according to the Standard Methods (1999). The detailed procedure of the GC-FID operation can be found in Chapter 3. Each of the chosen samples was run following the GC-FID method for eight times, and 99% of confidence interval was selected. Heptanoic acid was never detected in samples, so it is excluded from this report.

Table A2. Method detection limits of the VFAs in this study

compound	mg/l
acetate	1.52
propionate	1.03
isobutyrate	0.39
butyrate	1.76
isovaleric acid	0.34
valeric acid	0.66
isocaproic acid	0.84
caproic acid	1.74

C. The gas recirculation loop used in this study

At the very beginning of enrichment, methane was provided through a gas sampling bag attached to the outlet of the MEC. Since oxygen may diffuse into the gas sampling bag with time, a gas recirculation loop (Figure A3) was designed to replace the gas sampling bag. A 250 ml glass bottle (PYREX® Screw Cap Storage Bottles) with open top cap and rubber stopper was incorporated into the loop as the methane gas reservoir. The gas recirculation rate was set at 7 ml/min using a digital pump (Masterflex L/S peristaltic pump). The methane gas inside the glass bottle and the loop was refreshed once a week by purging with methane gas (99.97%, Praxair Canada).

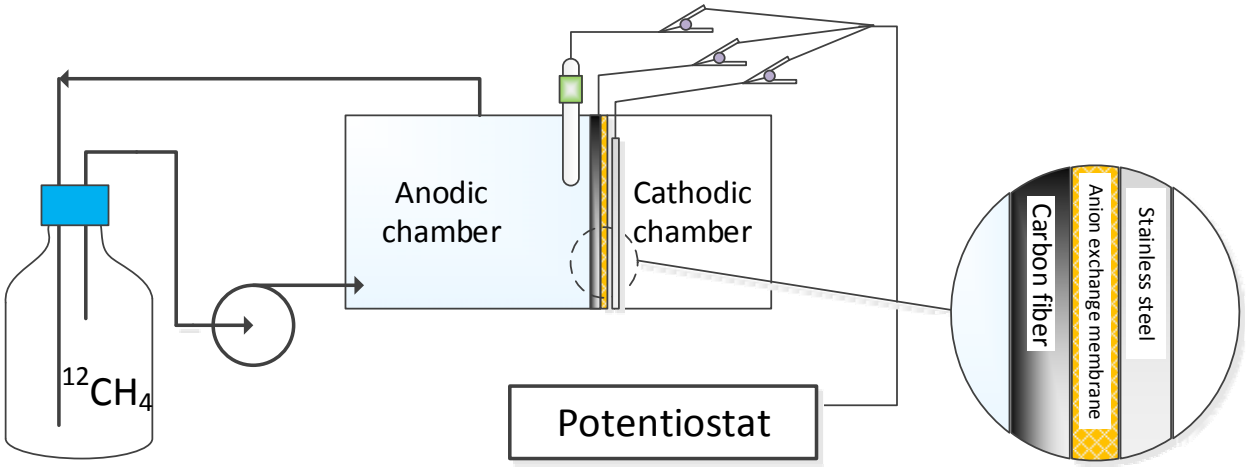

Figure A3. Supply of methane gas through a gas re-circulation loop during phase I, earlier phase II and phase III

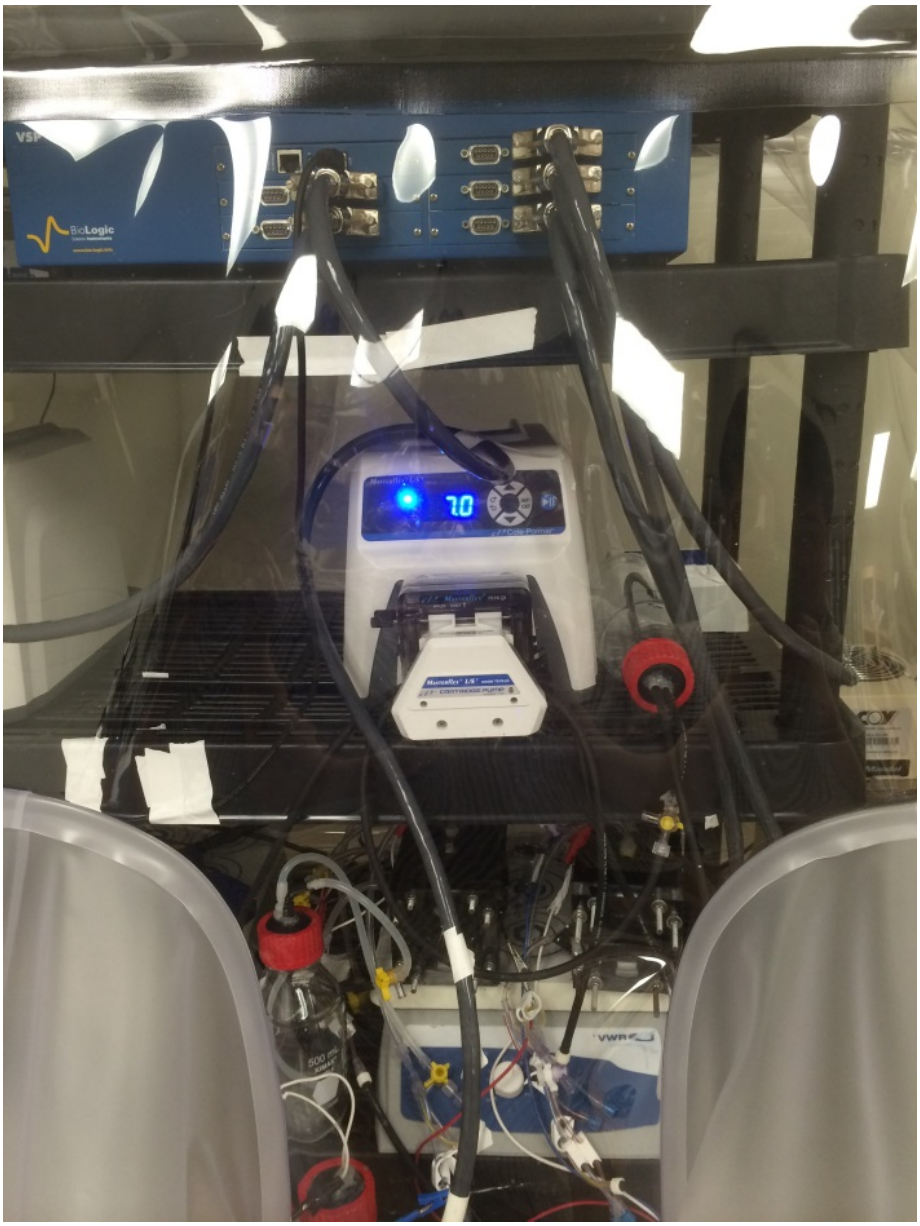

Figure A4. The MECs with gas recirculation loops (Phase III). Glass bottles, 500 ml, were incorporated into the loops to increase the headspace volume. Methane gas was used to fill the bottles and the tubes. The gas recirculation rate was set at 7 ml/min by a peristaltic pump.

D. Results from the isotopic analyses of carbon dioxide

The $\delta^{13}C$ values used for the computation in Chapter 5 were measured and provided by uwEILAB as shown in Table A3.

Table A3. Isotope analyses of the carbon dioxide generated from the anode chamber and the methane gas (feed)

Sample	$\delta^{13}C$	Result	Repeat	$\delta^{13}C$	Result	Repeat
	CO_2	$PDB_{standard}$		CH_4	$VPDB_{standard}$	
CO_2 from MEC		-56.4	-58.4			
CH_4 fed to MEC					-37.14	-37.23

E. Electric current profile and rates of anaerobic oxidation of methane from the H-type microbial electrochemical cell (Phase IV)

Methane-dependent current production was observed in the H-MEC. Overall, the current density (based on anode surface area, 22.5 cm^2) was one order of magnitude lower than that from sandwich type MEC. The first cycle with quantitative analysis was from day 6 to day 15, as shown in Figure A5. The current profile was broken around day 31 because the cable connecting the potentiostat and data acquisition system was dislodged from its socket. The ups and downs of the current were caused by the fluctuation of the room temperature plus that the temperature inside the anaerobic chamber was not controlled. Since the two graphite bars were freely emerged in the anolyte, movement or drift of the bars during operation might also have caused noise in the current.

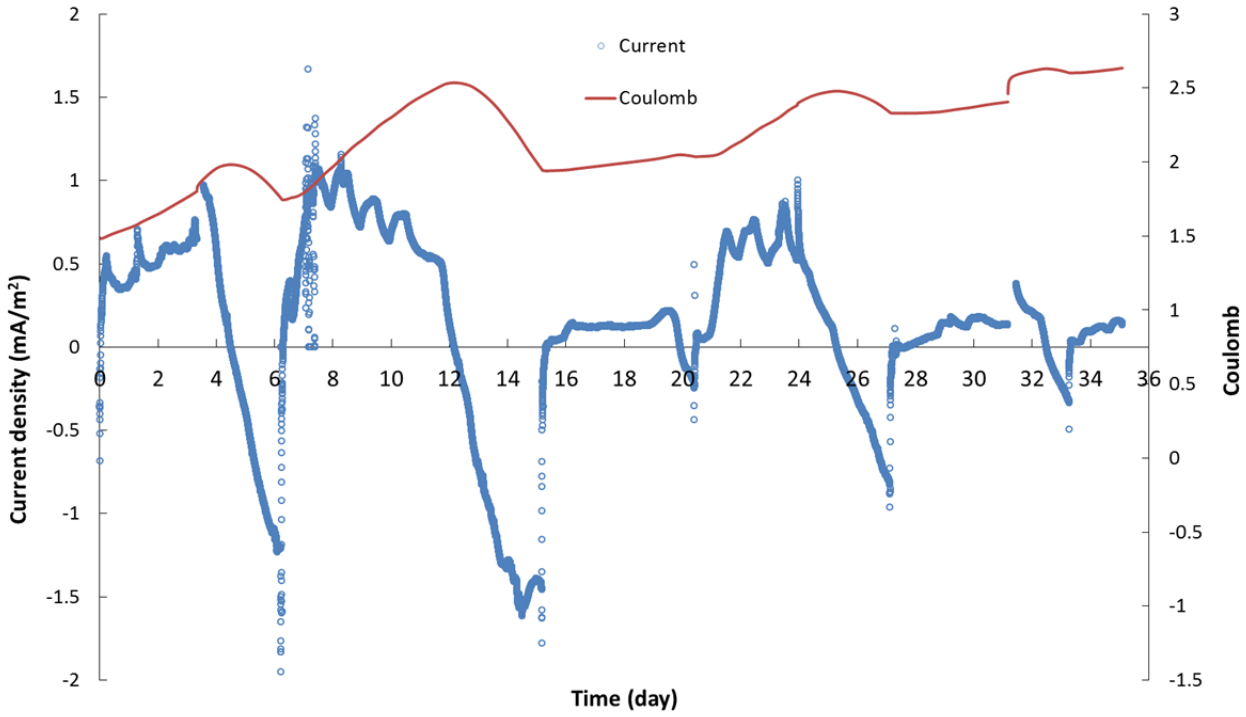

Figure A5. Current density and coulomb profiles from the H-type glass MEC, methane was the only external carbon and energy source.

The electric current dropped below zero at the end of each cycle. The reducing current can be attributed to the shift of the potential of the anode biofilm to more positive values with increasing concentration of oxidized terminal electron donor as indicated by the Nernst equation ($E = E^{\emptyset} - \frac{RT}{nF} ln \frac{a_{oxidized}}{a_{reduced}}$). To a point when the concentrations of the oxidized terminal electron donor and the reduced counterpart reach a certain ratio, the potential of the biofilm may exceed the set anode potential (-0.25 V vs Ag/AgCl), and reduction reaction can occur in this condition. The electrons flowed back to the biofilm may have been stored in the outer membrane cytochromes of ARB or some other electron carriers inside the biofilm matrix. The ability of anode biofilm to temporarily store electrons has been documented before (Uría et al., 2011).

To quantify the loss of methane due to diffusion through septa and the AEM, an abiotic control reactor (H-MEC-control in Figure 5-2, glass reactor of the same configuration as H-MEC) was operated. The same control test was repeated for six times. MilliQ water, instead of mineral medium, was used in control study. Methane was purged into the anode chamber for 1-2 hours, and the dissolved methane concentration was measured. The reactor was then sealed. After a certain time (Figure A6), the dissolved methane was measured again. The mass transfer equation used in the curve fitting can be found in Chapter 5. The results and the regression curve were plotted in Figure A6. Obviously, the diffusional loss was not significant during a four- to six-day batch operation, which was the time period for studying the

AOM rates during phase IV. Details of the measurement and computation of the AOM rate during the four cycles of methane oxidation are tabulated in Table A4.

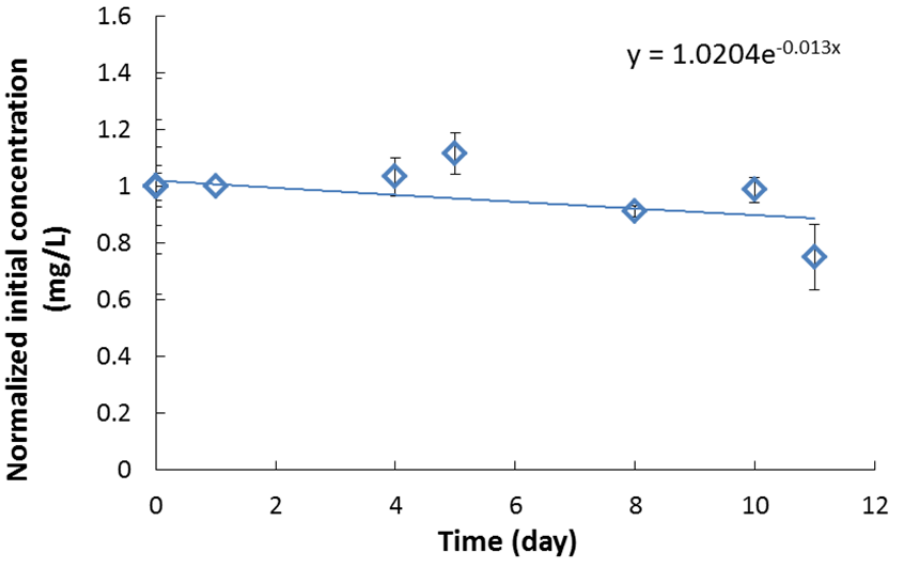

Figure A6. Abiotic control test for estimating the loss of methane via diffusion through the septa and the AEM. The blue line denotes the regression curve from the fit of the data points (top right). Error bars show one standard deviations from the means.

Table A4. Summary of the computation of AOM rates in an H-type MEC

Cycle #		First		Second		Third		Forth	
Date		June 9 2014	June 18 2014	June 18 2014	June 23 2014	June 23 2014	June 30 2014	June 30 2014	July 6 2014
Initial/end		Initial	end	Initial	end	Initial	end	Initial	end
Dissolved CH_4 (mg/l)	Average	6.836	0.166[@]	5.773	0.192	9.342	0.166[@]	4.935	1.005
	Standard deviation	0.849	-	1.042	0.170	1.297	-	-	-
Duration of each cycle (day)		8.95		5.23		6.71		6.14	
Final dissolved CH_4 if no biodegradation (mg/l)[*]		6.209		5.504		8.736		4.649	
Δ CH_4 due to biodegradation (mg/l)[#]		6.043		5.312		8.570		3.645	
AOM rate (mg CH_4/l/day)		0.675		1.016		1.277		0.594	

*: calculated based on correlation in Figure A5-4
#: (Final dissolved CH_4 if no biodegradation)-(Dissolved CH_4 at the end)

@: these two seem the same but are actually from two different sets of measurement: 0.2179 and 0.1142; 0.2438 and 0.088, respectively.

Table A5. Comparison of the Gibbs free energy gain from various AOM

Electron acceptor couple	Electron donor couple	Half reactions	$\Delta G^{o'}$ (kJ/mol e)	$\Delta G'$ (kJ/mol e)#	E' (V vs SHE*)	$\Delta G'_{rxn}$ (kJ/mol CH_4)	Note
SO_4^{2-}/ HS_2^-		SO_4^{2-} +8 ½ H^+ +7e^- →1/2HS_2^- +4H_2O	20.6	20.7	-0.21	-28.8	(Milucka et al., 2012), Table S3
	HCO_3^- /CH_4 (aq)	CH_4 (aq) + 3H_2O →HCO_3^- +9H^++8e^-	-24.9	-24.3	0.25		
NO_3^-/ NO_2^-		NO_3^- +2H^+ +2e^-→NO_2^- +H_2O	-41.65	-44	0.46	-539.2	(Haroon et al., 2013), Figure 3 and S12
	CO_2(g)/ CH_4 (g)	CH_4 (g) + 2H_2O →CO_2(g) +8H^++8e^-	-23.5	-23.4	0.24		
$Fe(OH)_3$/ Fe^{2+}		$Fe(OH)_3$+3H^+ +e^-→Fe^{2+} +3H_2O	-91.41	12.8	-0.13	-270.4	(Beal et al., 2009)
	HCO_3^- /CH_4 (aq)	CH_4 (aq) + 3H_2O →HCO_3^- +9H^++8e^-	19.9 (ΔG^o)	-46.6 (ΔG)	0.48		
electrode		N/A	N/A	N/A	-0.2	-38.6	This study
	CO_2(g)/ CH_4 (g)	CH_4 (g) + 2H_2O →CO_2(g) +8H^++8e^-	-23.5	-24.3‡	0.25		

#: the Gibbs free energy are computed according to the *in vitro* concentrations
*: SHE stands for standard hydrogen electrode
‡: Measured values at the end of batch incubation, average of triplicate measurements, CO_2=0.003187 atm, CH_4=0.135 atm, pH=7.4

F. Collection of background current density from sandwich-type microbial electrochemical cells (Phase III)

After the biofilm anode was sampled for the second SIP analysis, the residual anolytes (~250 ml) after dissolved methane quantification were filtered through 0.45 μm syringe filters (Nylon, Cole-Parmer Canada). The filtrate was re-injected into the anode chambers, which were cleaned thoroughly and sterilized while fresh deoxygenated mineral medium was used to make up the lost volume. The media were purged by methane gas for over 40 minutes. The same catholytes were used for these abiotic MECs. These cells were operated in the same condition for collecting background current density. This operation lasted for around 80 days.

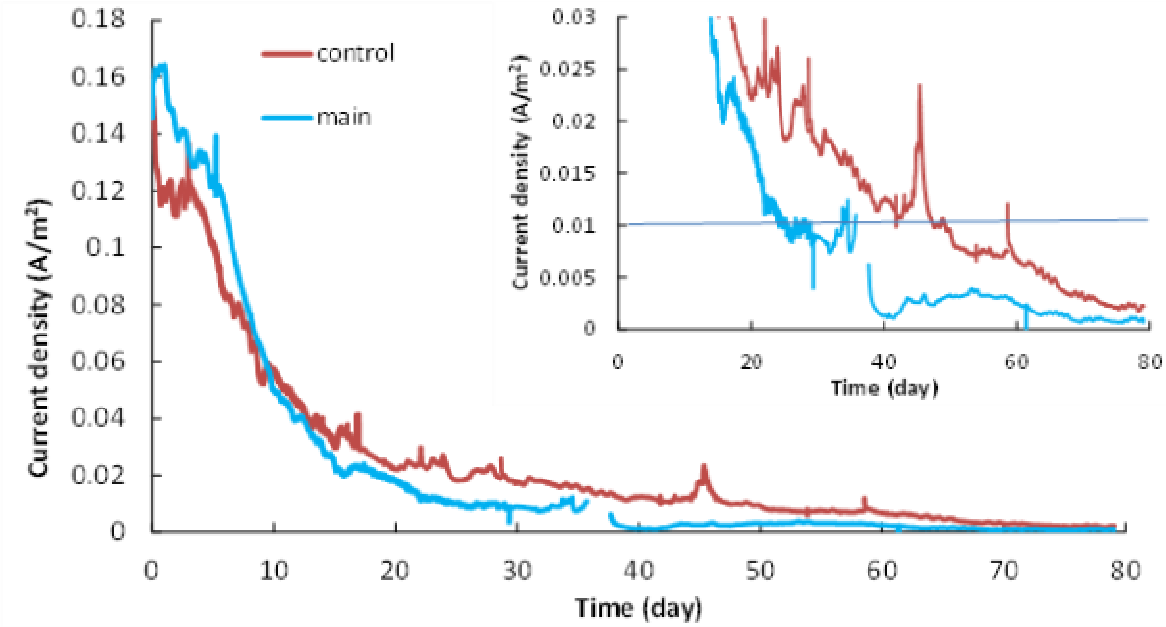

Figure A7. The background current from two identical microbial electrochemical cells. The anolytes that were collected after the biofilm anodes were sampled. New carbon fiber was used for the electric current collection. The insert highlights the difference between background current and the electric current when active AOM-biofilm anode is present (horizontal line).

G. Reasons for inconsistency in the microbial community structures in the control microbial electrochemical cell and the functional microbial electrochemical cell during SIP tests

The DGGE profiles from the control reactor show different dominant species from these in the functional reactor. The difference may be attributed to three reasons: (1) Due to the limitation of space, the first control reactor was not operated in parallel with the functional reactor. Instead, the control sample was the same as that used to inoculate the functional reactor. The new reactor was further enriched for four months during which continuous methane gas supply was adopted (Figure 5-2, phase II, the anode of MEC 1 was sacrificed for sequencing and was completely regrown). The microbial community could have undergone a shift during this enrichment phase. A long term shift or continuous variation of an AOM community was shown to exist in nitrite-dependent AOM (Haroon et al., 2013) where some archaeal species disappeared after long term incubation; (2) the second control reactor was inoculated by the anolyte from a functional reactor (Figure 5-2, phase III), not the anode biofilm. Although this method was recommended and followed by MEC researchers for growing ARB, it seems not appropriate for transferring AOM community from one reactor to another. Apparently, the successful growth of *Geobacter* species shown in Figure 5-8 supports this speculation. In future studies, a direct transfer of biofilm is recommended; (3) Two different sets of primers were used during the PCR amplification of archaea in the fractionated DNA samples, and the selective amplification can lead to different compositions of the final products.

H. Additional two-dimensional *FISH* images of the dissolved methane-oxidizing consortium on anode fibers

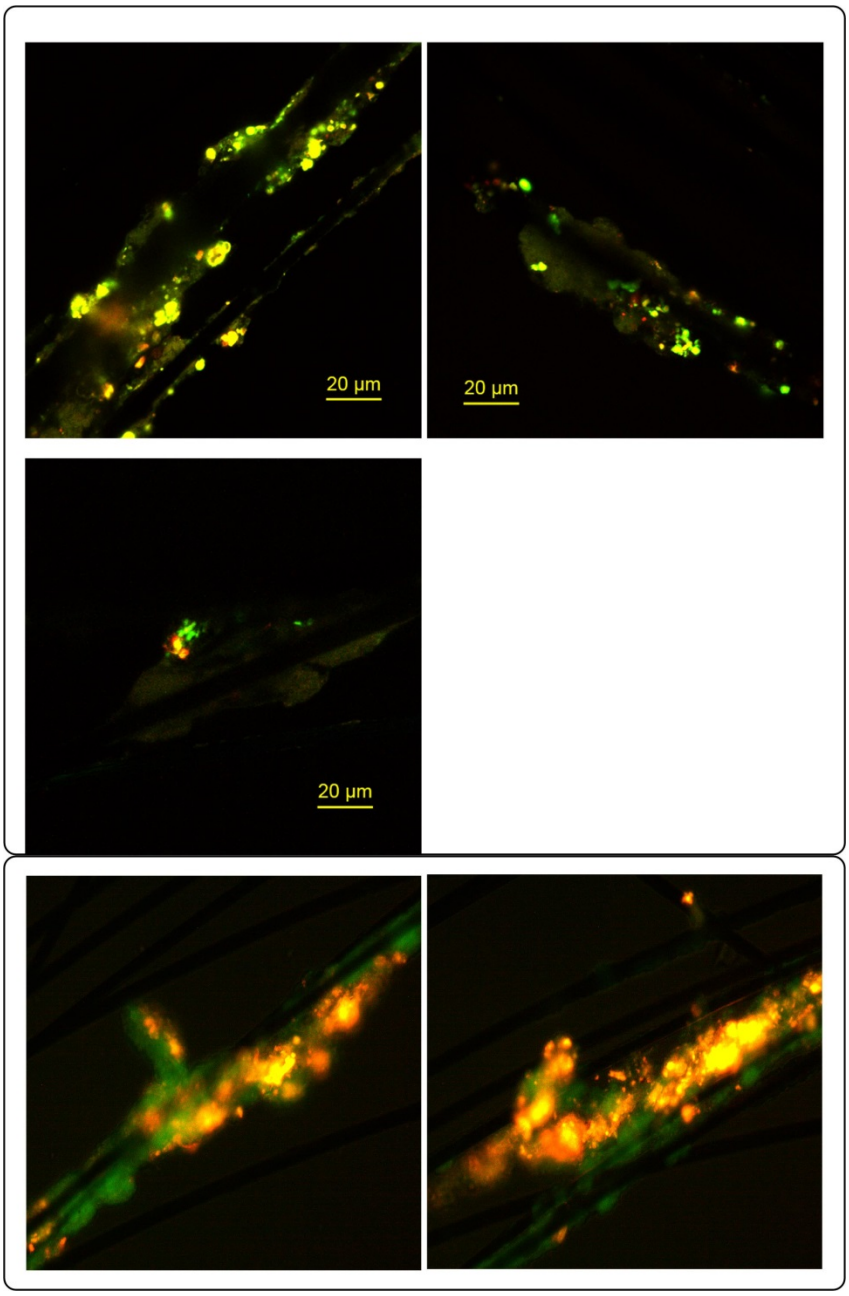

Figure A8. Additional two-dimensional *FISH* images from AOM consortium on carbon fibers. The three images in the top box (630X) are the hybridized samples observed via a Zeiss Axiovert 200 equipped with a Zeiss LSM510-Meta confocal module. The two images in the bottom box (400X) are observed by a Zeiss epifluorescence microscope (Axio Scope.A1).